

ELECTRONIC STRUCTURE OF LIQUID METALS
USING NONLOCAL, ENERGY DEPENDENT
MODEL POTENTIALS

by

TIN CHAN

B.Sc., University of Hong Kong, 1963
B.Sc., Special, University of Hong Kong, 1964
M.Sc., University of Hong Kong, 1967

A DISSERTATION SUBMITTED IN PARTIAL FULFILMENT
OF THE REQUIREMENTS FOR THE DEGREE OF
DOCTOR OF PHILOSOPHY
in the Department
of
Physics

© TIN CHAN 1971

SIMON FRASER UNIVERSITY

August 1971

APPROVAL

Name: Tin Chan
Degree: Doctor of Philosophy
Title of Thesis: Electronic Structure of Liquid Metals
using Nonlocal, Energy Dependent Model
Potentials

Examining Committee:

Chairman: K.E. Rieckhoff

L.E. Ballentine
Senior Supervisor

A.S. Arrott

E.D. Crozier

B.L. Jones

N.W. Ashcroft
External Examiner
Professor of Physics
Cornell University, USA

Date Approved

17 Sept 1971

ABSTRACT

The electronic structures of several liquid metals have been calculated numerically in a weak binding approximation using nonlocal, energy dependent electron-ion model potentials and measured liquid structure factors. Two different approaches are pursued to overcome the difficulties caused by the energy dependence of the potential.

In the first method, which is a slight modification of the Green function formalism of Edwards (1962), the energy dependence is approximately taken into account by absorbing the first order term into a redefined zero-order hamiltonian by means of an effective mass. This is equivalent to neglecting the energy dependence of the off-diagonal matrix elements of the potential. Using this method the densities of electronic states of liquid bismuth, indium, and mercury are calculated. The first two are found to be very free-electron-like, but for mercury there is a dip near the Fermi energy, quite similar to but less severe than was suggested by Mott.

To include the energy dependence exactly we have devised a method by which the total number of electronic states below an energy E is evaluated. It is based upon an idea of Lloyd (1967), which we have extended and developed into a form suitable for numerical calculation. Results of calculations for liquid bismuth are qualitatively similar to those obtained previously. The bandwidth for five valence electrons per atom is 1.18 Ry, which corresponds to a bandwidth effective mass of

0.63 electron mass, compared with the first order perturbation estimate of 0.87 used in the former method. Possible implications of this difference are discussed.

The effect of the structure in the density of states on the frequency-dependent conductivity has been studied by an approximate evaluation of the Kubo-Greenwood formula using parametrized Green functions which have been constructed to satisfy the sum rule automatically. We find insignificant departure from the Drude formula unless the density of states has structure much more drastic than that obtained for mercury. The zero frequency limit, however, is roughly proportional to the square of the density of states.

To Lilian and My Parents

TABLE OF CONTENTS

	Page
LIST OF TABLES.....	viii
LIST OF FIGURES.....	ix
ACKNOWLEDGEMENTS.....	xii
INTRODUCTION.....	1
PART I ELECTRONIC STRUCTURES OF LIQUID METALS	
1. BACKGROUND MATERIAL.....	8
1.1 Survey of Previous Quantitative Calculations...	8
1.2 The Green Function Formalism.....	11
1.3 Calculations with a Model.....	14
1.4 Ballentine's Work and its Relations to the Present Study.....	17
2. EFFECTIVE MASS APPROXIMATION.....	24
2.1 Modification of the Green Function Method to include an Effective Mass.....	24
2.2 Calculation of the Density of States.....	32
2.3 Application to Bismuth.....	34
2.4 Application to Indium.....	53
2.5 Application to Mercury.....	61
2.6 Comparison of the Three Metals.....	73
3. INTEGRATED DENSITY OF STATES.....	77
3.1 The Problem of an Energy Dependent Potential...	77
3.2 A Perturbation Expansion.....	80
3.3 Application to Bismuth.....	89
3.4 Discussion.....	98

PART II	FREQUENCY-DEPENDENT CONDUCTIVITY	
4.	FORMAL THEORY.....	102
4.1	Introduction.....	102
4.2	Reduction of the Kubo-Greenwood Formula.....	104
4.3	Diagrammatic Analysis.....	109
4.4	Approximations.....	114
5.	NUMERICAL CALCULATION WITH MODELS.....	117
5.1	The Lorentzian Model.....	117
5.2	A Parametrized Model.....	119
5.3	Zero-Frequency Conductivity and Density of States.....	132
6.	COMMENTS AND CONCLUSIONS.....	138
APPENDIX I	THE ENERGY SUM RULE FOR THE GREEN FUNCTION	142
APPENDIX II	MODEL POTENTIAL PARAMETERS.....	147
APPENDIX III	DIFFERENTIATION OF A FUNCTION OF AN OPERATOR WITH RESPECT TO A PARAMETER.....	148
REFERENCES.....		154

LIST OF TABLES

Table	Page
I Effective Masses.....	32
II Some Important Results.....	74
III Dependence of Zero-Frequency Conductivity and Relaxation Time on Density of States.....	134
IV Model Potential Parameters.....	147

LIST OF FIGURES

Figure		Page
1	Density of states $n(E)$ corresponding to the model Green function (1.9).....	16
2	(a) A typical reducible diagram in the expansion of $G(k, E)$. (b)-(d) Some irreducible diagrams in the expansion of $\Sigma(k, E)$	20
3	E_k^0 of Equation (2.6) vs. k^2	31
4	Structure factor for liquid bismuth.....	35
5	Model potential form factor for bismuth.....	40
6	Real part of self-energy for bismuth.....	47
7	Imaginary part of self-energy for bismuth.....	48
8	Spectral function $\rho(k, E)$ for bismuth.....	49
9	Density of states per unit volume (a.u.) per unit energy range, $n(E)$ for bismuth.....	51
10	Momentum distribution for occupied states of bismuth.....	52
11	Structure factor for liquid indium.....	54
12	Model potential form factor for indium.....	55
13	Real part of self-energy for indium.....	56
14	Imaginary part of self-energy for indium.....	57
15	Spectral function $\rho(k, E)$ for indium.....	58
16	Density of states per unit volume (a.u.) per unit energy range, $n(E)$ for indium.....	59
17	Momentum distribution for occupied states of indium.....	60
18	Structure factor for liquid mercury.....	64
19	Model potential form factor for mercury.....	67
20	Real part of self-energy for mercury.....	68
21	Imaginary part of self-energy for mercury.....	69

22	Spectral function $\rho(k, E)$ for mercury	70
23	Density of states per unit volume (a.u.) per unit energy range, $n(E)$ for mercury.....	71
24	Momentum distribution for occupied states of mercury.....	72
25	Diagrammatic representation of $-\langle\langle k \ln(1 - G W) k \rangle\rangle_{ave}$	82
26	Diagrams summed by the integral Eq. (3.18).....	90
27	$M(\lambda, E)/\lambda$ (per unit volume) versus λ for several values of E	93
28	Number $N(E)$ of electronic states per atom below energy E , calculated for liquid bismuth at 300°C	95
29	Similar to Figure 28 but $N^{2/3}$ plotted.....	97
30	Schematic frequency variation of the optical conductivity of mercury as measured by ellipsometry.....	103
31	Density of states $n(E)$ using parametrized model Green functions, a varied.....	120
32	Frequency dependence of normalized optical conductivity corresponding to $n(E)$ of Fig. 31..	121
33	Density of states $n(E)$ using parametrized model Green functions, b varied.....	122
34	Frequency dependence of normalized optical conductivity corresponding to $n(E)$ of Fig. 33..	123
35	Density of states $n(E)$ using parametrized model Green functions, c varied.....	124
36	Frequency dependence of normalized optical conductivity corresponding to $n(E)$ of Fig. 35.....	125
37	Density of states $n(E)$ using parametrized model Green functions, g varied.....	126
38	Frequency dependence of normalized optical conductivity corresponding to $n(E)$ of Fig. 37.....	127
39	Density of states $n(E)$ using parametrized model Green functions, g varied.....	128

40 Frequency dependence of normalized optical conductivity corresponding to $n(E)$ of Fig. 39..... 129

ACKNOWLEDGEMENTS

I wish to express my sincere gratitude to my supervisor, Dr. L.E. Ballentine, for suggesting this problem and for continual guidance through all stages of the work. I have benefited greatly from discussions or correspondence with many people, in particular Drs. E.D. Crozier, J.C. Jones, P. Lloyd, N.H. March, and J.M. Ziman. Thanks are also due to Dr. O.P. Gupta for lending me a computer program for calculating non-local screening and Mrs. Enid Britt for typing this thesis.

Finally, the financial support of the National Research Council of Canada and Canron Limited in the form of graduate scholarships is gratefully acknowledged.

INTRODUCTION

Theoretical and experimental studies of liquid metals can be conveniently classified into four categories: (i) liquid structure, (ii) electronic states, (iii) electronic transport properties, and (iv) mass transport properties. The work to be reported in this thesis is concerned with two of these aspects, namely, the electronic density of states per unit energy range and its influence on the frequency-dependent conductivity.

A comprehensive review of the entire subject of liquid metals will not be attempted here. Excellent reviews have been given by Cusack (1963, 1967), Wilson (1965), March (1968), and the various contributors to the Proceedings of the Brookhaven Conference (Adams et al. 1967). We shall only spell out the motivations and fundamental difficulties pertinent to the present investigation.

Although experimental work on liquid metals has been going on for a long time, significant progress in theory has been made only in the last decade or so with the development of Green function techniques (Edwards 1958, 1962) and pseudopotentials (see Ziman 1964 and Harrison 1966 for reviews). The main difficulty is that when a metal melts, its translational periodicity is lost so that Bloch's theorem no longer holds, an energy-momentum dispersion relation cannot be uniquely defined and the familiar methods of calculating band structures in solids cannot be used. A major revision in the concept of

electronic structures is necessary. Rather than obtaining a relation between energy and momentum we describe the electronic structure of the system by means of a density of states function, $n(E)$ which always has an exact meaning irrespective of the degree of disorder of the system.

One reason for studying $n(E)$ is that Ziman's nearly-free-electron theory has been remarkably successful in explaining the electronic transport properties of liquid metals (Ziman 1961, Bradley et al. 1962, Sundström 1965) and it is desirable to see whether the underlying assumption of the theory is justified i.e. whether $n(E)$ is approximately proportional to $E^{1/2}$. Knowledge of $n(E)$ by itself is also important because there are a number of experiments yielding information related to this quantity. Some of these are: (i) d.c. transport properties, (ii) optical conductivity, (iii) Pauli-spin susceptibility, (iv) Knight shift, (v) soft X-ray emission, (vi) photoelectric emission, (vii) positron annihilation, and (viii) Compton scattering of X-rays. Unfortunately most of the properties mentioned depend not only on $n(E)$ but also on transition-probabilities, among other things, so that it is not possible to extract $n(E)$ directly from the experiments. We shall comment further on this point in the final chapter.

Considerable effort has been devoted recently to study the electronic structure of disordered systems. As pointed out by Ziman (1968) there are two essentially distinct aspects of

disorder: topological or structural disorder -- the loss of long range order in the arrangement of the atomic sites, and cellular disorder -- the lack of strict periodicity from cell to cell in an otherwise almost periodic lattice. Examples of systems in which structural disorder is present are liquid metals, amorphous semi-conductors and glasses. In these systems one can no longer delineate the lines and planes in which the atoms lie. On the other hand in systems with cellular disorder such as hot solids and substitutional alloys the lattice planes, though deformed or containing different species of atoms, may still be recognized over large regions of the material. The latter type of disorder is better understood than the former because the presence of a periodic lattice simplifies the problem considerably. At present many sophisticated techniques for obtaining the electronic structure in systems with cellular disorder have been developed and applied successfully to the problems of alloys (see Ziman 1969a for a review, also Cohen* 1971). The same techniques are not directly applicable to topologically disordered systems. Recently Dy and Wu (1971) have been able to formally generalize them to topologically disordered systems. The practicability of their theory, however, has still to be tested by numerical calculations.

Results obtained using one-dimensional models (Mott 1967, Halperin 1968 and references given there), however rigorous they may be, cannot be generalized to real three-dimensional systems because all disordered linear chains are topologically

*Freed and Cohen (1971)

equivalent to a periodic linear lattice, and therefore no structural disorder can be built into the model.

The brief discussion above should suffice to indicate the great complexity to be expected in a theoretical study of the electronic structure of liquid metals. Most of the previous work has been concerned with developing formal methods. Few attempts have been made to carry out quantitative calculations on real liquid metals (see Section 1.1 below). The present work is intended primarily to be a contribution to this latter aspect. In the course of so doing we also hope to be able to shed some light on the general theory.

In a liquid metal the ions do not have a fixed configuration, so one has to calculate ensemble average quantities. The concept of a wave function is not a convenient one. Green functions (or equivalently spectral functions, density matrices, and cumulants), on the other hand, allow the averaging procedure to be performed in a natural way. The theory of Edwards (1962) which provides the basis for the present study is formulated in terms of Green functions.

This thesis consists of two parts. Part I which forms the greater part of the thesis deals with the electronic structure of liquid metals. Two different approaches are used and the densities of states of several real liquid metals are worked out. When the electronic structure of a liquid metal deviates significantly from free-electron behaviour, the

question arises as to whether such deviations are strongly reflected in the electronic transport properties. In Part II the effects of $n(E)$ on the frequency-dependent conductivity are explored by an approximate evaluation of the Kubo-Greenwood formula (Kubo 1957, Greenwood 1958) using parametrized models for the ensemble average Green function.

Throughout this work it is assumed that the conduction electrons are independent of each other, their interactions with the ions being represented by a weak effective potential and the motions of the ions can be neglected. The validity and limitations of these assumptions will be discussed at appropriate places.

PART I

ELECTRONIC STRUCTURES OF LIQUID METALS

The number of calculations of the electronic structure of liquid metals is very small in comparison with the number of such calculations for solid metals. This fact reflects both the greater novelty and the greater difficulty of the problem for liquids. For example, it is in principle not possible to classify electron states by a wavevector k or to obtain a unique energy versus k relation.

In Chapter 1, after a brief survey of previous work and an account of the Green function formalism, we demonstrate the inadequacy of the naive method of calculating the density of states, $n(E)$, of a liquid metal by differentiating the energy-momentum dispersion relation which has been obtained by means of ordinary perturbation theory. Next we discuss the simplifying approximations in Ballentine's (1966) calculations. The removal of these approximations is the initial purpose of the present investigation.

In Chapter 2 we calculate $n(E)$ numerically for liquid Bi, In and Hg using nonlocal model potentials and an effective mass approximation. Bismuth serves as the testing ground of our calculation. Among the metals considered by Ballentine it is the only one that shows substantial departures from free-electron behaviour. By evaluating the density of states for Bi to successively higher degrees of sophistication we hope to

reveal the extraneous structure introduced by each approximation and finally single out the inherent characteristic of the metal. Indium is chosen primarily for experimental reasons. The photoemission data of both Koyama et al. (1967) and Enderby (1969, unpublished) have indicated pronounced structures. Mercury being the only metal that exists in the liquid state at room temperatures is a natural candidate. The electronic transport properties of pure Hg and its alloys are strikingly different from those of other liquid metals (see Mott 1966 for a review). This so-called "mercury anomaly" has been interpreted by Mott (1966) in terms of a conjectured dip in the density of states near the Fermi energy. Our calculation should tell us whether this conjecture is well founded.

The problem introduced by the use of an energy dependent electron-ion model potential is treated in detail in Chapter 3. A method which remains valid for such a potential is presented for calculating the total number of electronic states below an energy E . As an example, the energy distribution of the electronic states in Bi is worked out and the results are compared to those obtained in Chapter 2.

CHAPTER 1

BACKGROUND MATERIAL

§1.1 Survey of Previous Quantitative Calculations

Edwards (1962) showed how the density of electronic states per unit energy could be obtained from a perturbation expansion of the single particle Green function averaged over the ensemble of possible atomic arrangements appropriate to the liquid state. The first quantitative application of Edwards' formalism was by Ballentine (1966), who found the density of states of liquid Al and Zn to be nearly free-electron-like, but predicted that of liquid Bi to differ significantly from the free-electron parabola. Ballentine represented the electron-ion interaction by a local pseudopotential.

If the imaginary part of the self-energy is very small one can, at least approximately, define a dispersion relation relating electron energy E to a wavevector k . By such a method Watabe and Tanaka (1964) predicted a very large peak near the Fermi energy in the density of states of liquid Zn. However, their result was shown to be entirely spurious (Ballentine 1966), due in part to their use of a very crude approximation (an exponentially screened coulomb potential) to the electron-ion pseudopotential. Similar calculations have since been carried out by several groups. Schneider and Stoll (1967) have obtained the electronic structure of Na, K and Pb using an empirical local model potential that has been fitted to experimental phonon dispersion curves. Their conclusion is

that as the solid melts there is an insignificant change in the density of states on the Fermi surface. In addition, a blurred image of the first Brillouin zone can be seen in the liquid. Shaw and Smith (1969) have performed a similar calculation for Li, Cd, and In, using a nonlocal energy-dependent model potential. Their results resemble the densities of states of the corresponding solids but with all van Hove singularities smoothed out. Only for Li is their result much different from the free-electron curve. A similar calculation for nine metals has been reported by Srivastava and Sharma (1969), however, they give only the density of states at the Fermi level and not the entire curve. Very recently Jena and Halder (1971) have repeated the work of Shaw and Smith on Cd using a different nonlocal pseudopotential and found a much larger difference between the densities of states of the liquid and the solid, apparently in agreement with the Knight shift data (Seymour and Styles 1964, Borsa and Barnes 1966, Sharma and Williams (1967)). The limitations of this approach are the use of second order perturbation theory and the assumption of an $E(k)$ relation for a liquid. Both become suspect as the electronic structure becomes non-free-electron-like, which is of course the most interesting case. Although one can artificially define an $E(k)$ for a liquid such that it yields the correct density of states, that same $E(k)$ cannot be used for other applications such as the Boltzmann equation (Lloyd 1968). Furthermore the neglect of the imaginary part of the self-energy may not be justified as we will illustrate with a numerical example in Section 1.3.

The work of Ballentine (1966) and the present thesis are not strictly perturbation methods since infinite classes of terms are summed by means of integral equations. Nevertheless they are weak binding approximations.

Cyrot-Lackmann (1966) has developed a tight binding approximation for the moments of density of states function. It is applicable only to strictly bound bands, since moments do not exist for free-electron-like bands. Lloyd (1967) has developed an interesting theory which uses the phase shifts of (assumed) non-overlapping ions rather than a pseudopotential. No realistic calculations have been done with this method, but he has shown by means of a simple model that his theory can describe the formation of a gap between a "free" and a "bound" band as the potential strength increases. Rousseau, Stoddard and March (1970) have developed a form of strong coupling theory based on the density matrix, rather than the Green function, and have applied their method to Be. They find the density of states to be qualitatively similar in the liquid and solid phases, and quite different from what it would be for a random distribution of atoms.

This brief review is believed to cover all quantitative calculations of the electronic density of states for liquid metals which have been published (excluding one dimensional models and disordered lattices).

§1.2 The Green Function Formalism

In Edwards' (1962) Green function formalism of the liquid metal problem an independent-electron model was used. The effects of electron-electron interaction can be included, at least formally (Langer 1961), but in the present state of knowledge such complication is not expected to be very rewarding and, in an actual calculation, the interaction is accounted for only in the screening of the electron-ion potential by an electron gas. The ionic motions may also be neglected because the electronic motions are much more rapid. This is just the analog of the Born-Oppenheimer approximation in solid state theory (see Ziman 1965 section 6.10). Thus we consider the motion of a single electron under the influence of the potential V due to a disordered system of ions in a "frozen" liquid.

The Green operator is defined as

$$\begin{aligned} G(E) &= (E - H)^{-1} \\ &= \sum_n \frac{|\psi_n\rangle \langle \psi_n|}{E - E_n}, \end{aligned} \quad (1.1)$$

where $H = H_0 + V$ is the single electron hamiltonian, and $|\psi_n\rangle$ and E_n are its eigenvectors and eigenvalues. We refer to its diagonal matrix element in the momentum representation as the Green function,

$$G(\underline{k}, E) \equiv \langle \underline{k} | G(E) | \underline{k} \rangle .$$

In terms of $G(E)$ we can define the spectral operator

$$\begin{aligned} \rho(E) &= \lim_{\eta \rightarrow 0^+} \left(\frac{-1}{2\pi i} \right) \{ G(E+i\eta) - G(E-i\eta) \} \\ &= \sum_n |\psi_n\rangle \langle \psi_n| \delta(E-E_n) . \end{aligned} \quad (1.2)$$

Its diagonal matrix element in the momentum representation, the spectral function

$$\begin{aligned} \rho(\underline{k}, E) &\equiv \langle \underline{k} | \rho(E) | \underline{k} \rangle \\ &= \lim_{\eta \rightarrow 0^+} \left(\frac{-1}{\pi} \right) \text{Im} \{ \langle \underline{k} | G(E+i\eta) | \underline{k} \rangle \} \\ &= \sum_n | \langle \underline{k} | \psi_n \rangle |^2 \delta(E-E_n) , \end{aligned} \quad (1.3)$$

tells us the momentum distribution of electrons with energy E . For a perfect crystal the $|\psi_n\rangle$'s are eigenstates of crystal momentum and $\rho(\underline{k}, E)$ is just a sum of delta functions. From the completeness of the set of states $\{\psi_n\}$ we have the sum rule (Edwards 1965)

$$\int_{-\infty}^{\infty} \rho(\underline{k}, E) dE = 1 . \quad (1.4)$$

The trace of the spectral operator gives us the density of states per unit energy per spin state,

$$\begin{aligned} \text{tr } \rho(E) &= \sum_{\underline{k}} \rho(\underline{k}, E) \\ &= \sum_n \delta(E-E_n) \\ &= n(E) . \end{aligned} \quad (1.5)$$

Since the trace is an invariant of the operator, (1.4) and (1.5) hold for any representation. The momentum representation has been chosen solely for convenience. In particular, it does not imply that we are using the plane wave states $|k\rangle$ as the zero-order states for electrons in a liquid metal.

To obtain the ensemble average Green function, we consider the formal expansion of the Green operator

$$G(E) = (E - H_0 - V)^{-1} \\ = G_0 + G_0 V G_0 + G_0 V G_0 V G_0 + \dots \quad (1.6)$$

where $G_0(E) = (E - H_0)^{-1} = (E - k^2)^{-1}$ in "semi-atomic" units ($\hbar = 2m = \frac{1}{2}e^2 = 1$). Now introduce the self-energy,

$$\Sigma(\underline{k}, E) = \langle \underline{k} | V | \underline{k} \rangle + \sum_{\underline{k}' \neq \underline{k}} \langle \underline{k} | V | \underline{k}' \rangle G_0(\underline{k}', E) \langle \underline{k}' | V | \underline{k} \rangle \\ + \sum_{\substack{\underline{k}' \neq \underline{k} \\ \underline{k}'' \neq \underline{k}}} \langle \underline{k} | V | \underline{k}' \rangle G_0(\underline{k}', E) \langle \underline{k}' | V | \underline{k}'' \rangle G_0(\underline{k}'', E) \langle \underline{k}'' | V | \underline{k} \rangle + \dots \quad (1.7)$$

If we expand $(E - k^2 - \Sigma(\underline{k}, E))^{-1}$ in a power series in $\Sigma(\underline{k}, E)$ and substitute from (1.7) we get back the diagonal element of (1.6). Hence

$$G(\underline{k}, E) = \frac{1}{E - k^2 - \Sigma(\underline{k}, E)} \quad (1.8)$$

This result is none other than the solution of the well known Dyson equation (see e.g. Ziman 1969b section 3.10)

$$G(\underline{k}, E) = G_0(\underline{k}, E) + G_0(\underline{k}, E) \Sigma(\underline{k}, E) G(\underline{k}, E)$$

If we further assume the validity of what Edwards (1962) called the "geometric approximation" in which the average of a product

like $G_0(k, E) \Sigma(k, E) G_0(k, E) \Sigma(k, E) G_0(k, E)$ is replaced by the product of the average of the separate terms, then we obtain the ensemble average Green function simply as

$$\langle G(k, E) \rangle_{ave} = \frac{1}{E - k^2 - \langle \Sigma(k, E) \rangle_{ave}}$$

Ballentine (1965) has argued that this replacement is actually exact in the limit of an infinite system with a finite range of order. A proof of this assertion has been provided by Taylor (1966) in a more general context. The problem of finding the Green function and hence the spectral function and the density of states is thus reduced to the calculation of $\langle \Sigma(k, E) \rangle_{ave}$. In what follows we shall simply denote the ensemble average quantities by $G(k, E)$ and $\Sigma(k, E)$ when there is no danger of ambiguity.

§1.3 Calculations with a Model

At the beginning of this chapter we raised some objections on general grounds against the naive method of calculating the density of states of liquid metals by first obtaining a dispersion relation using ordinary perturbation theory. Here we attack the same problem on different grounds. Suppose we set aside the question of existence of a dispersion relation and consider a fictitious liquid metal represented by the parametrized model,

$$G(k, E) = \{E - \epsilon(k) + i b E^{1/2}\}^{-1}, \quad (1.9)$$

where

$$\varepsilon(k) = k^2 + c \left\{ [1 + e^{(g-k)/a}]^{-1} - [1 + e^{g/a}]^{-1} \right\} \quad (1.10)$$

is a model dispersion relation. The parameter a controls the sharpness of the dip in the density of states, b controls the width of the spectral function and indirectly the depth of the dip, c controls the depth of the dip, and g controls the position of the dip. The last term in (1.10) ensures that $\varepsilon(0) = 0$. The Green function (1.9) is of a form that automatically satisfies the sum rule (1.4) (see Appendix I). This point has also been confirmed by numerical integration.

In the naive method the density of states per unit volume per spin state is given by

$$n(\varepsilon) = \frac{1}{2\pi^2} k^2 \left[\frac{\partial \varepsilon(k)}{\partial k} \right]^{-1} . \quad (1.11)$$

The correct method is of course to calculate $n(\varepsilon)$ from the trace of the spectral function. The question we ask is whether these two different approaches yield the same or nearly the same results. Figure 1 shows the density of states calculated for the model with parameters $a = 0.01$; $b = 0.05, 0.1, 0.2, 0.5$; $c = 0.1$; $g = 0.975$ (in units for which $\hbar = 2m = k_F = 1$). As b gets smaller and smaller, the correct $n(\varepsilon)$ does seem to approach the dashed curve obtained by the naive method, but even for $b = 0.05$, the naive method gives a dip 40 percent deeper than the true one. Similar results have also been obtained with various other values of the parameters. $b = 0.05$

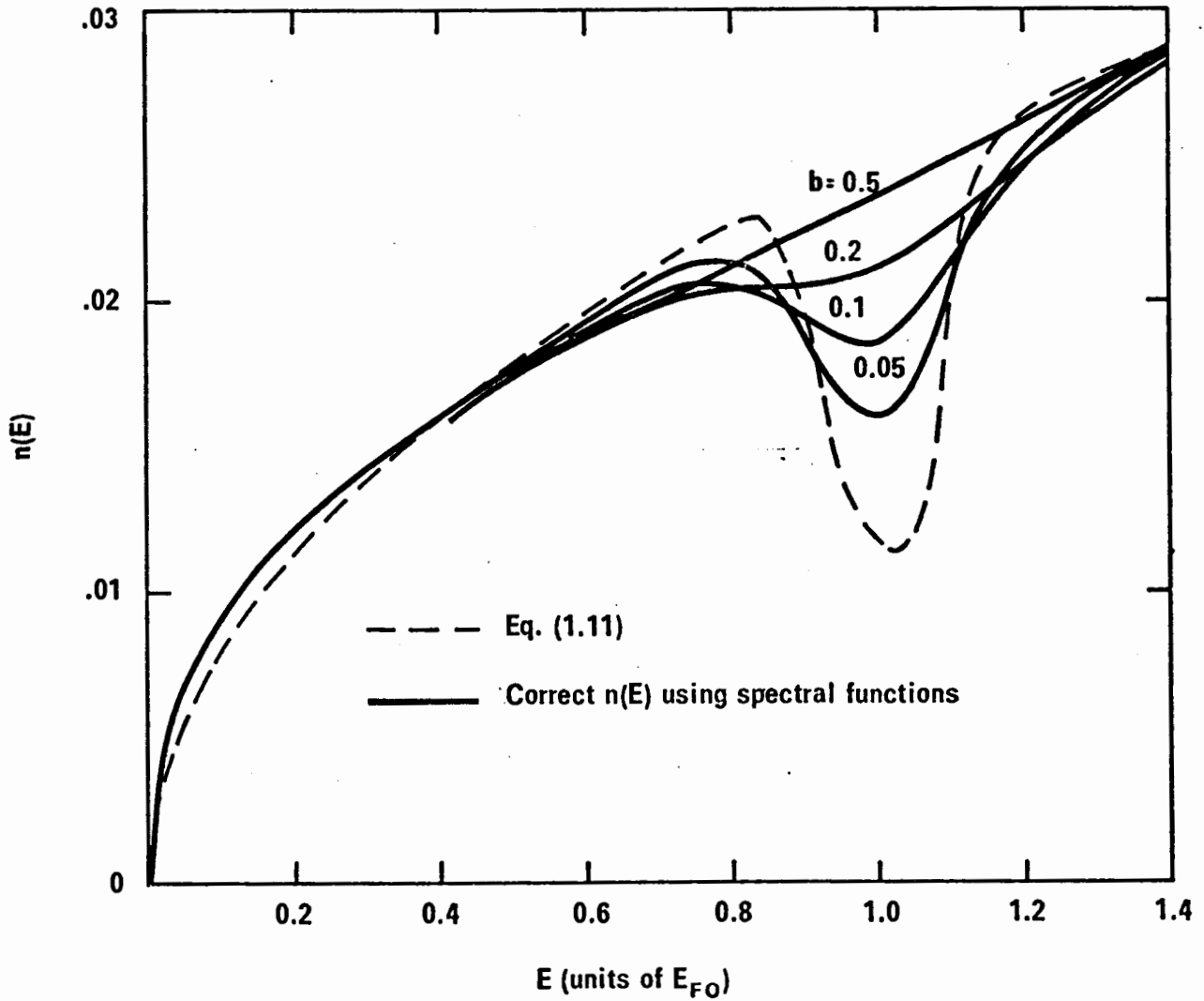


Figure 1 Density of states $n(E)$ corresponding to the model Green function (1.9).

means that at the free-electron Fermi energy E_{F_0} ($E_{F_0} = 1$ in the units we are using) the imaginary part of the self-energy $\text{Im}\Sigma$ equals 5 percent of the conduction bandwidth. Anticipating the results of our calculation on liquid Hg in the next chapter, we find that for $E \approx E_F$, $\text{Im}\Sigma(k, E)$ has a maximum value of about 7 percent of the conduction bandwidth. This implies that a calculation of the density of states of liquid Hg using the naive method would be in error by more than 40 percent in the interesting region.

Our numerical investigation in this section should dispel any doubt that the Green function method is to be preferred over the naive method in spite of the apparent advantage of simplicity of the latter, unless the metal in question is very free-electron-like--and we have no reliable a priori criterion to tell us when it is so.

§1.4 Ballentine's Work and its Relation to the Present Study

In Edwards' weak binding formalism the ensemble average Green function is obtained from the self-energy, which in turn is calculated by a partial summation of a perturbation series in the scattering potential V . The validity of such a scheme relies on the weakness of the potential. The true potentials due to the ions in a real liquid metal are certainly not weak. In order to apply Edwards' formalism to perform quantitative calculations, Ballentine (1966) replaced the deep ionic

potential by a weak pseudopotential. An extensive discussion of the theory of pseudopotentials is beyond the scope of this thesis and we refer to Harrison's book (1966) for details.

The fundamental idea behind the pseudopotential concept as first introduced into solid state theory by Phillips and Kleinman (1959) is quite simple. The conduction electron wave functions must be orthogonal to the core wave functions and therefore must oscillate rapidly inside the core regions. The large positive kinetic energy associated with these oscillations almost completely cancels the deep negative potential within the cores, resulting in a weak net effective potential. Thus Austin, Heine and Sham (1962) (hereafter referred to as AHS) have shown that the Schrödinger equation for an electron in a metal

$$H\psi \equiv (T+V)\psi = E\psi \quad (1.12)$$

can be transformed into

$$(T+W)\phi = E\phi \quad (1.13)$$

so that the true potential V is replaced by a pseudopotential W which is much weaker in the core region, the true wave function ψ is replaced by the pseudowave function ϕ which is smooth inside the core, and the valence energy eigenvalue E is preserved. Depending on its form W is either known as a pseudopotential (see AHS for the general form) or a model potential (Heine and Abarenkov 1964, Abarenkov and Heine 1965) (hereafter referred to as HA).

Within the small core approximation the total screened pseudopotential W can be written as a sum of spherically symmetric terms w centred on each of the N ions,

$$W(\underline{r}) = \sum_{\alpha} w(\underline{r} - \underline{R}_{\alpha})$$

and the plane wave matrix element can be factored as

$$\langle \underline{k} | W | \underline{k}' \rangle = \langle \underline{k} | w | \underline{k}' \rangle \sum_{\alpha} \exp [i(\underline{k}' - \underline{k}) \cdot \underline{R}_{\alpha}] \quad , \quad (1.14)$$

the first term depending only on the properties of a single ion and the second term being a function of the positions \underline{R}_{α} of all the ions. The n^{th} -order term in the diagonal element of the expansion (1.6) of $G(E)$ can be written (in "semi-atomic" units) as

$$\begin{aligned} & G_0(\underline{k}, E) \sum_{\substack{\underline{k}', \dots, \underline{k}^{(n-1)}}} \langle \underline{k}' | w | \underline{k} \rangle G_0(\underline{k}', E) \langle \underline{k}' | w | \underline{k}'' \rangle \dots \\ & \dots G_0(\underline{k}^{(n-1)}, E) \langle \underline{k}^{(n-1)} | w | \underline{k} \rangle G_0(\underline{k}, E) C_n(\underline{k} - \underline{k}', \underline{k}' - \underline{k}'', \dots, \underline{k} - \underline{k}^{(n-1)}) \end{aligned} \quad (1.15)$$

where

$$C_n(\underline{p}_1, \underline{p}_2, \dots, \underline{p}_n) = \sum_{\alpha_1, \dots, \alpha_n} \exp [i(\underline{p}_1 \cdot \underline{R}_{\alpha_1} + \underline{p}_2 \cdot \underline{R}_{\alpha_2} + \dots + \underline{p}_n \cdot \underline{R}_{\alpha_n})] \quad . \quad (1.16)$$

The ensemble average of $G(\underline{k}, E)$ is obtained by replacing C_n with its average,

$$\bar{C}_n(\underline{p}_1, \underline{p}_2, \dots, \underline{p}_n) \equiv \langle C_n \rangle_{\text{ave}} \quad ,$$

which is related to the n -particle correlation function. It is convenient to introduce diagrams to represent the various terms. Some examples are shown in Figure 2. A solid line represents a

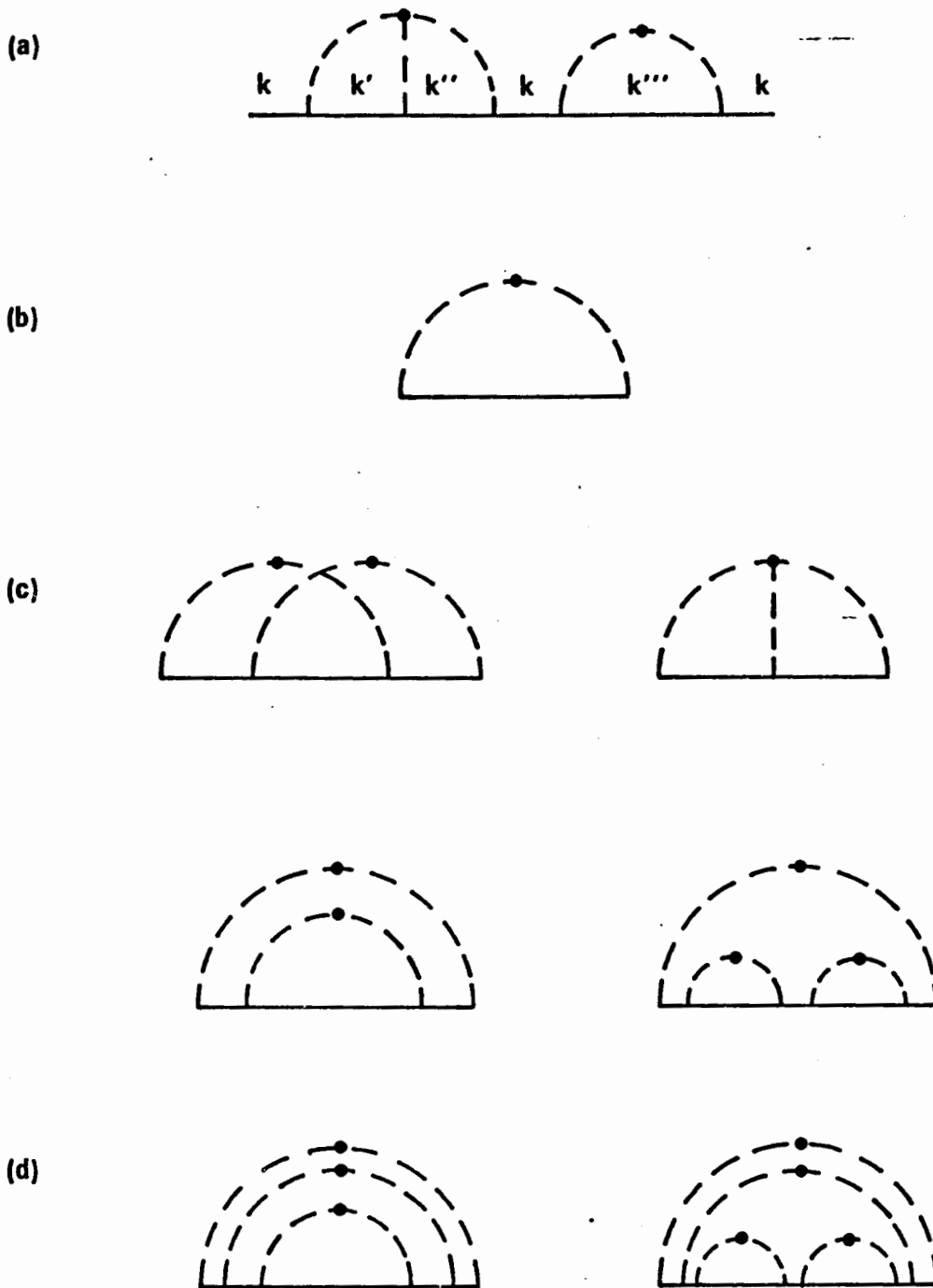


Figure 2 (a) A typical reducible diagram in the expansion of $G(k, E)$.
(b)-(d) Some irreducible diagrams in the expansion of $\Sigma(k, E)$.

propagator $G_0(k, E) = (E - k^2)^{-1}$, an intersection of two solid lines with a dashed line (a vertex) represents a factor $\langle k|w|k' \rangle$, and a node connecting n dashed lines represents a factor \bar{C}_n . The self-energy $\Sigma(k, E)$ defined by (1.7) consists of the sum of all irreducible diagrams i.e. those that cannot be separated into two disconnected parts by cutting a propagator line, such as those in Figure 2 (b), (c), (d). $G(k, E)$ is the sum of all reducible diagrams, like the one in Figure 2 (a).

If the pseudopotential is local, meaning that its matrix element $\langle k|w|k' \rangle$ depends only on the momentum transfer $q = k' - k$ but not on k , then the first-order term in $\Sigma(k, E)$ is just the average potential energy and may be chosen to be zero, and the simplest nontrivial contribution is the second-order term Σ_2 represented by the diagram in Figure 2(b). Ballentine has found that this "one diagram approximation" leads to a certain inconsistency which may be removed by "renormalizing" the diagram i.e. replacing the zero-order Green function by the full Green function. $\Sigma(k, E)$ is now obtained by a self-consistent solution of the integral equation,

$$\Sigma(k, E) = \frac{\pi}{(2\pi)^3} \int \frac{d^3k' |u(q)|^2(q)}{E - (k')^2 - \Sigma(k', E)} \quad , \quad (1.17)$$

which sums the infinite set of diagrams illustrated in Figure 2(b) and (d). Here

$$u(q) = L^3 \langle k|w|k' \rangle = \int \exp(iq \cdot r) w(r) d^3r \quad (1.18)$$

is the Fourier transform of the potential, L^3 is the normaliza-

tion volume, and $n = N/L^3$ is the atomic density. The structure factor $a(q)$ is equal to the continuous part of $N^{-1}\bar{C}_2$, and measured in diffraction experiments.

Ziman (1969c) has argued, on the basis of a calculation for polycrystalline material, that Σ_2 cannot give the correct features of the structure. To obtain a reasonable result a term that he calls Σ_4 has to be included. An inspection of his expression for Σ_4 reveals that it is just the term represented by the first diagram in Figure 2(d), which is certainly included by (1.17). On the contrary, the naive method which is equivalent to an approximate evaluation of Σ_2 is indeed invalidated by Ziman's argument.

The HA model potential which Ballentine adopted in his calculations is nonlocal and dependent on an energy parameter. Ballentine used an approximate local, energy independent form derived from its Fermi energy shell matrix elements. This, together with the assumption that $\Sigma(k, E)$ in the denominator of (1.17) could be replaced by a constant, enabled him to perform all the angular integrations analytically and greatly simplify the solution of the integral equation. The work of Shaw and Smith (1969) mentioned before indicates that retaining the nonlocal and energy dependent nature of the model potential will tend to smooth out some of the structure predicted from a local pseudopotential. This is not surprising, for Ballentine found that the relative position of the zero of the pseudopotential (in momentum space) and the peak of the structure factor is an

important parameter, and for a nonlocal pseudopotential the zero is effectively varying with energy or momentum. To include a nonlocal pseudopotential and to solve the integral equation (1.17) without further approximation, as we shall do in our calculations in the next chapter, we need to take care of the first order term, perform one of the angular integrations numerically and solve an integral equation in the two variables k and E . Such complications are entirely computational in nature. The energy dependence of the model potential, however, causes difficulties in principle for the Green function method. The solution of these difficulties is the subject of Chapter 3.

CHAPTER 2

EFFECTIVE MASS APPROXIMATION

§2.1 Modification of the Green Function Method to include an Effective Mass

The HA model potential, like many other pseudopotentials that are useful in calculating properties of metals, is non-local and energy dependent. Weaire (1967) has shown that some of the largest effects of the k and E dependence can be absorbed into an effective mass. In this chapter we combine a similar effective mass with the Green function method to obtain the density of states of three liquid metals.

Consider the hamiltonian $H = \frac{p^2}{2m} + W(E)$ (units $\hbar = 1$), where p is the momentum operator, m is the free-electron mass and $W(E)$ is the electron-ion model potential containing a parameter E such that the computed energy eigenvalue of the model wave equation is equal to the true energy eigenvalue only when E is itself set equal to the true eigenvalue to be solved for. It is customary in perturbation theory to break H up into two terms, $H = H_0 + H_1$ with the free-electron hamiltonian $H_0 = \frac{p^2}{2m}$ as the unperturbed part and $H_1 = W(E)$ as the perturbation. This is not the only possible decomposition. An equally legitimate alternative is the following:

$$H = H^0 + H^1, \quad (2.1)$$

where

$$H^0 = \frac{\mathbf{k}^2}{2m} + \sum_{\mathbf{k}} |\mathbf{k}\rangle \langle \mathbf{k}| W(E_{\mathbf{k}}^0) |\mathbf{k}\rangle \langle \mathbf{k}| \quad (2.2)$$

and

$$\begin{aligned} H^1 &= \sum_{\substack{\mathbf{k}, \mathbf{k}' \\ \mathbf{k} \neq \mathbf{k}'}} |\mathbf{k}\rangle \langle \mathbf{k}| W(E) |\mathbf{k}'\rangle \langle \mathbf{k}'| \\ &+ \sum_{\mathbf{k}} |\mathbf{k}\rangle \langle \mathbf{k}| \left\{ \langle \mathbf{k}| W(E) |\mathbf{k}\rangle - \langle \mathbf{k}| W(E_{\mathbf{k}}^0) |\mathbf{k}\rangle \right\} \\ &= H_{od}^1 + H_d^1 . \end{aligned} \quad (2.3)$$

Here we have expanded the potential operator $W(E)$ in terms of the complete set of plane wave states $\{|\mathbf{k}\rangle\}$. The symbols H_d^1 , H_{od}^1 denote the diagonal and off-diagonal parts of the perturbing term H^1 , respectively and $E_{\mathbf{k}}^0$ is the solution of the equation,

$$H^0 |\mathbf{k}\rangle = E_{\mathbf{k}}^0 |\mathbf{k}\rangle . \quad (2.4)$$

Assuming that $W(E)$ depends linearly on the energy we have

$$\begin{aligned} E_{\mathbf{k}}^0 &= \frac{\mathbf{k}^2}{2m} + \langle \mathbf{k}| W(E_{\mathbf{k}}^0) |\mathbf{k}\rangle \\ &= \frac{\mathbf{k}^2}{2m} + \langle \mathbf{k}| W(E_F) |\mathbf{k}\rangle + (E_{\mathbf{k}}^0 - E_F) \langle \mathbf{k}| \left(\frac{\partial W}{\partial E} \right)_{E_F} |\mathbf{k}\rangle , \end{aligned} \quad (2.5)$$

which can be solved self-consistently to yield

$$E_k^0 = \frac{\frac{k^2}{2m} + \langle k | W(E_F) | k \rangle - E_F \langle k | (\frac{\partial W}{\partial E})_{E_F} | k \rangle}{1 - \langle k | (\frac{\partial W}{\partial E})_{E_F} | k \rangle} \quad (2.6)$$

In (2.6) the Fermi energy E_F is given by

$$E_F = \frac{k_F^2}{2m} + \langle k_F | W(E_F) | k_F \rangle \quad (2.7)$$

As the parameters (and their derivatives) for the model potentials that we shall be using are tabulated at $E = E_F$, it is a straightforward matter to evaluate E_k^0 . We can define an effective mass m^* by the equation

$$E_k^0 = \frac{k^2}{2m^*} + E_0 \quad (2.8)$$

The constant E_0 can be taken as zero by a suitable choice of origin. It is convenient to define a dimensionless parameter

$$\mu = \frac{m^*}{m} \quad (2.9)$$

This is equivalent to the product $\mu_{\mu}^{E,k}$ of Weaire (1967) who differentiated the equation,

$$\frac{k^2}{2m^*} = \frac{k^2}{2m} + \langle k | W(E) | k \rangle \quad (2.10)$$

with respect to k and made use of the relation,

$$\frac{dW}{dk} = \frac{\partial W}{\partial k} + \frac{dE}{dk} \frac{\partial W}{\partial E} \quad (2.11)$$

to obtain

$$\mu = \mu^E \mu^k, \quad (2.12)$$

with

$$\mu^E = 1 - \frac{\partial W}{\partial E}, \quad (2.13)$$

and

$$\mu^k = \left(1 + \frac{m}{k} \frac{\partial W}{\partial k} \right)^{-1}. \quad (2.14)$$

Here we have abbreviated $\langle k | W(E) | k \rangle$ by W . The ensemble average Green function can now be written as

$$G(k, E) = \frac{1}{\{G^0(k, E)\}^{-1} - \Sigma(k, E)}, \quad (2.15)$$

where (in units $\hbar = 2m = \frac{1}{2}e^2 = 1$),

$$G^0(\underline{k}, E) \equiv \langle \underline{k} | (E - H^0)^{-1} | \underline{k} \rangle$$

$$= \frac{1}{E - \frac{k^2}{\mu}} \quad (2.16)$$

The self-energy is given by

$$\Sigma(\underline{k}, E) = \langle \underline{k} | H' | \underline{k} \rangle + \sum_{\underline{k}' \neq \underline{k}} \frac{|\langle \underline{k} | H' | \underline{k}' \rangle|^2}{E - \frac{(k')^2}{\mu} - \Sigma(\underline{k}', E)} \quad , \quad (2.17)$$

to the same order of approximation as Eq. (1.17). The first order term,

$$\langle \underline{k} | H' | \underline{k} \rangle = \langle \underline{k} | H'_d | \underline{k} \rangle$$

$$= \langle \underline{k} | W(E) | \underline{k} \rangle - \langle \underline{k} | W(E_k^0) | \underline{k} \rangle \quad ,$$

is zero if we approximate the parameter E here by E_k^0 . The second term in (2.17) contains only off-diagonal matrix elements,

$$\langle \underline{k} | H' | \underline{k}' \rangle = \langle \underline{k} | H'_{od} | \underline{k}' \rangle$$

$$= \langle \underline{k} | W(E) | \underline{k}' \rangle \quad .$$

If we neglect the energy dependence of the off-diagonal part, we have a hamiltonian of the form $H = H^0 + H^1$, where the perturbation H^1 is independent of energy. Hence the usual Green function method for calculating the density of states is applicable. The self-energy is now given by

$$\Sigma(\underline{k}, E) = \frac{n}{(2\pi)^3} \int \frac{|u(\underline{k}, \underline{k}', E_F)|^2 a(\underline{q})}{E - \frac{(\underline{k}')^2}{\mu} - \Sigma(\underline{k}', E)} d^3k', \quad (2.18)$$

where

$$\begin{aligned} u(\underline{k}, \underline{k}', E_F) &\equiv L^3 \langle \underline{k} | w(E_F) | \underline{k}' \rangle \\ &= \iint e^{-i\underline{k}\cdot\underline{r}} \langle \underline{r} | w(E_F) | \underline{r}' \rangle e^{i\underline{k}'\cdot\underline{r}'} d^3r d^3r'. \end{aligned} \quad (2.19)$$

Equation (2.18) has the same form as (1.17), but now the model potential is nonlocal and an effective mass has been introduced.

The neglect of the energy dependence of the off-diagonal elements can be justified to some extent by perturbation theory. These matrix elements occur only in the second order of the perturbation expansion for the energy eigenvalues, whereas the diagonal elements occur in the first order. Thus the primary effect of the energy dependence has been taken into account.

Perhaps we should mention that our formalism does not preclude the possibility that μ may depend on k . Whether or not we need to use a k -dependent effective mass in our actual calculations is a question that can be answered by computing μ numerically at different values of k . From Figure 3, in which we have plotted E_k^0 of Equation (2.6) against k^2 for liquid Bi, In, and Hg it is clear that the corresponding effective masses can be regarded as constant for all practical purposes. We have also listed in Table I the various effective masses defined above and related quantities for future use. The overall effective mass μ which we shall use in Equation (2.18) is the average value deduced from the slope of the best fitting straight line in Figure 3. Our effective masses for mercury are different from Weaire's (shown in parentheses) because we used Evans' (1970) model potential (see Figure 19, Section 2.5 below) which differs radically from the HA potential he used.

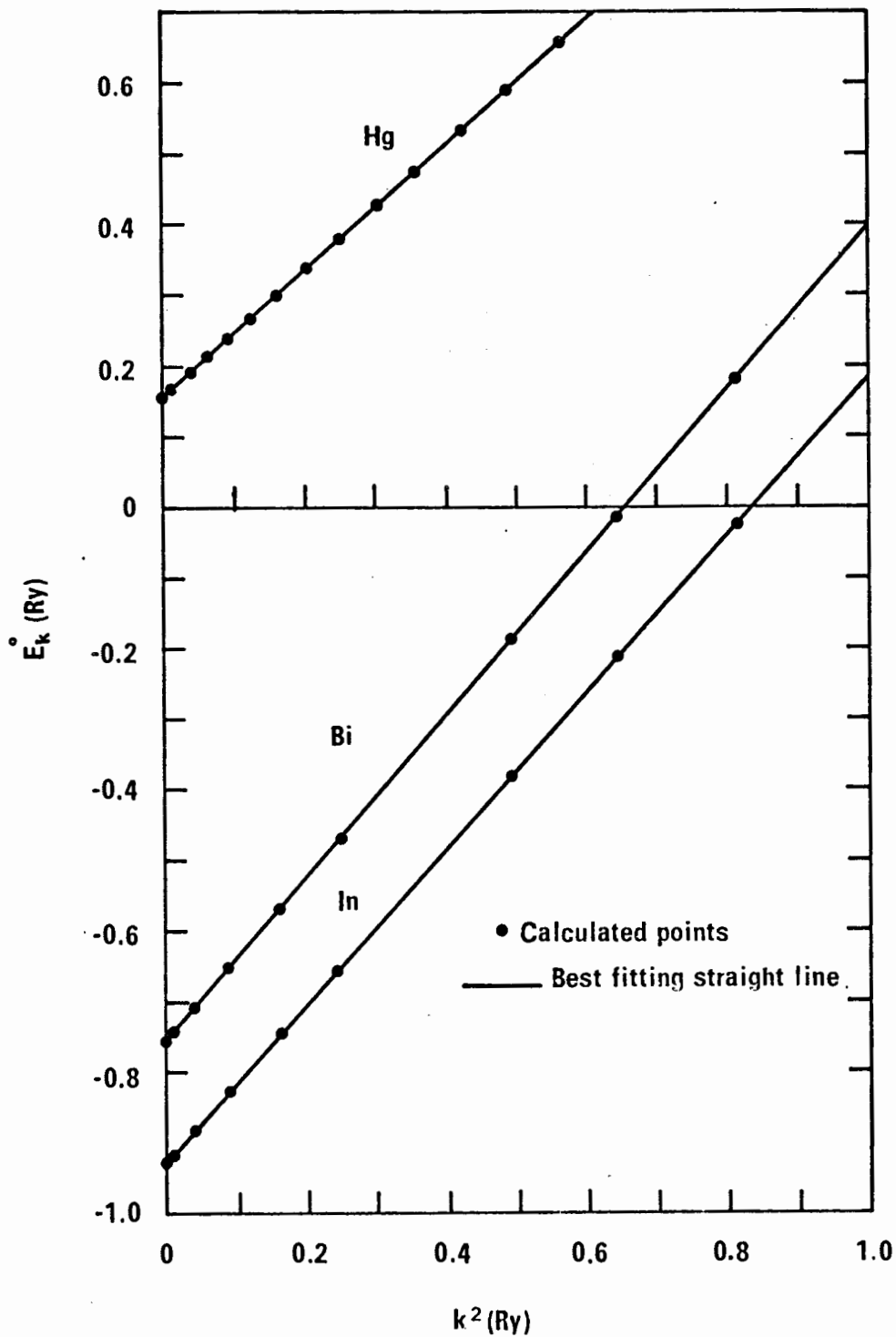


Figure 3 E_k^0 of Equation (2.6) vs. k^2 .

TABLE I Effective Masses

	Bi	In	Hg
μ^k	0.93	1.00	1.23 (1.02)
μ^E	0.93	0.90	0.91 (0.78)
$\mu^k \mu^E$	0.87	0.90	1.12 (0.80)
μ^k / μ^E	1.00	1.10	1.35 (1.30)
μ	0.87	0.90	1.12

§2.2 Calculation of the Density of States

The essential step in calculating the density of states $n(E)$ is to obtain the self-energy $\Sigma(k, E)$. Equations (1.8) and (1.3) then give the Green function and spectral function, which yields $n(E)$ upon integrating over k . In order to solve equation (2.18) self-consistently for $\Sigma(k, E)$ we first transform the integral into polar co-ordinates with the polar axis along the direction of k so that

$$\Sigma(k, E) = \frac{n}{(2\pi)^2} \int_0^\infty \frac{f(k, k', E_F) (k')^2 dk'}{E - \frac{(k')^2}{\mu} - \Sigma(k', E)} \quad (2.20)$$

The angular integral yields

$$f(k, k', E_F) = \int_{-1}^1 |u(k, k', \beta, E_F)|^2 a(q) d\beta, \quad (2.21)$$

with u given by (2.19), β being the cosine of the angle between \mathbf{k} and \mathbf{k}' and $q = (k^2 + k'^2 - 2kk'\beta)^{\frac{1}{2}}$. It can be tabulated for different values of k and k' , and need not be recalculated during the solution of (2.20). The numerical solution, though not trivial, turned out to be quite straight-forward because a direct iterative scheme converges. This is somewhat fortuitous since nonlinear integral equations such as (2.20) are not generally solvable by simple iteration. Some important details of the numerical procedure will be discussed in connection with the calculations for bismuth.

In addition to the density of states we shall also calculate the momentum distribution of the conduction electrons,

$$P(\mathbf{k}) = \int_{-\infty}^{E_F} \rho(\mathbf{k}, E) dE. \quad (2.22)$$

This quantity measures the probability that the momentum state $|\mathbf{k}\rangle$ is occupied. The Fermi energy E_F is to be obtained by integrating $n(E)$ up to the energy below which the Z valence electrons per atom can be accommodated.

§2.3 Application to Bismuth

The structure factor $a(q)$ of liquid bismuth (at 300°C), taken from the neutron diffraction data of North, Enderby and Egelstaff (1968), is plotted in Figure 4. We have used the nonlocal model potential of Heine, Abarenkov and Animalu (Heine and Abarenkov 1964, Abarenkov and Heine 1965, Animalu and Heine 1965, to be referred to as HAA). Certain local potential contributions have been treated slightly differently from HAA, for reasons which are not particularly important here (see Ballentine and Gupta 1971, to be abbreviated BG). For the sake of completeness we briefly state the potential actually used.

The self-consistently screened model potential in a metal,

$$W = V_M + V_{sc} + V_{xc} \quad , \quad (2.23)$$

is the sum of the bare model potential V_M , the screening potential V_{sc} due to the redistribution of the conduction electron charge and the exchange and correlation effective potential V_{xc} of the conduction electrons. V_M is a sum of similar model potentials v_M centered around each ion, of the form

$$\begin{aligned} v_M(r) &= -e^2 \sum_{l=0}^{\infty} A_l(E) P_l \quad , \quad r < R_M, \\ &= -Ze^2/r \quad , \quad r > R_M, \end{aligned} \quad (2.24)$$

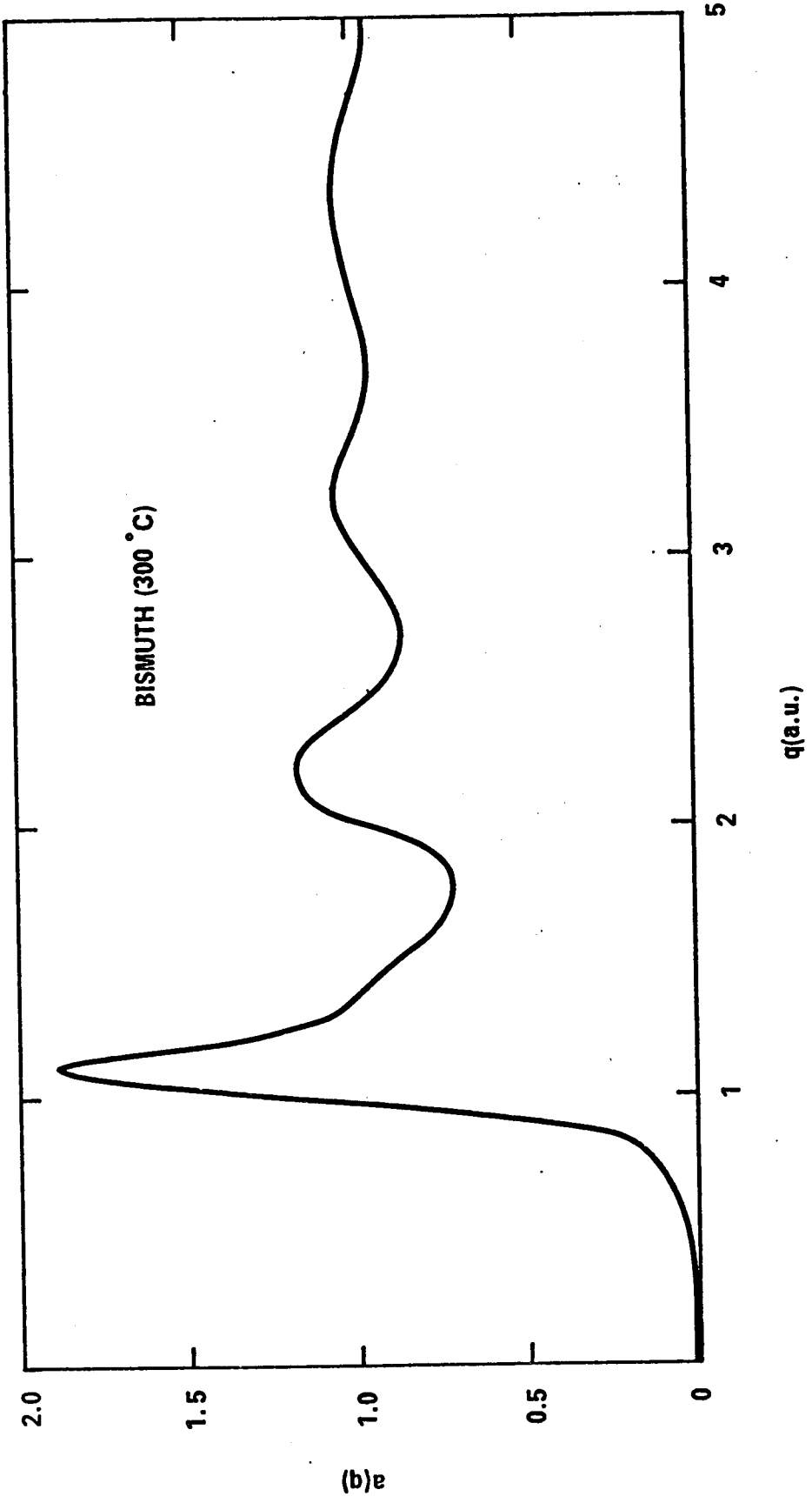


Figure 4 Structure factor for liquid bismuth.

where P_ℓ is the projection operator for angular momentum quantum number ℓ . The model radius R_M is chosen rather arbitrarily within the range between the ionic core radius R_C and the Wigner-Seitz radius of the atom in a solid. For $\ell \leq 2$ the depth parameter $A_\ell(E)$ is adjusted so that for energy E the logarithmic derivative of the pseudo-wave function is the same as that for the true wave function at $r = R_M$. This is done by fitting the spectroscopic term values of the single ion and linearly extrapolating to other energies. For $\ell > 2$ A_ℓ is set equal to A_2 . V_{sc} is related to the screening charge density ρ_{sc} by Poisson's equation,

$$V_{sc}(\underline{q}) = \frac{4\pi e^2}{q^2} \rho_{sc}(\underline{q}) \quad (2.25)$$

First order perturbation gives

$$\rho_{sc}(\underline{q}) = \frac{4}{L^3} \sum_{\underline{k} (\underline{k} < k_F)} \frac{2m/\mu^{\underline{k}}}{\mu^E} \frac{\langle \underline{k} + \underline{q} | W(E_{\underline{k}}) | \underline{k} \rangle}{k^2 - (\underline{k} + \underline{q})^2}, \quad (2.26)$$

where the ratio $\mu^{\underline{k}}/\mu^E$ of the effective masses enters in the same way that it does in the case of the structure-dependent energy (Weaire 1968). BG have obtained V_{xc} by applying the formalism of Hohenberg and Kohn (1964) and Kohn and Sham (1965). Both V_{sc} and V_{xc} must of course be calculated self-consistently. The final result for the momentum space matrix element of the

screened model potential for a single ion is

$$\begin{aligned} \langle \mathbf{k} + \mathbf{q} | \psi(\mathbf{r}) | \mathbf{k} \rangle &= \langle \mathbf{k} + \mathbf{q} | V_M(E) | \mathbf{k} \rangle + v_{ic}(q) / \epsilon(q) \\ &+ \frac{1}{\epsilon(q)} \left[\frac{4\pi e^2}{q^4} + C_0(q) \right] \frac{4}{(2\pi)^3} \int \frac{d^3 k'}{\mu E} \frac{\langle \mathbf{k} + \mathbf{q} | V_M(E) | \mathbf{k}' \rangle}{k'^2 - (\mathbf{k} + \mathbf{q})^2} d^3 k'. \end{aligned} \quad (2.27)$$

The inhomogeneity correction potential arises from the fact that the potential corresponding to an exchange and correlation charge density $C_0 \rho_{sc}$ is an overestimate of V_{xc} inside the ion core. It is approximated by the form

$$v_{ic}(q) = E_{ic} \frac{4}{3} \pi R_c^3 g(x), \quad (2.28)$$

where $x = qR_c$ and

$$g(x) = 3(\sin x - x \cos x) / x^3 \quad (2.29)$$

is the form factor of a uniform spherical charge distribution. Formulas for evaluating $C_0(q)$ and E_{ic} can be found in section 3 of BG. The dielectric function is

$$\epsilon(q) = 1 + \left[\frac{4\pi e^2}{q^2} + C_0(q) \right] \frac{\mu^k}{\mu E} X(q), \quad (2.30)$$

where

$$\begin{aligned}
 X(q) &= -\frac{4}{(2\pi)^3} \int_{k < k_F} \frac{2m d^3k}{k^2 - (\underline{k} + \underline{q})^2} \\
 &= \frac{mk_F}{\pi^2} \left\{ \frac{1}{2} + \frac{4k_F^2 - q^2}{8k_F q} \ln \left| \frac{2k_F + q}{2k_F - q} \right| \right\} .
 \end{aligned}
 \tag{2.31}$$

In (2.30) it has been assumed that the ratio μ^k/μ^E is independent of k .

Within the framework of our effective mass approximation we only need to evaluate the model potential at $E = E_F$. To further simplify the computation we have replaced $\langle \underline{k} + \underline{q} | v_M(E_F) | \underline{k} \rangle$ in the screening term by the Fermi energy shell matrix element $\langle \underline{k} + \underline{q} | v_M(E_F) | \underline{k} \rangle_F$ ($|\underline{k} + \underline{q}| = k = k_F$ for $q \leq 2k_F$, and $k = k_F$, $|\underline{k} + \underline{q}| = q - k_F$ for $q > 2k_F$). Equation (2.27) now becomes, after some manipulation

$$\begin{aligned}
 \langle \underline{k} + \underline{q} | w(E_F) | \underline{k} \rangle &= \langle \underline{k} + \underline{q} | v_{nl}(E_F) | \underline{k} \rangle + \frac{v_{loc}(q) + v_{ic}(q)}{\epsilon(q)} \\
 &+ \left(\frac{1}{\epsilon(q)} - 1 \right) \langle \underline{k} + \underline{q} | v_{nl}(E_F) | \underline{k} \rangle_F .
 \end{aligned}
 \tag{2.32}$$

Here v_{loc} and v_{nl} represent the local and nonlocal parts of v_M respectively. Only the first term in (2.32) is nonlocal.

Values of the model potential parameters for the three

metals considered are tabulated in Appendix II. Figure 5 shows our Fermi energy shell form factor for bismuth normalized to the atomic volume Ω . Shown also are the HAA form factor for comparison and the position q_p of the main peak in $a(q)$. There is not much difference between the two curves. Ours is in slightly better agreement with Cohen and Heine's (1970) estimates of the node of the form factor from liquid structure data. The slight difference in the long wave limits is due to the different atomic volumes used. Our value is appropriate to the liquid whereas HAA used the solid state value.

Numerical computation

Throughout our numerical work we have used "semi-atomic" units so that energies are in rybergs and momenta in a_0^{-1} where $a_0 = \frac{\hbar^2}{me^2}$ is the Bohr radius. The calculations did not involve any special techniques of numerical analysis and therefore need not be described in full. We mention here only those aspects which are important for accuracy or computational efficiency.

(1) The angular integral $f(k, k')$ in (2.21) was first tabulated at 29 values of k and 58 values of k' in the interval $0 \leq k, k' \leq 6.5$. The points were distributed more densely where the function was more rapidly varying. More points were needed for k' than for k because the structure of $f(k, k')$ was more complicated than that of $\Sigma(k, E)$, and the iterative solution of (2.20) required us to integrate a product involving

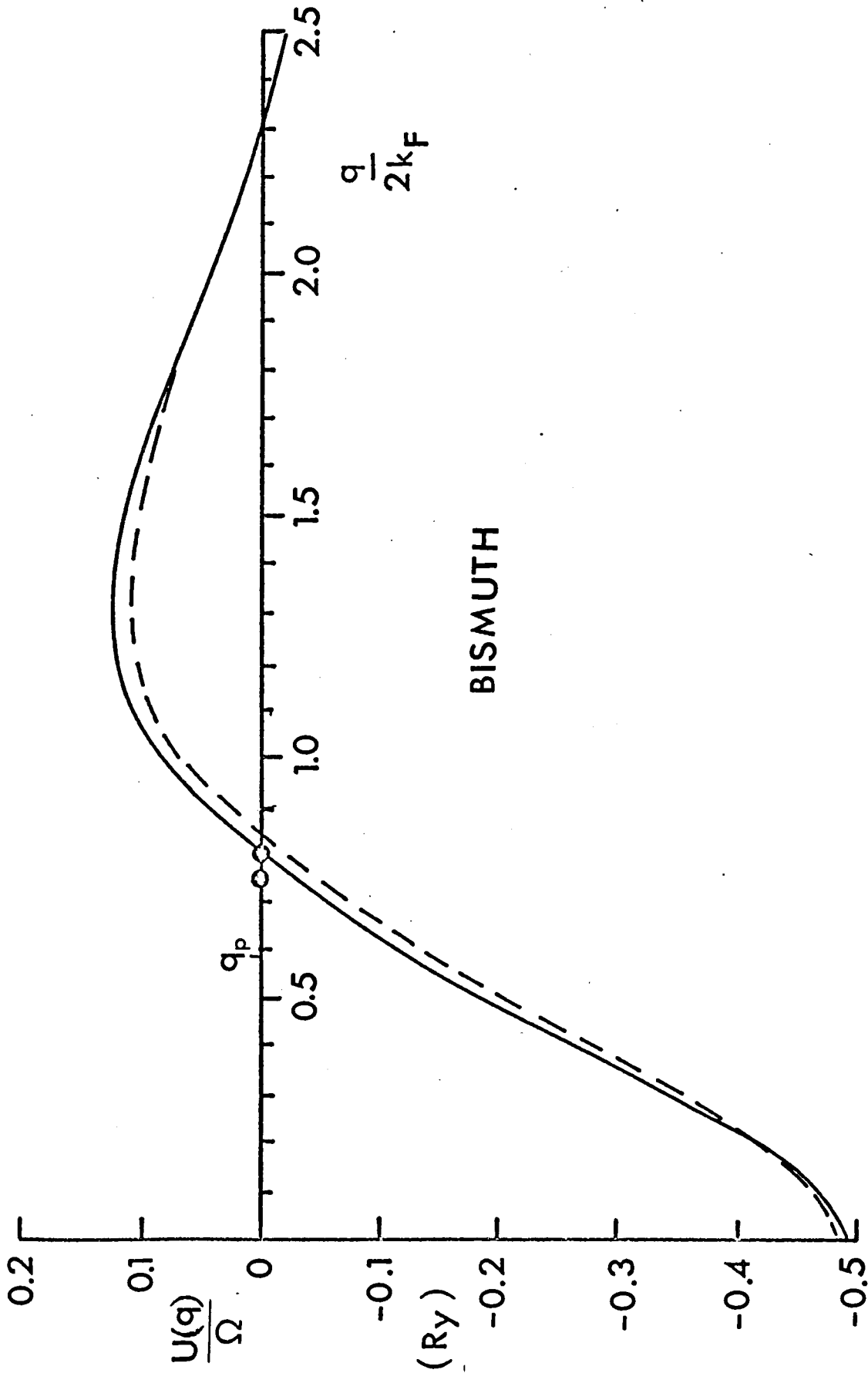


Figure 5 Model potential form factor for bismuth. Solid curve: Fermi energy shell form factor used in this calculation. Dashed curve: Fermi energy shell form factor of Animalu and Heine (1965). Points: estimates of the node of form factor from liquid structure data (Cohen and Heine, 1970).

$f(k, k')$ over k' . A Romberg quadrature (see e.g. section 4.4, Conte 1965) was used to perform the integration. It has the advantage of proceeding automatically until the specified absolute or relative accuracy is achieved.

(2) Equation (2.20) was solved by complex integration rather than separating it into real and imaginary parts. In this way the interpolation for the real and imaginary parts of the integrand could be done simultaneously.

(3) We can easily estimate the truncation errors $\Delta\Sigma$ and $\Delta n(E)$ in Σ and $n(E)$, which may arise from the use of a finite upper limit of integration, k_M say, in (2.20) and in the final integration for the density of states. From (2.20) we have

$$\Delta \Sigma(k, E) = \frac{1}{4\pi^2} \int_{k_m}^{\infty} \frac{f(k, k') (k')^2 dk'}{E - \frac{(k')^2}{\mu} - \Sigma(k', E)}$$

or

$$\text{Re } \Delta \Sigma(k, E) = \frac{1}{4\pi^2} \int_{k_m}^{\infty} \frac{f(k, k') \text{Re } \Sigma(k', E) (k')^2 dk'}{\left[E - \frac{(k')^2}{\mu} - \text{Re } \Sigma(k', E) \right]^2 + \left[\text{Im } \Sigma(k', E) \right]^2}, \quad (2.33)$$

and

$$\text{Im} \Delta \Sigma(k, E) = \frac{1}{4\pi^2} \int_{k_m}^{\infty} \frac{f(k, k') \text{Im} \Sigma(k', E) (k')^2 dk'}{\left[E - \frac{(k')^2}{\mu} - \text{Re} \Sigma(k', E) \right]^2 + \left[\text{Im} \Sigma(k', E) \right]^2} . \quad (2.34)$$

Our particular choice of $k_m = 6.5$ insures that in the denominator $(k')^2 \gg E$ for the entire range of E in which we are interested, and $(k')^2 \gg \text{Re} \Sigma(k', E), \text{Im} \Sigma(k', E)$ (from the results of our calculations). Equations (2.33) and (2.34) thus reduce to

$$\text{Re} \Delta \Sigma(k, E) \approx \frac{1}{4\pi^2} \int_{k_m}^{\infty} \frac{f(k, k') \text{Re} \Sigma(k', E)}{(k')^2} dk' , \quad (2.35)$$

and

$$\text{Im} \Delta \Sigma(k, E) \approx \frac{1}{4\pi^2} \int_{k_m}^{\infty} \frac{f(k, k') \text{Im} \Sigma(k', E)}{(k')^2} dk' . \quad (2.36)$$

Consider, for example, the case $E = 0.6, k = 0.2$. The relevant quantities have the values $\text{Re} \Sigma(0.2, 0.6) = -0.092, \text{Im} \Sigma(0.2, 0.6) = -0.0858, \text{Re} \Sigma(6.5, 0.6) = -0.031, \text{Im} \Sigma(6.5, 0.6) = -10^{-4}$, and

$f(0.2, 6.5) = 0.0113$. The asymptotic behaviour of the functions $\text{Re}\Sigma$, $\text{Im}\Sigma$, and f were estimated by log-log plots. They were found to vary as $(k')^{-2}$, $(k')^{-4}$, and $(k')^{-4}$ respectively. Inserting these into (2.35) and (2.36) we obtain

$$|\text{Re } \Delta \Sigma(k, E)| \approx \frac{1}{28\pi^2} f(k, k_m) \text{Re} \Sigma(k_m, E) k_m^{-7}, \quad (2.37)$$

and

$$|\text{Im } \Delta \Sigma(k, E)| \approx \frac{1}{36\pi^2} f(k, k_m) \text{Im} \Sigma(k_m, E) k_m^{-9}. \quad (2.38)$$

In particular,

$$|\text{Re } \Delta \Sigma(0.2, 0.6)| \approx 2.6 \times 10^{-12},$$

and

$$|\text{Im } \Delta \Sigma(0.2, 0.6)| \approx 1.5 \times 10^{-16}.$$

These errors are obviously negligible in comparison with the numerical values for $\text{Re}\Sigma(0.2, 0.6)$ and $\text{Im}\Sigma(0.2, 0.6)$ quoted above. This is expected to hold for other values of k and E .

Similarly, from Equations (1.5), (1.3), and (1.8),

$$\begin{aligned} \Delta n(E) &= \frac{1}{2\pi^2} \int_{k_m}^{\infty} \rho(k, E) k^2 dk \\ &\approx \frac{1}{2\pi^3} \int_{k_m}^{\infty} \frac{\text{Im} \Sigma(k, E)}{k^4} k^2 dk \\ &\approx -\frac{1}{10\pi^3} k_m^{-5} \text{Im} \Sigma(k_m, E) \\ &< 10^{-6} |\text{Im} \Sigma(k_m, E)|, \quad k_m = 6.5. \end{aligned} \tag{2.39}$$

For illustration we quote some numerical results: $n(0.06) = 0.0166$, $\text{Im}\Sigma(6.5, 0.6) = -10^{-4}$, $n(-0.05) = 0.0041$, and $\text{Im}\Sigma(6.5, -0.05) = -3.3 \times 10^{-6}$. Evidently Δn is negligible except at the very bottom of the band ($E_0 \approx -0.09$).

The above considerations should not be taken to imply that our final results for the density of states will be accurate to the order indicated in (2.39). Ultimately the accuracy of our calculations is limited by the available experimental data for $a(q)$. The point is that no extraneous numerical error has been introduced.

(4) The interval of integration (0, 6.5) for both Σ and $n(E)$ was divided into three subintervals (0, $k_0 - 2\Delta k$), ($k_0 - 2\Delta k$, $k_0 + 2\Delta k$), and ($k_0 + 2\Delta k$, 6.5) where k_0 is the peak position of the spectral function $\rho(k, E)$ and is given by the solution of the equation,

$$E - k^2 - \text{Re} \Sigma(k, E) = 0 \quad , \quad (2.40)$$

Δk is the "half-width" of $\rho(k, E)$ if Σ were independent of k so that $\rho(k, E)$ would be a Lorentzian. Provided that $k_0 \gg \Delta k$, which is satisfied except for E very close to the bottom of the band, Δk is given to a good approximation by $\text{Im} \Sigma(k_0, E)/k_0$. The purpose of this subdivision of the interval is to reduce the computer time since $\rho(k, E)$ is a sharply peaked function of k and the integration in the region outside the peak converges much more rapidly.

As a test of our programs we have calculated the self-energy and hence the density of states for bismuth using free-electron mass (i.e. $\mu = 1$) and Ballentine's (1966) values of $|u(q)|^2 a(q)$ in which a local approximation of the HAA model potential was used. In Figure 9 the $n(E)$ so obtained (case 2) is compared to Ballentine's (case 1) which he calculated by making the "complex energy approximation" of replacing $\Sigma(k, E)$ in the denominator of (1.17) by a constant $\Sigma(k_0, E)$. The coincidence of the two curves at all points except at the small peak around $k = -0.14$ testifies to the general correctness of

our programs. At the same time it also shows that the "complex energy approximation" did not introduce serious errors apart from a slight spurious enhancement of the structure. We have also plotted on the same graph the results for $n(E)$ with effective mass correction using local (case 3) and nonlocal (case 4) model potentials respectively. A comparison of cases 2 and 3 shows that the structure is somewhat reduced by the inclusion of the energy dependence of the potential through an effective mass. When a nonlocal model potential is used (case 4) the structure is further reduced so that the shoulder of the $n(E)$ curve, which is still quite distinct in case 3, is now barely visible. Thus we find the density of electronic states of bismuth to be more nearly-free-electron-like as the calculations become more exact. To understand what is happening we need only consider the origin of the structure obtained with a local, energy independent model potential. In bismuth it is the large value of $|u(q)|^2 a(q)$ at the position of the main peak of $a(q)$ which gives rise to the structure (Ballentine 1966). For a nonlocal, energy dependent model potential the position of the zero of $\langle k|u(E)|k+q\rangle$ varies with k and E , with the effect of smoothing out the structure.

The real and imaginary parts of the self-energy $\Sigma(k, E)$ corresponding to case 4 are shown in Figures 6 and 7. These have about the same amount of structure as found by Ballentine (1966) but the values are typically smaller by factors of two and three respectively. By comparing the values of $\Sigma(k, E)$ for

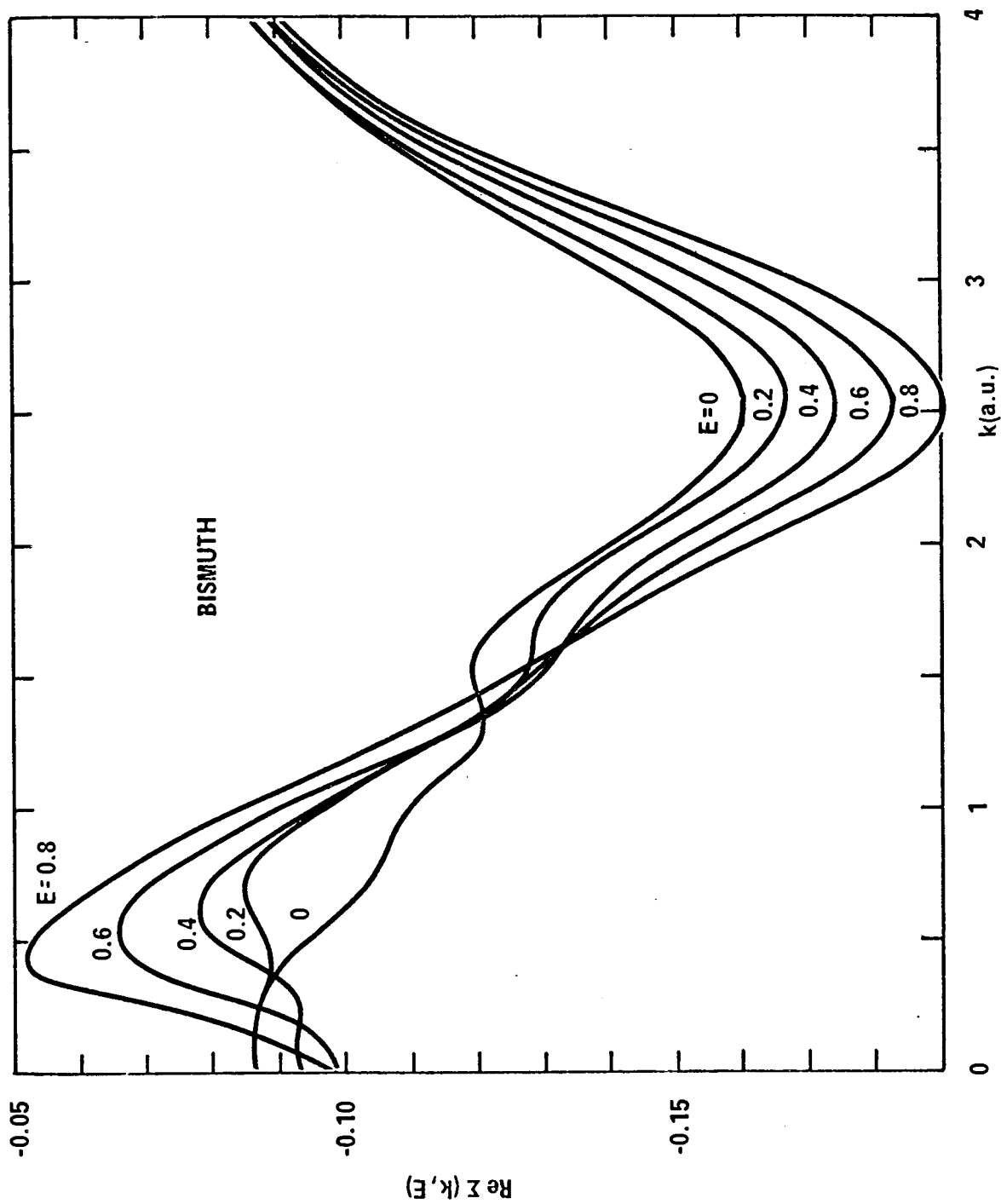


Figure 6 Real part of self-energy for bismuth.

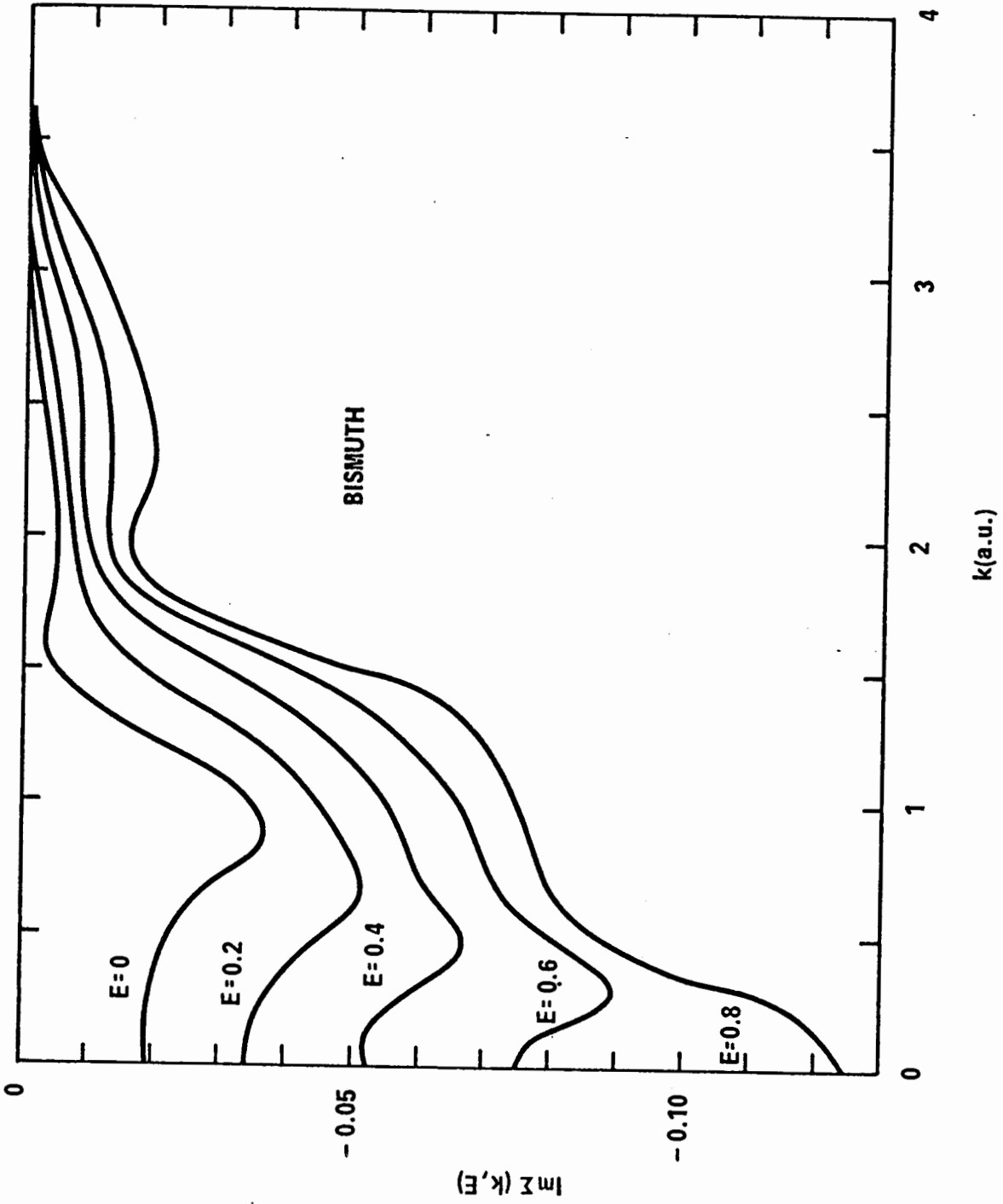


Figure 7 Imaginary part of self-energy for bismuth

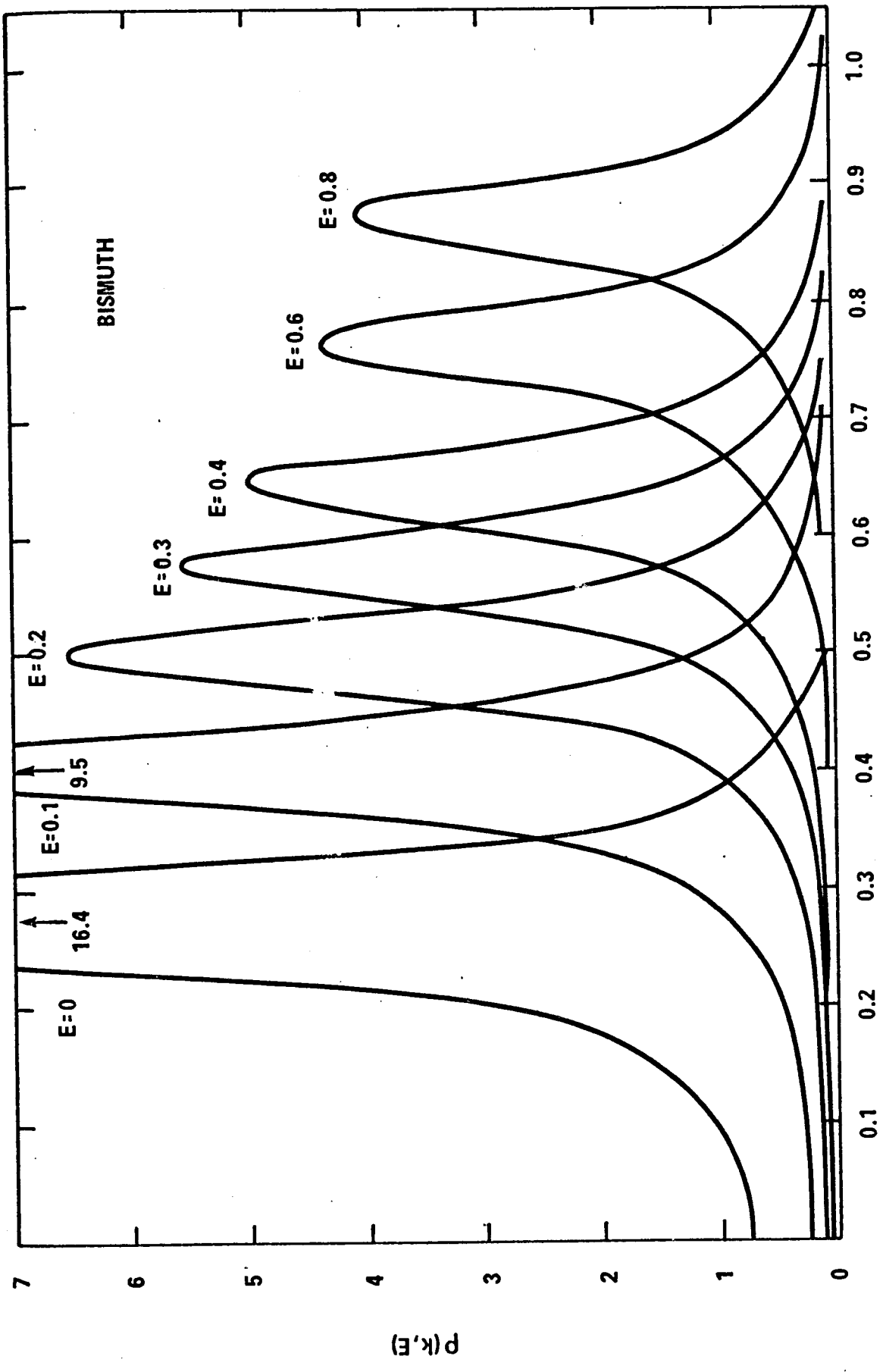


Figure 8 Spectral function $\rho(k, E)$ for bismuth

Figure 9 Density of states per unit volume (a.u.) per unit energy range, $n(E)$ for bismuth.

- △— Case 1 Local, energy independent model potential, "complex energy approximation" -- Ballentine (1966)

- ⊙— Case 2 Local, energy independent model potential

- Case 3 Local model potential, effective mass correction

- Case 4 Nonlocal model potential, effective mass correction

- - — Free-electron parabola (origin shifted)

- — Free-electron parabola corresponding to $\mu = 0.87$

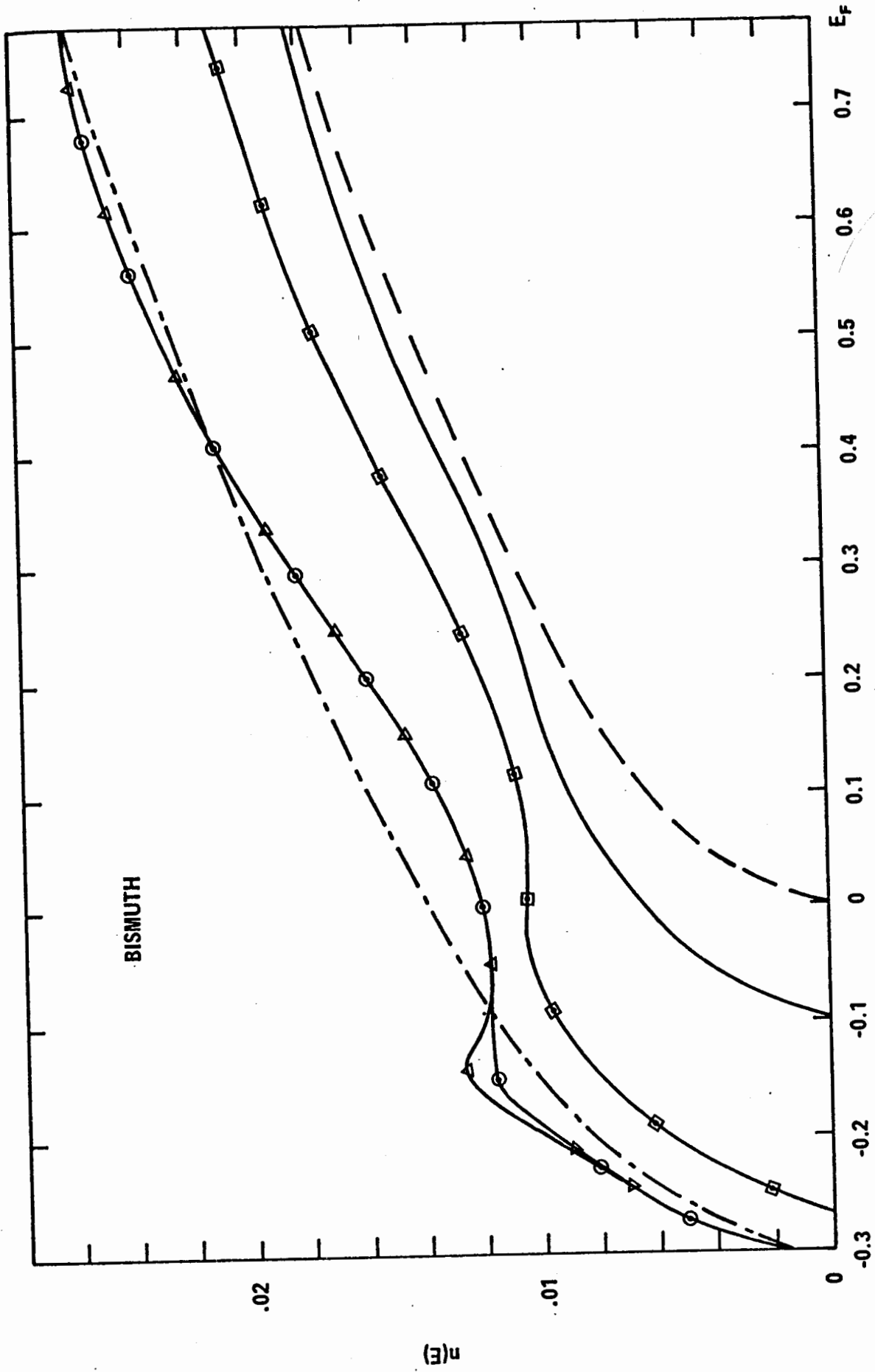


Figure 9

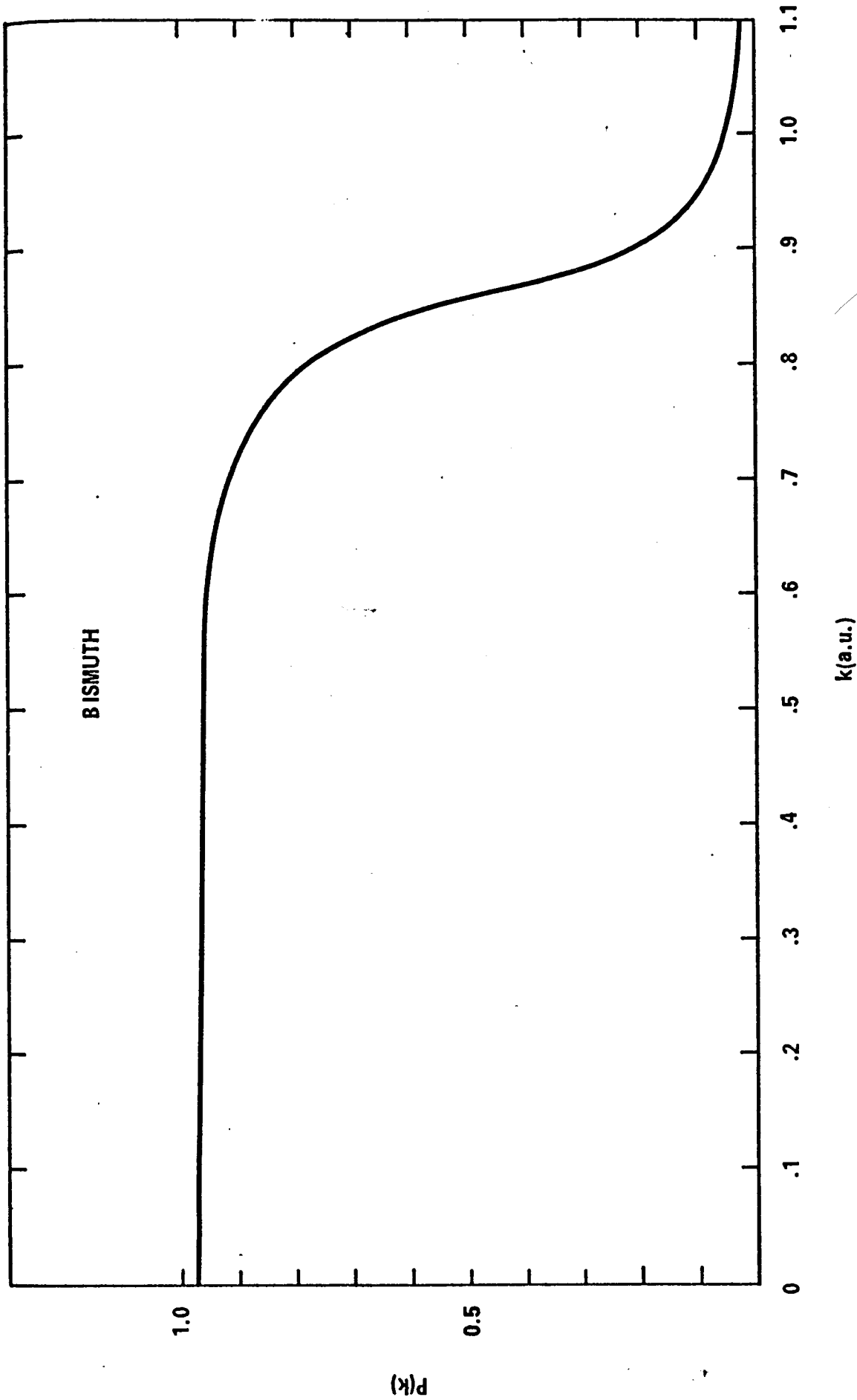


Figure 10 Momentum distribution for occupied states of bismuth.

the four cases mentioned above we observe that it is mainly the use of a nonlocal model potential which is responsible for the drastic reduction. The smaller values of $\text{Im}\Sigma(k, E)$ are reflected in the narrower width of the spectral function $\rho(k, E)$ (Figure 8). Moreover, if we define a thickness of the Fermi surface, Δk_F , as the distance between the points where a tangent to the momentum distribution curve for occupied states (Figure 10) at $P(k) = 0.5$ intercepts $P = 0$ and 1 , we obtain a thickness of $0.087 a_0^{-1}$. This is much smaller than Ballentine's (1966) value of $0.205 a_0^{-1}$. We conclude that the electronic states of bismuth have nearly-free-electron behaviour.

§2.4 Application to Indium

In their photoemission experiments on indium Koyama et al. (1967) and Enderby (1969, unpublished) have found a pronounced structure in the energy distributions of the photoemitted electrons, which has been tentatively attributed to structure in the density of occupied states (Koyama et al. 1967). It is therefore of considerable interest to calculate the density of states in this metal. The structure factor $a(q)$ for indium at 170°C (Figure 11) was taken from the X-ray diffraction data of Ocken and Wagner (1966). A nonlocal model potential (Figure 12) similar to the one for bismuth was used, but in this case the parameter E_{iC} (see Eq. (2.28)) was adjusted to make the form factor fit the points deduced from the Fermi surface data and the pressure dependence of the de Haas-van

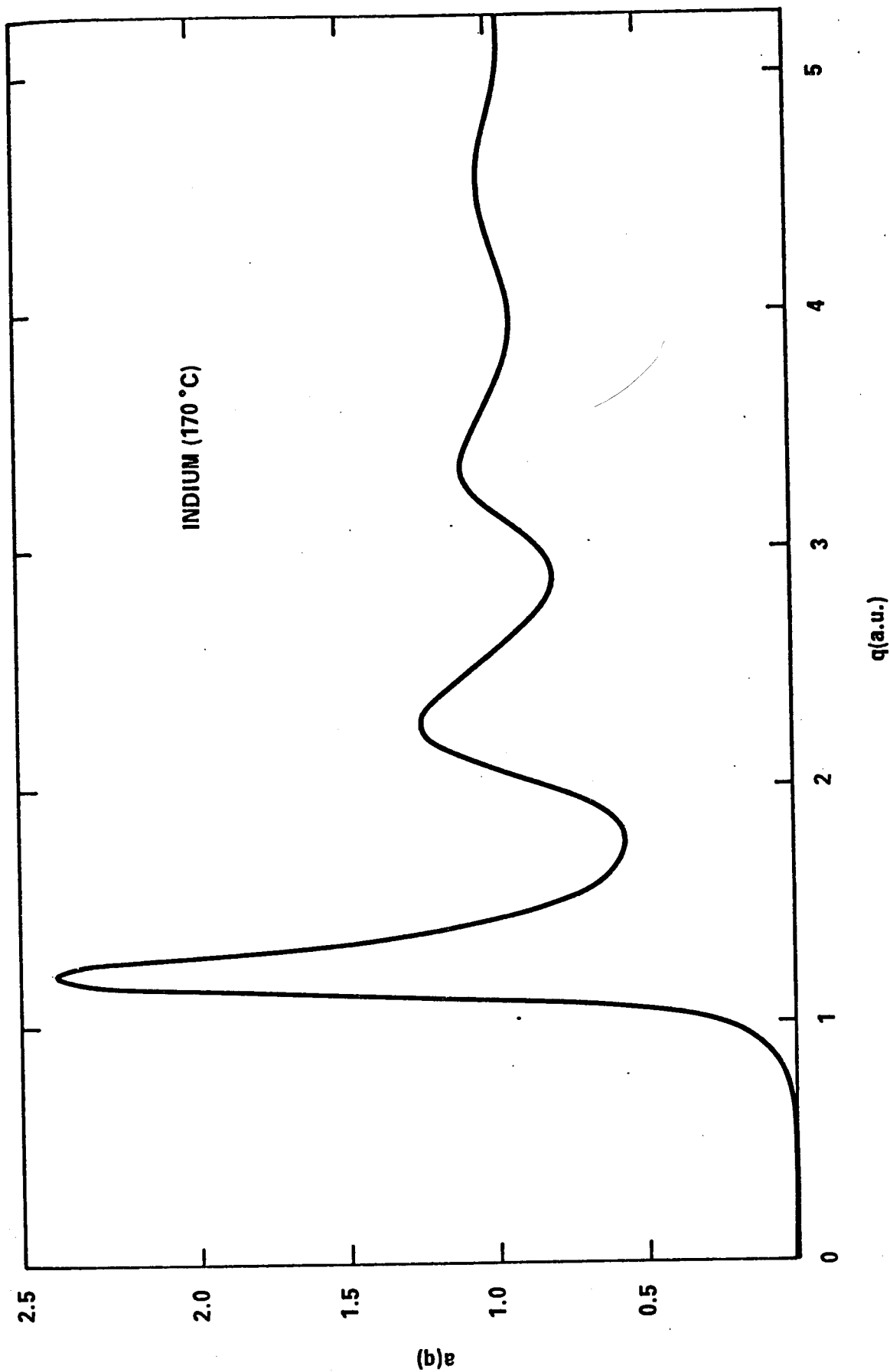


Figure 11 Structure factor for liquid indium.

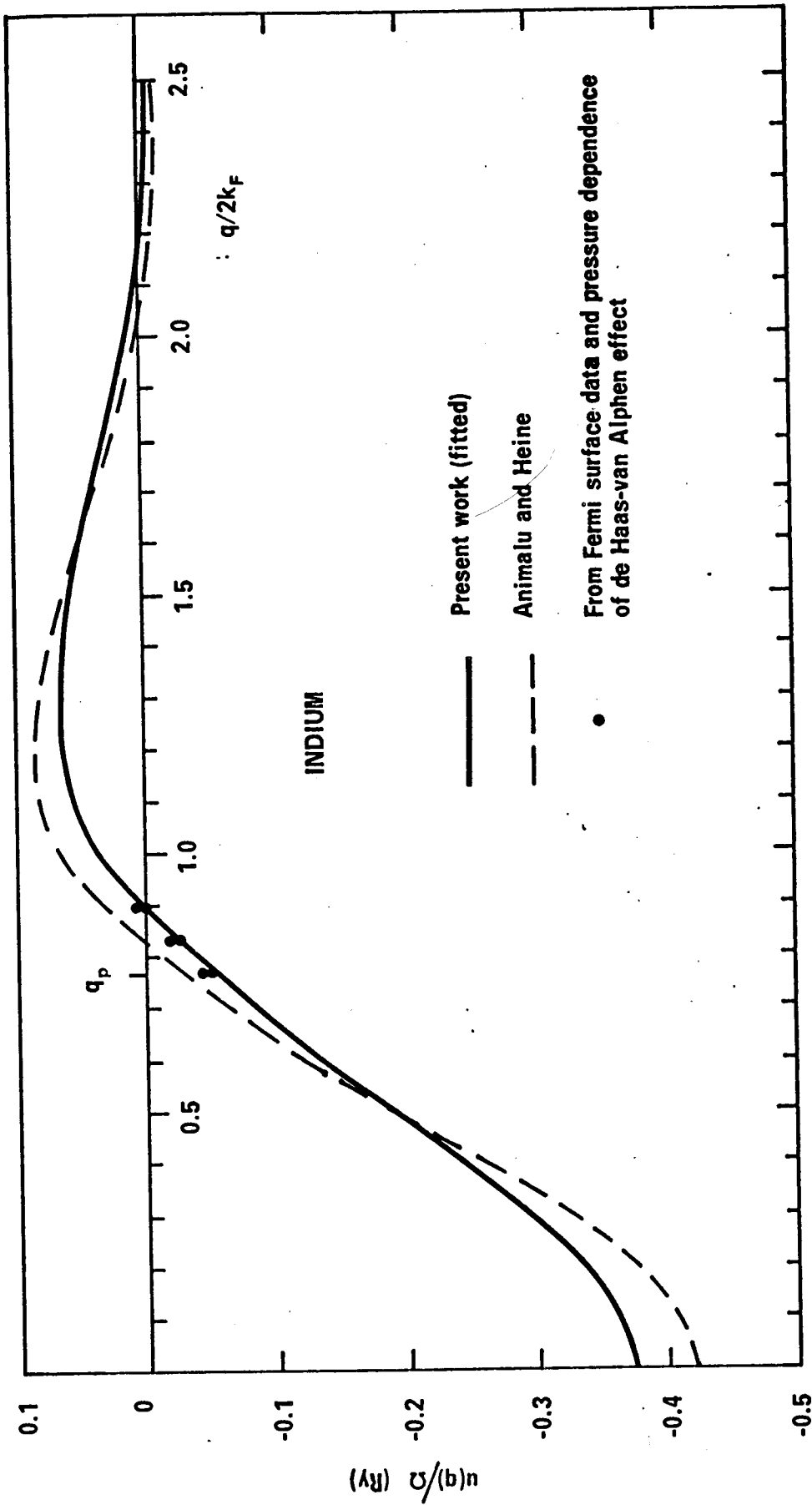


Figure 12 Model potential form factor for indium.

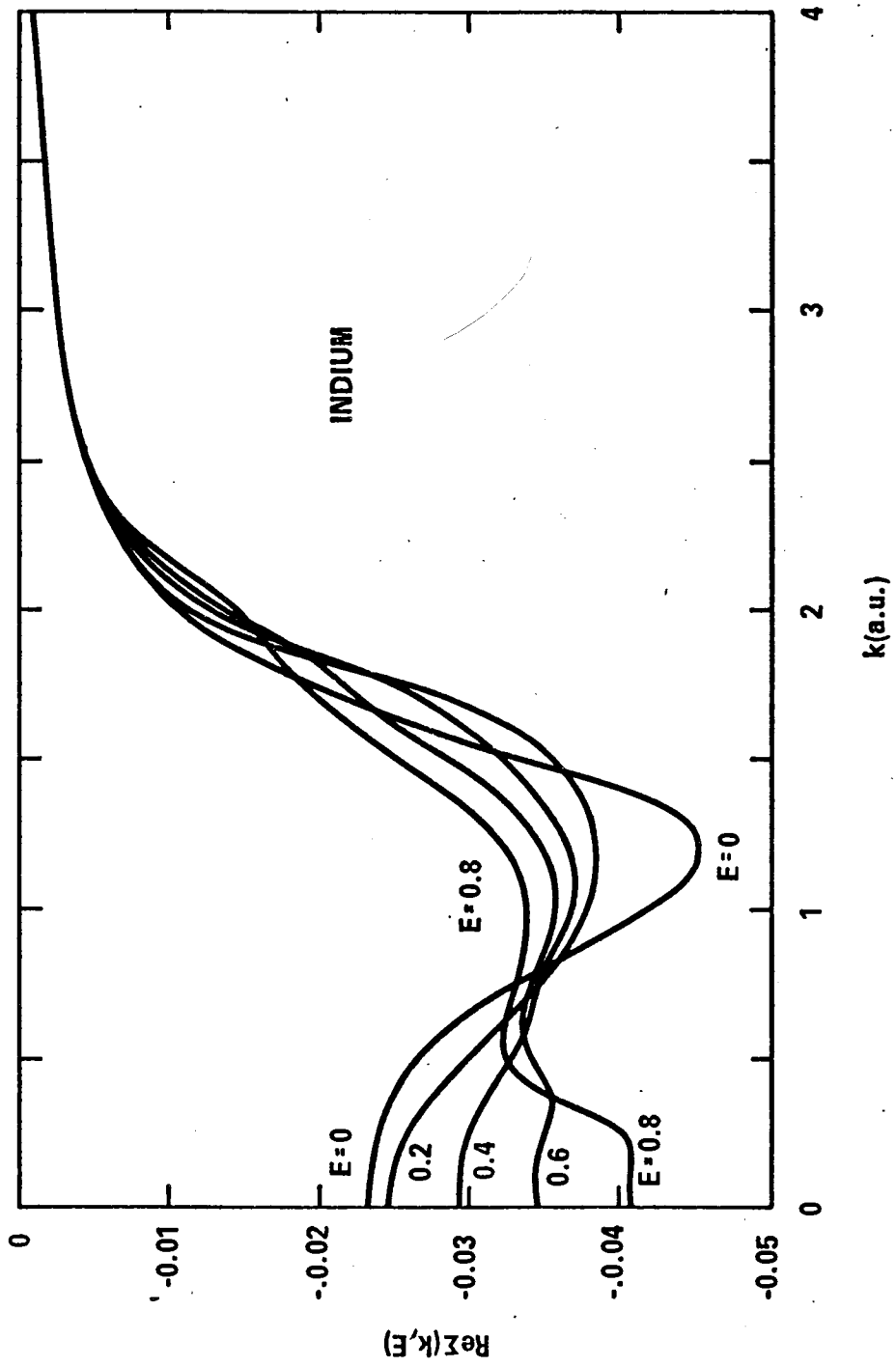


Figure 13 Real part of self-energy for indium.

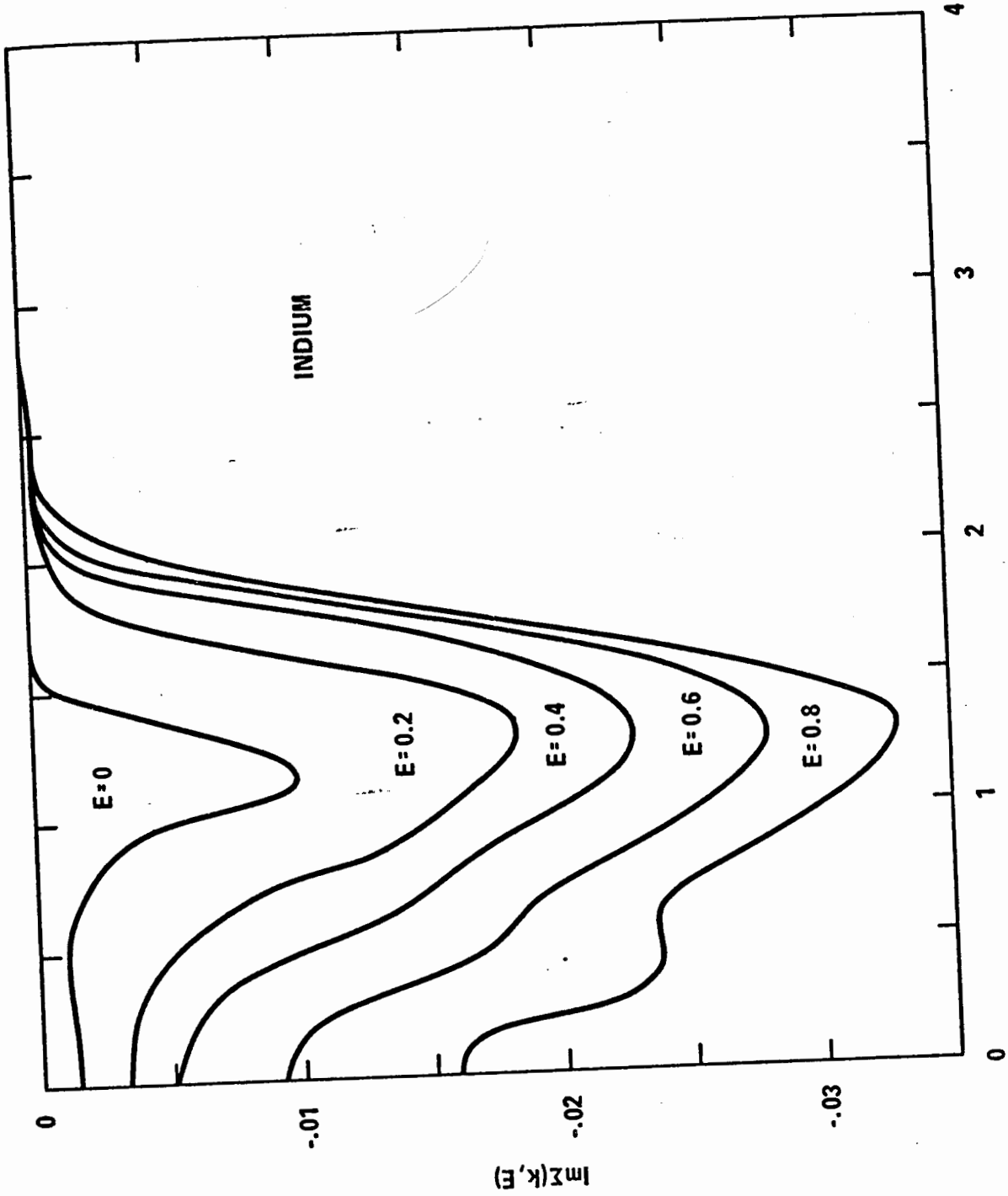


Figure 14 Imaginary part of self-energy for indium.

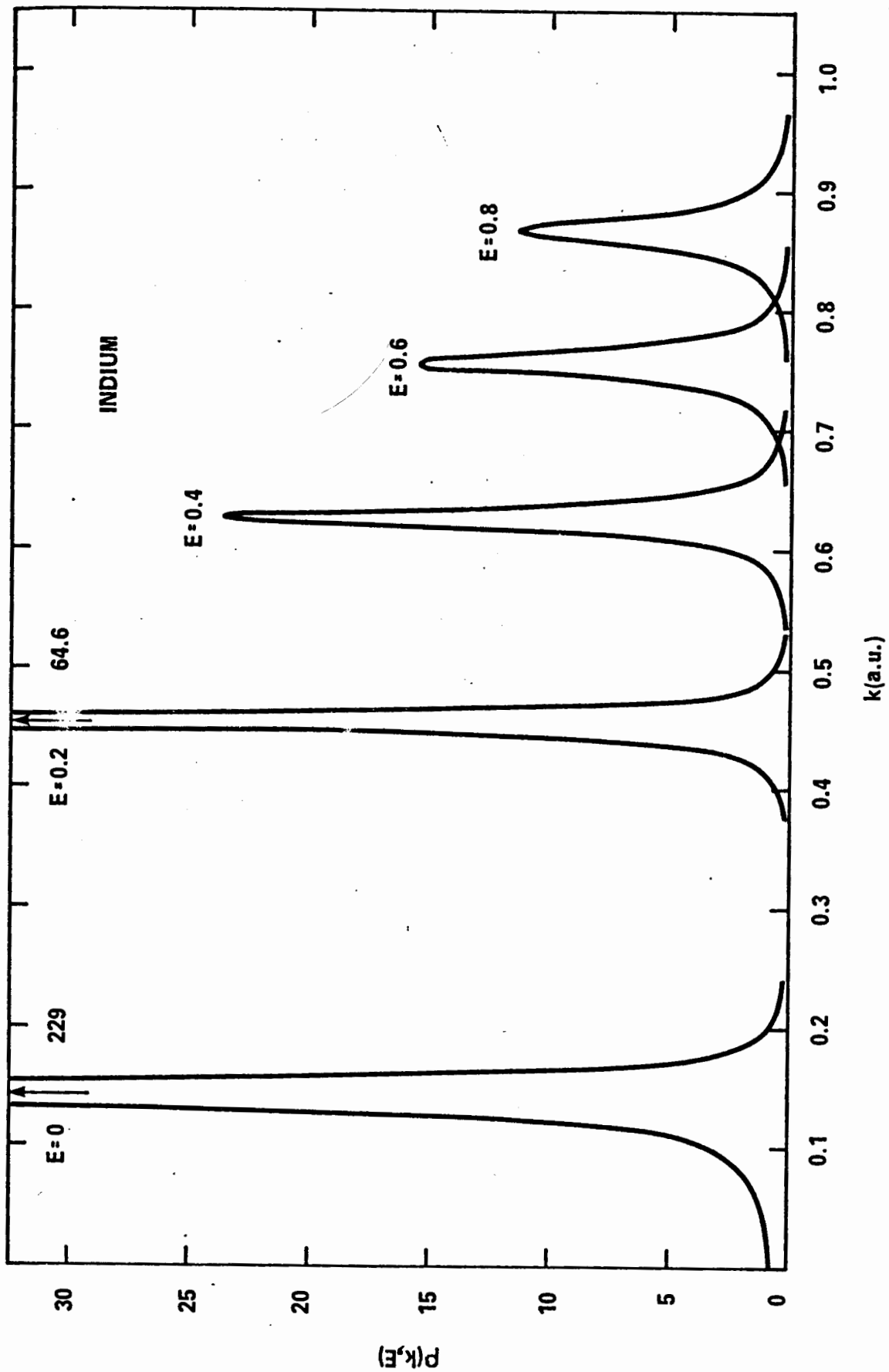


Figure 15 Spectral function $\rho(k, E)$ for indium.

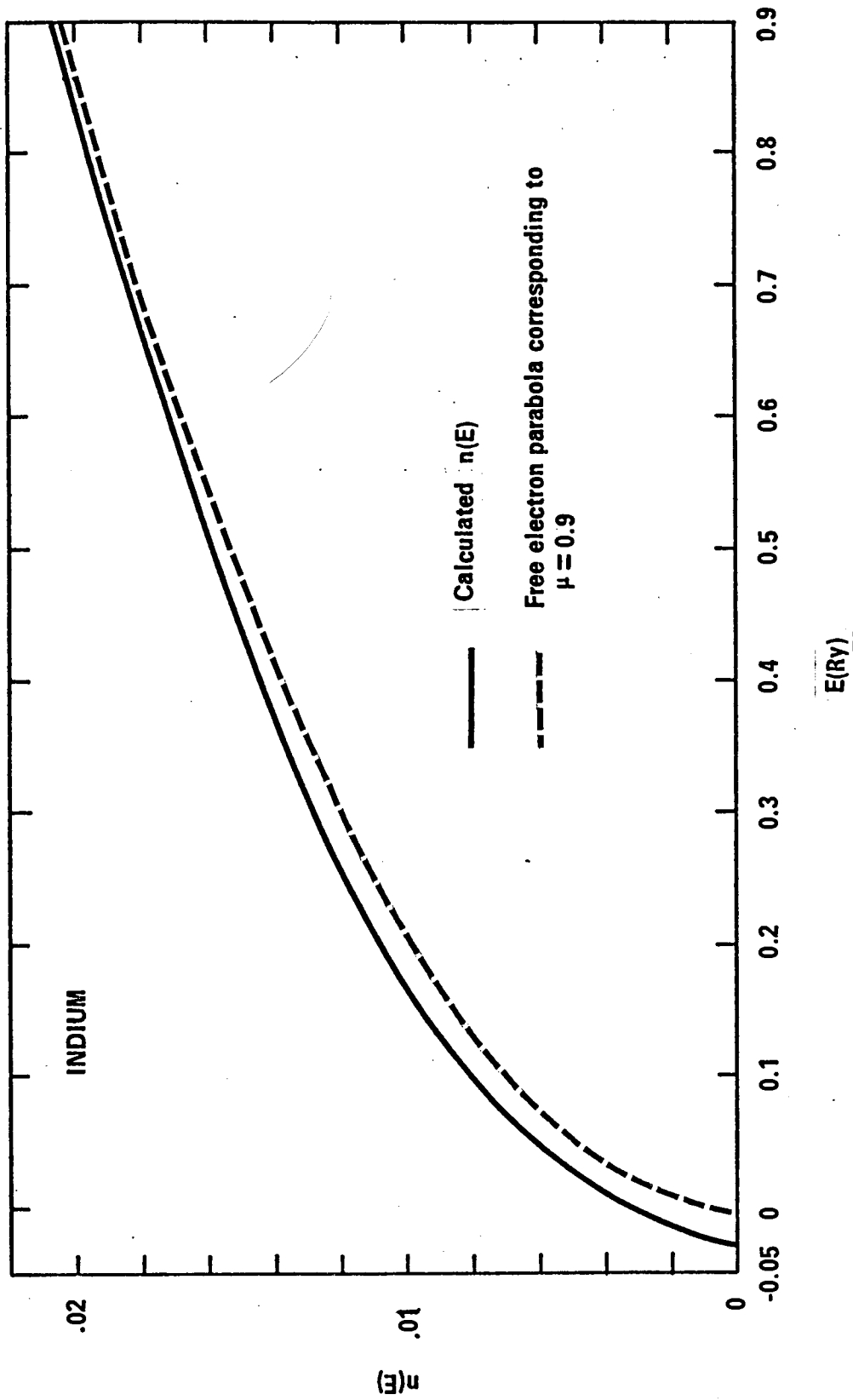


Figure 16 Density of states per unit volume (a.u.) per unit energy range, $n(E)$ for indium.

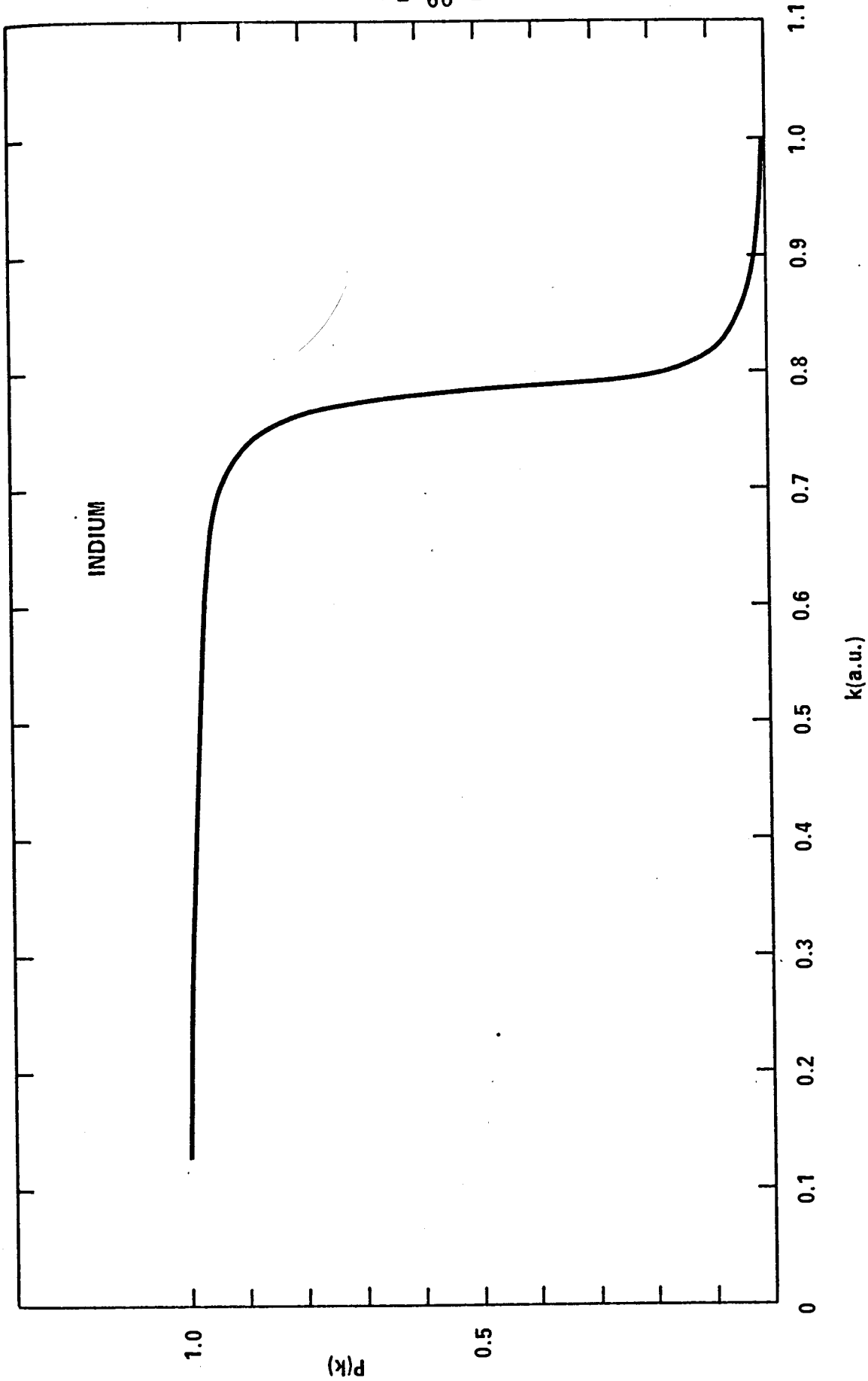


Figure 17 Momentum distribution for occupied states of indium.

Alphen effect (Cohen and Heine 1970, and references given there). The best fit was obtained when E_{ic} , considered as a parameter, had the value -0.45. The ratio $\mu^k/\mu^E = 1.1$ in Equation (2.30) is responsible for the difference between the long wave limit of our form factor and that of the HAA potential. Figures 13 to 17 display the results of the calculations.

Indium is even more free-electron-like than bismuth in every respect. Both the real and imaginary parts of the self-energy (Figure 13 and 14) have smaller values and the imaginary part has less structure. The spectral function (Figure 15) is narrower and there is less disorder broadening in the momentum distribution $P(k)$ (Figure 17). Above all, the density of states (Figure 16) differs very little from the free-electron parabola corresponding to the appropriate effective mass. In the light of our present results the interpretation of the photoemission data by Koyama et al. (1967) appears dubious. Shaw and Smith (1969) have come to a similar conclusion on the basis of their second order perturbation calculation.

§2.5 Application to Mercury

Liquid mercury possesses electronic properties which are strikingly different from those of other liquid metals. Some of these are: (a) very high d.c resistivity and thermoelectric power, (b) sharp decrease in resistivity on alloying with metals other than the alkalis, and (c) optical conduc-

tivity that cannot be fitted to the Drude formula* (see Mott 1966 for a review). By postulating a dip in the electronic density of states near the Fermi energy Mott was able to give a qualitative interpretation to a large body of experimental data, although Adams (1968) later showed that the resistivity of Hg-Au alloys is an exception to Mott's model.

The theoretical origin of the dip in $n(E)$, as calculated either by second order perturbation theory or by the Green function techniques used in this thesis, is the sharp peak in the structure factor $a(q)$. Because $a(q)$ occurs multiplied by the square of the model potential form factor $u(q)$ (see Eq. (1.17)), which according to Animalu and Heine (1965) should be zero near the peak position q_p of $a(q)$ for mercury, Mott's hypothesis appeared for some time to be poorly founded.

However more recently Evans et al. (Evans et al. 1969, Evans 1970) showed that the model potential for mercury should have a considerably different form from the HAA model potential, and in particular $u(q)$ should not pass through zero near q_p . Using Ziman's theory (Ziman 1961, Bradley et al. 1962, Faber and Ziman 1965) they obtained reasonable quantitative agreement with most (though not all) of the resistivity and thermoelectric power measurements, without employing Mott's hypothesis about the density of electronic states.

* Experimental workers are not unanimous regarding this point. See Part II below.

The form of the Evans model potential suggests that the density of states in mercury might indeed have an interesting structure. Accordingly we have calculated $n(E)$ for mercury (Chan and Ballentine 1971a) using such a model potential in conjunction with the structure factor (Figure 18) taken from the X-ray diffraction data of Kaplow et al. (1965).

Several features distinguish the model potential of Evans from that of HAA:

- (a) the core potential is replaced by a square well of depth A_ℓ only for $\ell < \ell_0$, where ℓ_0 ($= 2$ for Hg) is the largest angular momentum for which there are core states and the energy dependence in A_ℓ is retained in calculating the screening; for higher ℓ the true potential is used;
- (b) the arbitrariness in the choice of the core radius R_ℓ is removed by an optimization procedure to obtain the smoothest model wave function, which requires that

$$A_\ell = \frac{Z}{R_\ell} \quad ; \quad (2.41)$$

- (c) in extrapolating A_ℓ from the free-ion term values to conduction band energies a quantum defect method (Ham 1955) is used instead of linear extrapolation.

The first two modifications are due to Shaw (1968) whereas the last, particularly important for mercury in which the 5d states of the core of the free ion come close to the con-

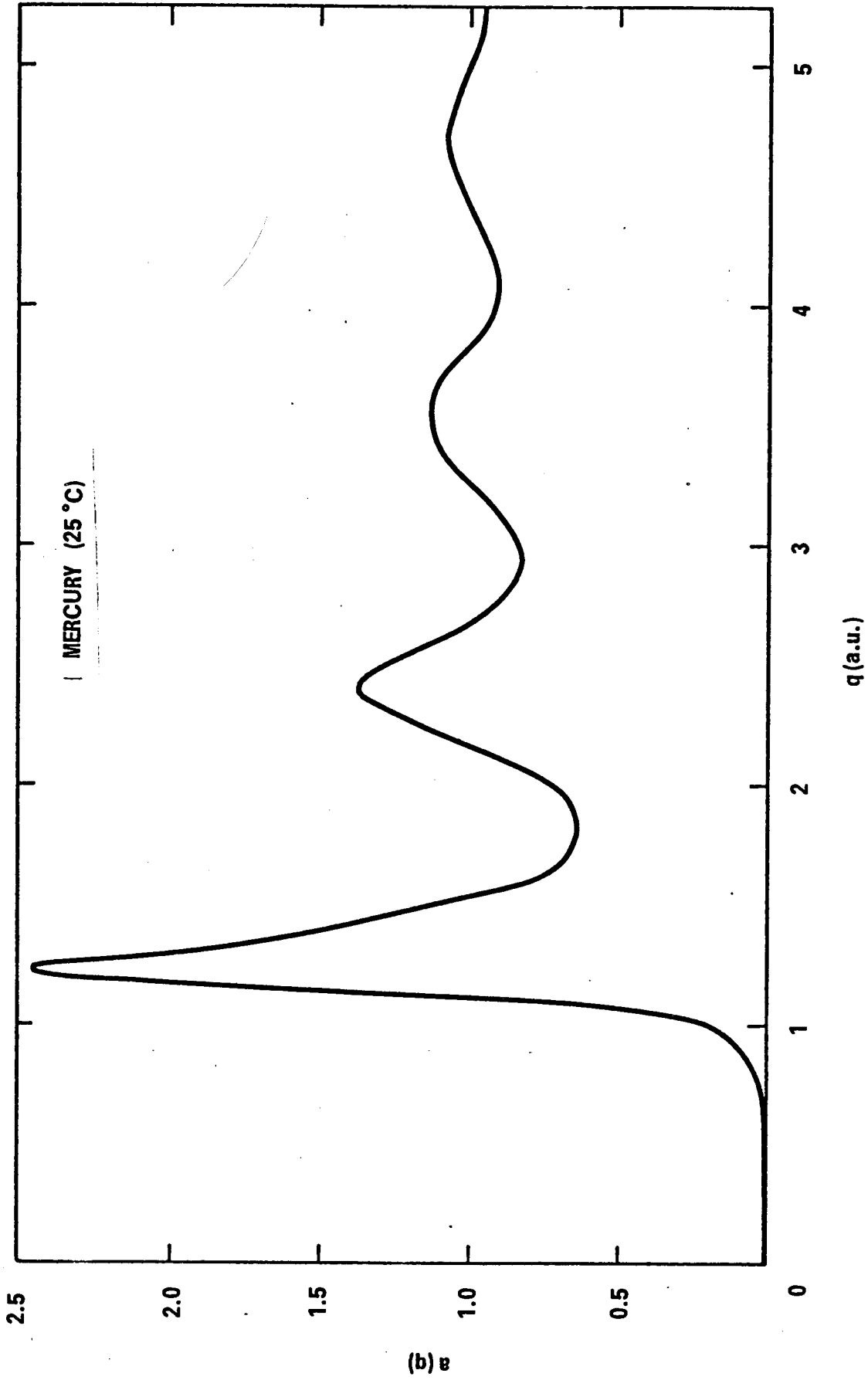


Figure 18 Structure factor for liquid mercury.

duction band, is the contribution of Evans. He also found that for $\ell = 2$ Equation (2.41) could not be satisfied and $R_2(E)$ had to be determined by minimizing $|A_2(E) - Z/R_2(E)|$.

We have used the bare model potential of Evans (1970) but have treated the screening and the depletion potential slightly differently. The matrix element of our screened model potential has the form

$$\begin{aligned} \langle \underline{k} + \underline{q} | w(E) | \underline{k} \rangle &= \langle \underline{k} + \underline{q} | v_{nl}(E) | \underline{k} \rangle + \frac{v_{sc}(q) + v_d(q)}{\epsilon(q)} \\ &+ \frac{1}{\epsilon(q)} \left[\frac{4\pi e^2}{q^2} + C_0(q) \right] \frac{4}{(2\pi)^3} \int \frac{2m\mu^k}{\mu^E} \frac{\langle \underline{k} + \underline{q} | v_{nl}(E_k) | \underline{k} \rangle d^3k}{k^2 - (\underline{k} + \underline{q})^2} . \end{aligned} \quad (2.42)$$

The screening was calculated in the same way as described in Section 2.3.1 except that this time we retained the nonlocal and energy dependent nature of the model potential in evaluating the integral in (2.42). The depletion potential v_d arises from the difference between the charge density corresponding to the model wave function and that corresponding to the true wave function in the core region and is taken to be

$$v_d(q) = - \frac{4\pi e^2 Z\alpha}{q^2} g(x) , \quad (2.43)$$

where $g(x)$ is given by (2.29) and $-Z\alpha$ is the total depletion charge. The latter is related to the effective mass μ^E by

(Shaw and Harrison 1967)

$$\alpha = \left(\frac{1}{\mu} - 1 \right) . \quad (2.44)$$

We have not included v_{ic} because Evans (1970) did not include it and, moreover, Ballentine and Gupta (1971) found that an energy shift in E_F , due to v_{ic} , tends to cancel the direct contribution of v_{ic} .

Figure 19 shows our model potential form factor calculated with and without effective mass correction, compared to that of Evans. The curve for free-electron mass is in general agreement with that of Evans but differs slightly around the region $q = 2k_F$. The origin of this discrepancy is not clear, for the difference in the treatment of screening and the depletion potential should have little effect for these values of q . Jones (1970) has fitted Fermi surface data for solid mercury to determine an empirical pseudopotential. He found three possible solutions, one of which is quite close to the Evans potential but closer to ours. Using such a pseudopotential he obtained a conduction bandwidth smaller than the free-electron value, in conformity with an effective mass μ greater than unity (see Table I above).

The results of our calculations for liquid mercury are depicted in Figures 20-24. The more complicated structure of $\Sigma(k, E)$, especially in the imaginary part, suggests that one might expect $n(E)$ to have more pronounced structure in mercury

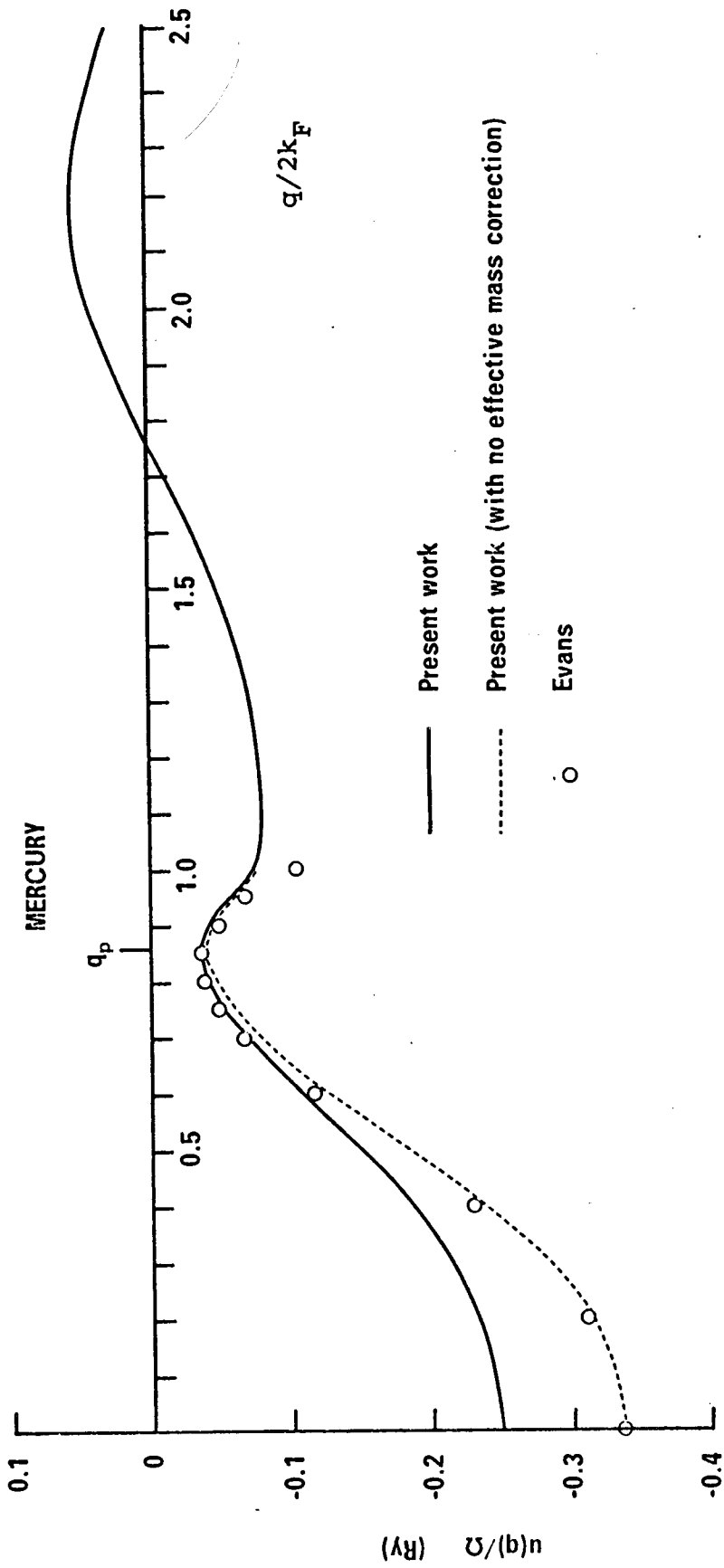


Figure 19 Model potential form factor for mercury.

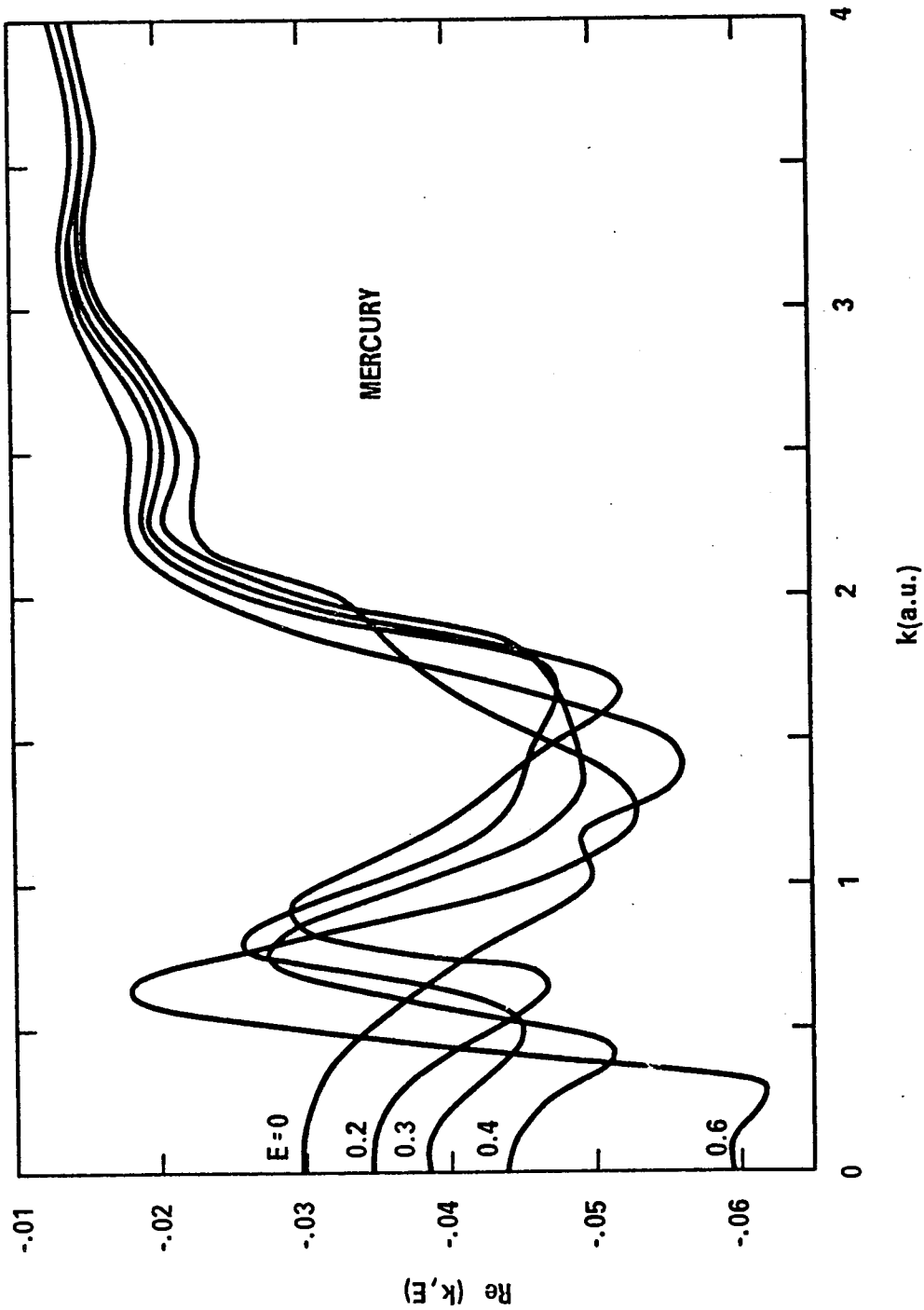


Figure 20 Real part of self-energy for mercury.

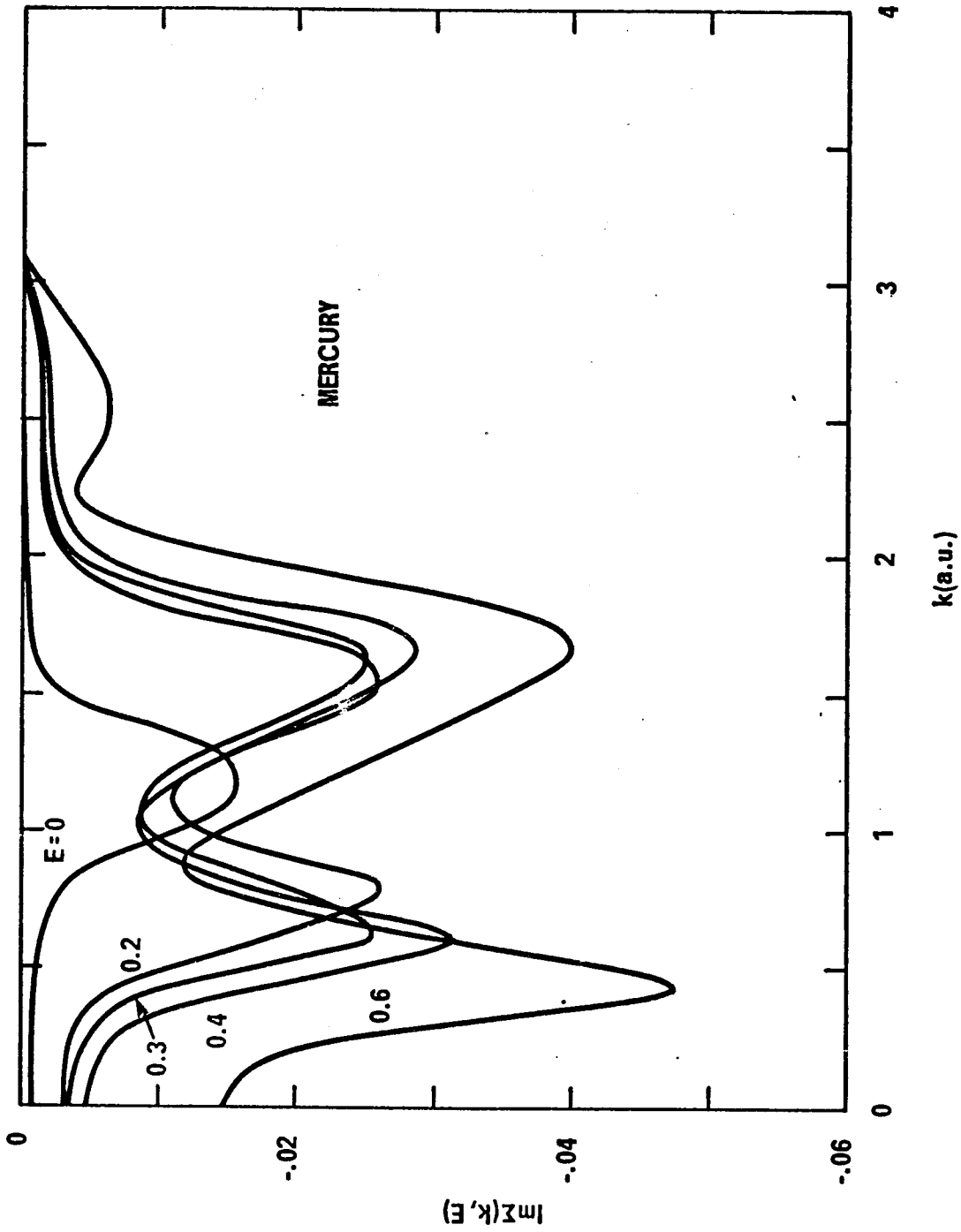


Figure 21 Imaginary part of self-energy for mercury.

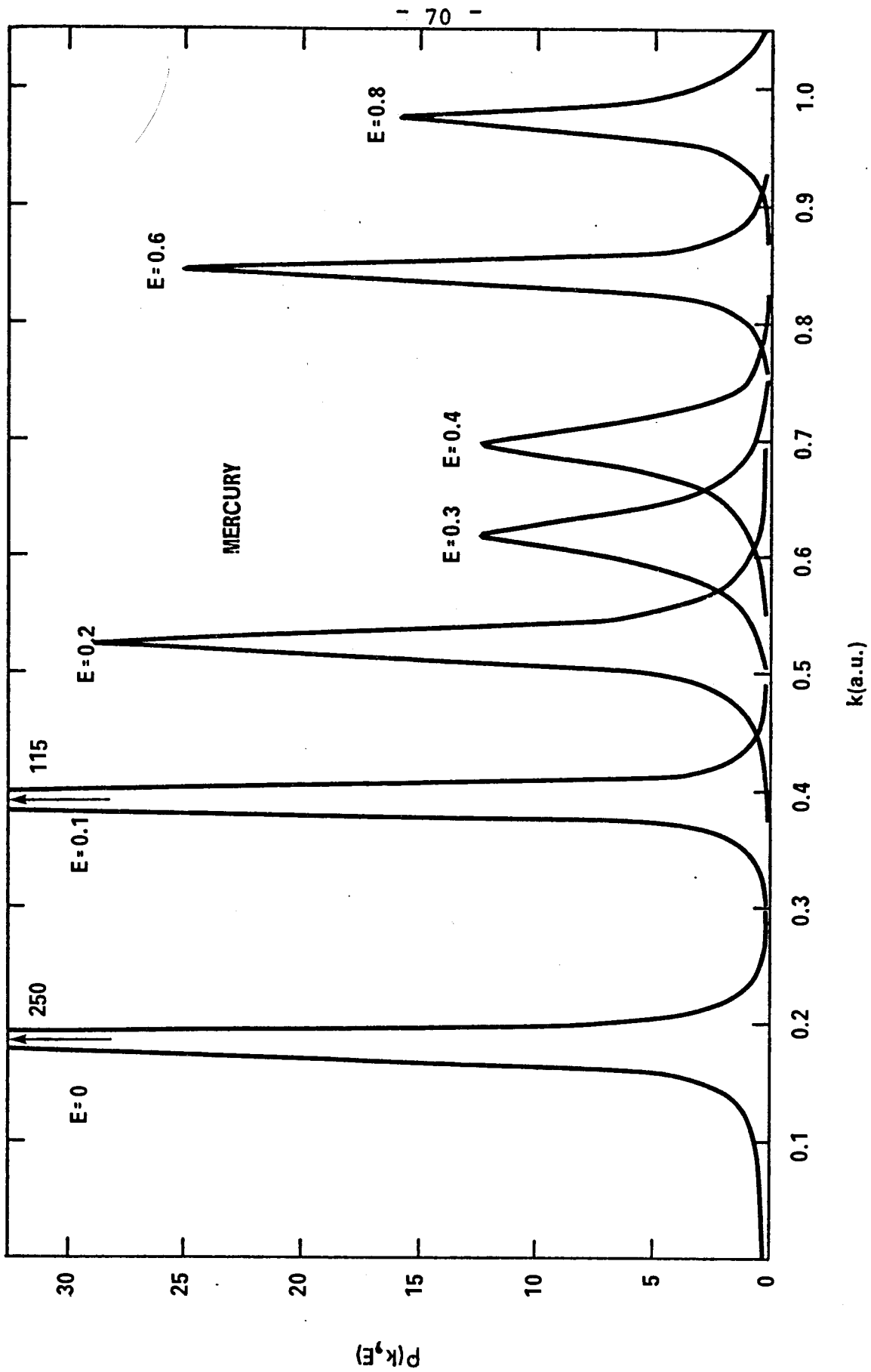


Figure 22 Spectral function $\rho(k, E)$ for mercury.

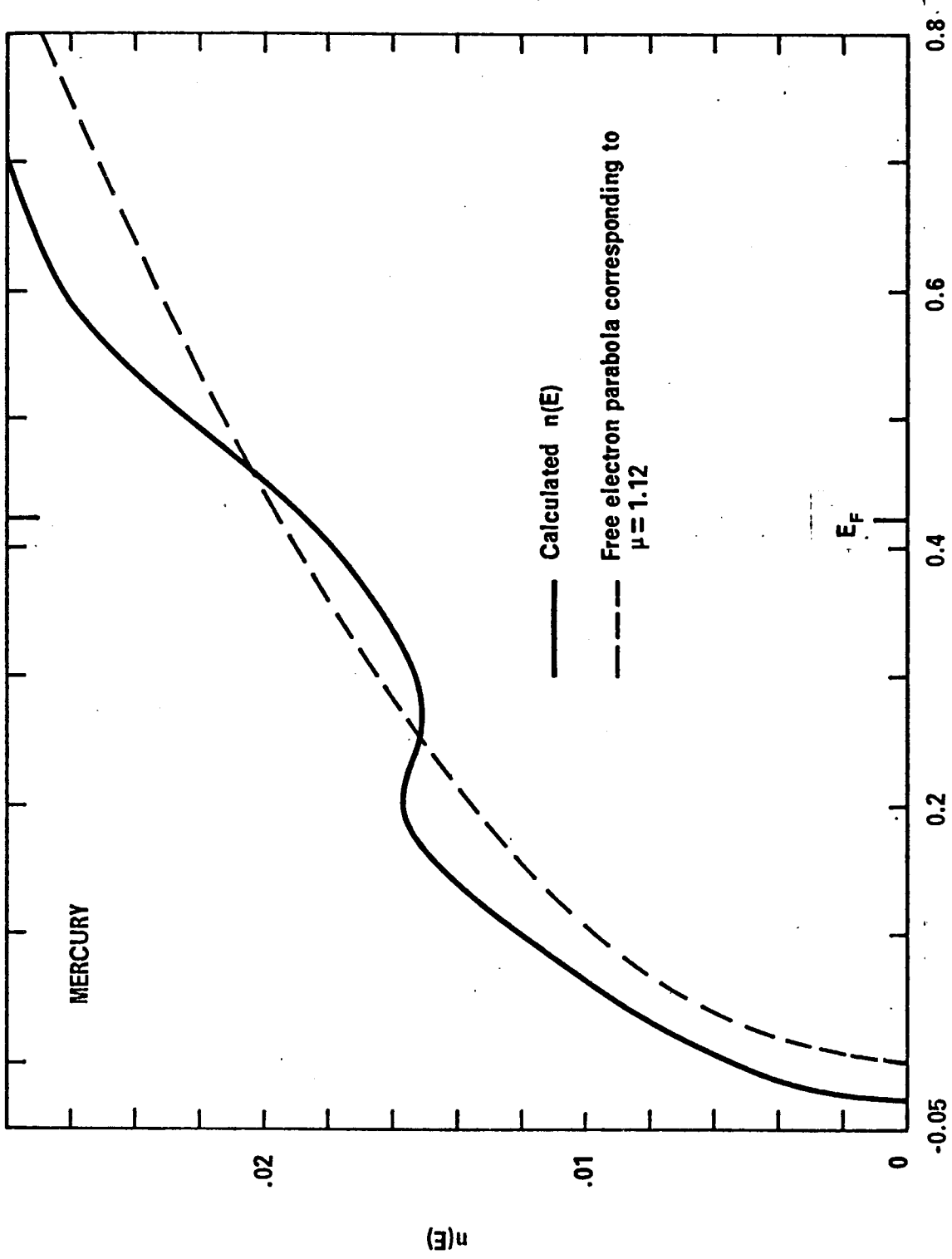


Figure 23 Density of states per unit volume (a.u.) per unit energy range, $n(E)$ for mercury.

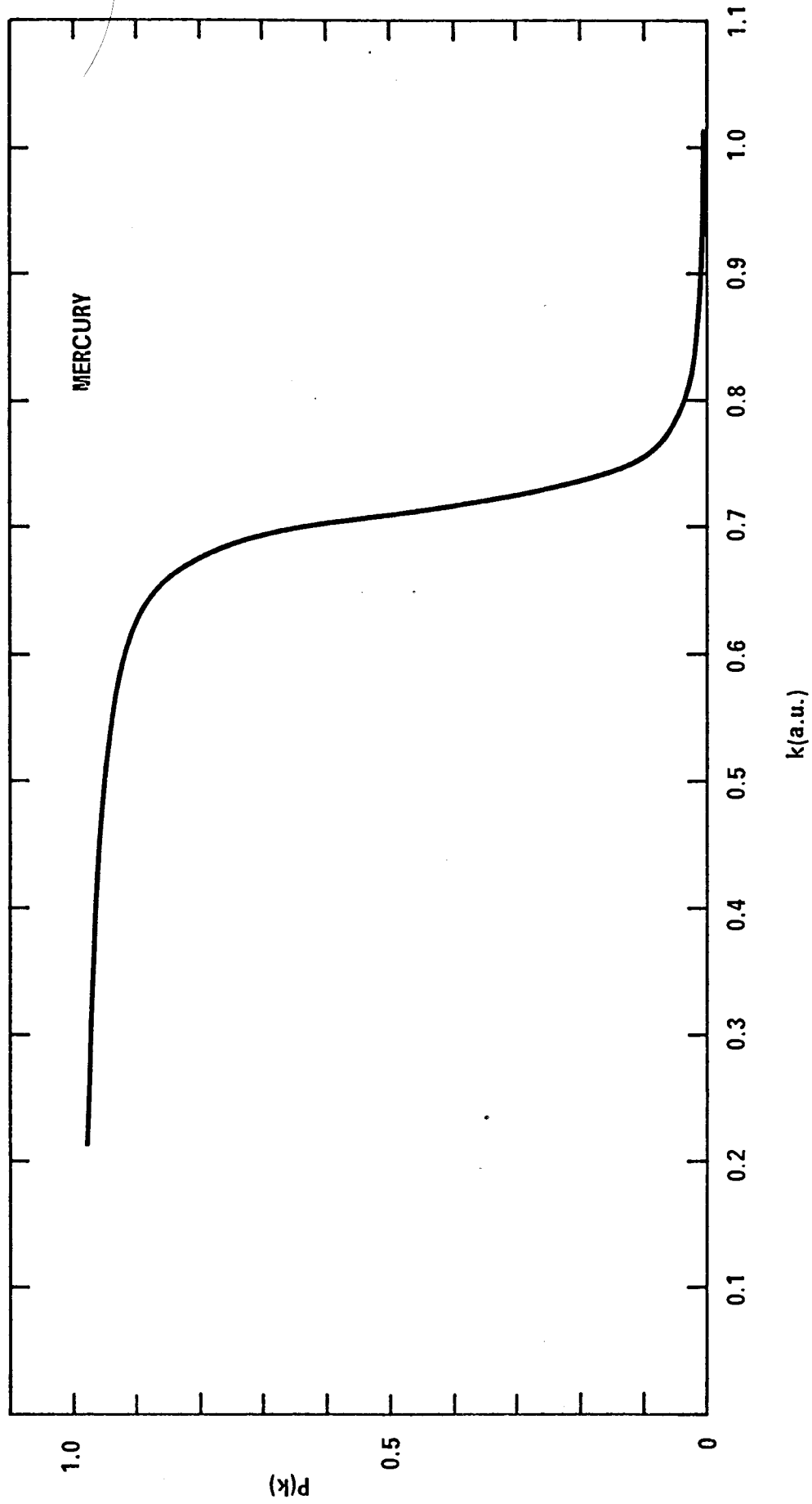


Figure 24 Momentum distribution for occupied states of mercury.

than in the other two metals previously discussed. As a matter of fact we did obtain a dip in $n(E)$ (Figure 23) but its magnitude is much smaller than that estimated by Mott (1966), and it is not likely to have any serious effect on the d.c. transport properties. Taking our results together with those of Evans (1970), we may say that the structure in $n(E)$ and the unusual transport properties of Hg and its alloys are results of the same cause (the peculiar shape of the model potential), rather than one being the cause of the other as Mott had suggested. The depletion in the density of states around $E = 0.3$ is also manifested as reduced peak height in the spectral function $\rho(k, E)$ (Figure 22), or equivalently an increase in $\text{Im}\Sigma$. We can roughly estimate the position in momentum space of the relative minimum in $n(E)$. Denoting the bottom of the band by E_0 and the energy for the minimum by E_m we have $\{\mu(E_m - E_0)\}^{\frac{1}{2}} \approx 0.59 a_0^{-1}$. This is remarkably close to the first spherical Brillouin zone boundary, $q_p/2 = 0.61 a_0^{-1}$, considering that a unique dispersion relation does not exist for a liquid and a parabolic $E - k$ relation is a poor approximation for mercury.

§2.6 Comparison of the Three Metals

We observe that the width of the spectral function (Figures 8, 15, 22) and the thickness of the Fermi surface, Δk_F (Table II) both indicate that the scattering is strongest in bismuth, weakest in indium, with mercury intermediate. This

TABLE II Some Important Results

		Bi	In	Hg
$k_F (=k_{F0})$	(a_0^{-1})	0.8582	0.7850	0.7091
Δk_F	(a_0^{-1})	0.087	0.040	0.055
E_{F0} (a)	(Ry)	0.7365	0.6162	0.5028
E_{F0}^* (b)	(Ry)	0.850	0.685	0.448
E_F	(Ry)	0.775	0.650	0.422
ΔE	(Ry)	0.861	0.675	0.452
$n_0(E_{F0})$	$(Ry^{-1} a_0^{-3})$	0.02174	0.01994	0.0180
$n_0^*(E_{F0}^*)$	$(Ry^{-1} a_0^{-3})$	0.0188	0.0179	0.0202
$n(E_F)$	$(Ry^{-1} a_0^{-3})$	0.0185	0.0178	0.0186

(a) Subscript 0 refers to free-electron values.

(b) Asterisk indicates quantities obtained with effective mass correction.

is in accord with the experimental data for d.c. resistivity ρ_L (quoted in Cusack 1963) and the values of $|u(q_p)|^2 a(q_p)/(\Delta E)^2$, where $\Delta E = E_F - E_0$ is the conduction bandwidth:

	Bi	Hg	In
ρ_L (μ ohm-cm)	128.1	90.96	33.1
$ u(q_p) ^2 a(q_p)/(\Delta E)^2$	0.0409	0.0225	0.0131

One may then wonder why it is that the density of states for mercury has more pronounced structure than bismuth. The answer lies in the difference in the shapes of the model potentials. In bismuth the form factor (Figure 5) has a steep slope at q_p and passes through zero nearby so that, as explained in Section 2.3, the use of a nonlocal model potential tends to wipe out most of the structure in $n(E)$ predicted by a local approximation. This is much less likely to happen in the case of mercury because the form factor remains quite stationary over an appreciable range of q around q_p . As regards the resistivity a local model potential should give the correct picture since only those electrons on the Fermi surface are involved. So there is actually no paradox between the different properties.

Finally we note that the value of k at which the momentum distribution $P(k) = 0.5$ is practically the same as the free-electron Fermi momentum for each of the three metals. For in-

dium and mercury we found that we could not reliably calculate $P(k)$ at small values of k because it was difficult to locate the bottom of the conduction band precisely.

CHAPTER 3

INTEGRATED DENSITY OF STATES

§3.1 The Problem of an Energy Dependent Potential

We have seen in Chapter 2 how the energy dependence of the model potential can be included approximately by means of an effective mass. Now we investigate in detail the difficulty introduced by the use of an energy dependent model potential.

Suppose we take the hamiltonian of an electron in a liquid metal to be $H = p^2/2m + W(E)$ ($= H(E)$, say), the electron-ion interaction being represented by the energy dependent model potential $W(E)$. Its eigenvectors and eigenvalues will be energy dependent,

$$H(E) | \phi_n(E) \rangle = \epsilon_n(E) | \phi_n(E) \rangle . \quad (3.1)$$

The true energy levels E_n are obtained when the parameter E in the model potential is equal to the current eigenvalue, that is,

$$E_n = \epsilon_n(E_n) . \quad (3.2)$$

Now, when we try to calculate the Green operator, as in Section 1.2, from the equation $G(E) = (E - H)^{-1}$ we obtain results similar to (1.1)-(1.5) but with $\epsilon_n(E)$ instead of the true eigenvalue E_n . Thus, in place of (1.5), we obtain

$$\sum_n \delta(E - \varepsilon_n(E)) = \sum_n \left\{ 1 - \left. \frac{\partial \varepsilon_n}{\partial E} \right|_{E=\varepsilon_n} \right\}^{-1} \delta(E - \varepsilon_n), \quad (3.3)$$

which is not equal to the density of states.

Lloyd (1967) showed that one could formally circumvent this difficulty by calculating the integrated density of states $N(E)$ using the equation

$$N(E) = -\frac{1}{\pi} \text{Tr} \text{Im} [\ln \{H - (E + i\eta)\}] \quad (3.4)$$

It is easy to show that (3.4) indeed evaluates the total number of eigenstates up to the energy E regardless of the energy dependence of the model potential. Thus, from (3.4), we have

$$\begin{aligned} N(E) &= -\frac{1}{2\pi i} \text{Tr} [\ln \{H - (E + i\eta)\} - \ln \{H - (E - i\eta)\}] \\ &= -\frac{1}{2\pi i} \sum_n [\ln \{\varepsilon_n(E) - (E + i\eta)\} - \ln \{\varepsilon_n(E) - (E - i\eta)\}] \\ &= \sum_n \theta \{E - \varepsilon_n(E)\}, \end{aligned} \quad (3.5)$$

where the step function $\theta(x)$ is equal to unity for $x > 0$ and is zero for $x < 0$.

The last step follows from the fact that the value of the logarithm changes discontinuously from $-i\pi$ to $+i\pi$ as one crosses the branch cut on the negative real axis. Equation (3.5) says that $N(E)$ is equal to the number of eigenvalues $\epsilon_n(E)$ of $H(E)$ which are less than E . The true eigenvalues E_n are determined from Equation (3.2). The number of these below energy E will also be given by $N(E)$ provided that $\partial\epsilon_n/\partial E$ is less than unity, that is as E increases $\epsilon_n(E)$ must not increase so rapidly that a level ϵ_n from just below E rises above E .

If one differentiates the right hand side of (3.5) one immediately obtains $\sum_n \delta(E - E_n)$, which is just the density of states. This leads to the hope that it may be possible to calculate $n(E)$ from

$$-\frac{1}{\pi} \text{Tr} \text{Im} \left[\frac{d}{dE} \ln \{ H - (E + i\eta) \} \right].$$

The differentiation of a function of an operator with respect to a parameter is by no means trivial because the operator does not usually commute with its derivative. We have managed to derive a general formula for this differentiation (see Appendix III), but unfortunately it turns out to involve multiple commutators which are too complicated for the present application. Finding it rather fruitless to pursue this line

of approach we turn to a direct evaluation of (3.4) (Chan and Ballentine 1971b) for the less convenient quantity $N(E)$.

§3.2 A Perturbation Expansion

The formalism for the integrated density of states presented in the last section is similar to that of Edwards (1962) except that where the Green function occurs in Edwards' formalism, we now have the logarithm. It might appear from the similarity that we could employ Edwards' technique of expanding in a formal perturbation series, taking the ensemble average and resumming the terms. However, an examination of the diagrammatic expansion reveals that such a straightforward analogy with Edwards' method will not work.

Consider the operator

$$\ln(H-E) = \ln \{ (H_0 - E)(1 - G_0 W) \}, \quad (3.6)$$

where $H = H_0 + W$, and $G_0 = (E - H_0)^{-1}$ is the free-electron Green operator. The energy dependence of G_0 and W is not explicitly indicated. Now $\ln(AB) \neq \ln A + \ln B$, in general, if the operators A and B do not commute. Nevertheless, one still has equality of the traces of the operators.

$$\begin{aligned} \text{Tr} \ln(AB) &= \ln(\det |AB|) \\ &= \ln(\det A) + \ln(\det B) \end{aligned}$$

$$= \text{Tr} \ln A + \text{Tr} \ln B^* \quad (3.7)$$

From (3.4), (3.6), and (3.7), we then obtain

$$N(E) = -\frac{1}{\pi} \text{Tr} \text{Im} \{ \ln(H_0 - E) + \ln(1 - G_0 W) \} \quad (3.8)$$

The first term is just $N_0(E)$, the number of energy levels below E for the free-electron hamiltonian H_0 .

To evaluate the second term it is natural to try a formal expansion,

$$-\ln(1 - G_0 W) = G_0 W + \frac{1}{2} G_0 W G_0 W + \frac{1}{3} G_0 W G_0 W G_0 W + \dots \quad (3.9)$$

The ensemble average, $\langle \langle \mathbf{k} | -\ln(1 - G_0 W) | \mathbf{k} \rangle \rangle_{\text{ave}}$, of the diagonal matrix element in the momentum representation can be represented by the diagrammatic series shown in Figure 25. The notation here is the same as in Section 1.4. If the n^{-1} factors were not present, we would be able to sum up "propagator renormalization" diagrams of all orders. Indeed, since these diagrams differ from ordinary Green function diagrams only by the lack of a G_0 line on their right hand ends, the sum of all diagrams omitting n^{-1} factors would be $(G - G_0)G_0^{-1}$.

*We are indebted to Dr. P. Lloyd for pointing out this relation.

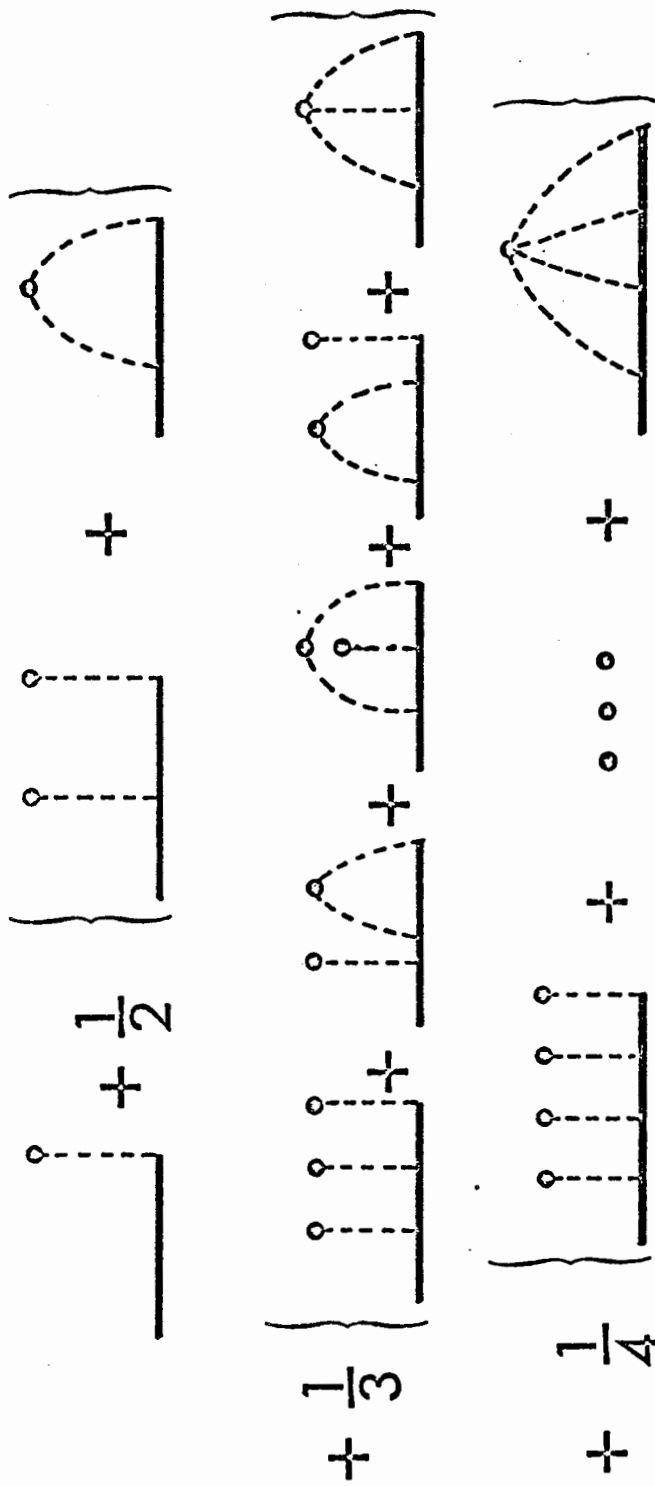


Figure 25 Diagrammatic representation of $-\langle\langle k | \ln(1 - G W) | k \rangle\rangle_{\text{ave}}$

The troublesome n^{-1} factors can be eliminated if we consider instead the expression $-\lambda \left(\frac{d}{d\lambda} \right) \ln(1 - G_0 \lambda W)$. This can be represented by the same diagrams as in Figure 25 except that now the vertex corresponds to $\lambda \langle k|w|k' \rangle$ rather than $\langle k|w|k' \rangle$ and the n^{-1} factors are absent. Examining the set of diagrams, we see that they are those for the ensemble average diagonal matrix element of $(G_\lambda - G_0) G_0^{-1}$, or equivalently of $G_\lambda \lambda W$. Here we have defined a Green operator

$$G_\lambda(E) = [E - H_0 - \lambda W(E)]^{-1}. \quad (3.10)$$

Its ensemble average diagonal matrix element can be written in the form (units $\hbar = 2m = \frac{1}{2}e^2 = 1$)

$$\langle\langle \tilde{k} | G_\lambda(E) | \tilde{k} \rangle\rangle_{ave} = [E - \tilde{k}^2 - \Sigma_\lambda(\tilde{k}, E)]^{-1}, \quad (3.11)$$

where the self-energy function $\Sigma_\lambda(k, E)$ is defined by this equation and is formally given by the sum of all irreducible diagrams (Edwards 1958, 1962; Ballentine 1966; see also Sections 1.2 and 1.4, this thesis).

The result of this diagrammatic analysis is

$$\begin{aligned} & \left\langle - \left\langle \tilde{k} \left| \lambda \frac{d}{d\lambda} \ln(1 - G_0 \lambda W) \right| \tilde{k} \right\rangle \right\rangle_{ave} \\ &= \left\langle \left\langle \tilde{k} \left| (G_\lambda - G_0) G_0^{-1} \right| \tilde{k} \right\rangle \right\rangle_{ave} \end{aligned} \quad (3.12)$$

$$= \sum_{\lambda} (\kappa, E) [E - \kappa^2 - \Sigma_{\lambda}(\kappa, E)]^{-1}.$$

The problem of evaluating (3.8) is thus reduced to the computation of the self-energy function Σ_{λ} of a Green operator containing λW as the potential energy, and familiar techniques and approximations (Ballentine 1966) may be used.

The result (3.12) can also be derived algebraically without reference to diagrams although it is unlikely that we would have discovered it without diagrammatic analysis. If $A(\lambda)$ is an operator depending upon a parameter λ , then the usual rule of calculus

$$\frac{d}{d\lambda} (\ln A) = A^{-1} \frac{dA}{d\lambda}$$

is valid, in general, only if the two operators A and $dA/d\lambda$ commute (see Appendix III). For $A = (1 - G_0 \lambda W)$, this condition is clearly satisfied.

Hence

$$\begin{aligned} -\lambda \frac{d}{d\lambda} \ln(1 - G_0 \lambda W) &= \lambda (1 - G_0 \lambda W)^{-1} G_0 W \\ &= (G_0^{-1} - \lambda W)^{-1} \lambda W \\ &= (E - H_0 - \lambda W)^{-1} \lambda W \end{aligned}$$

$$= G_{\lambda} \lambda W .$$

It is not convenient to calculate the ensemble average of this expression because both factors G_{λ} and W depend upon the arrangement of the ions. However, with a little manipulation one obtains

$$\begin{aligned} G_{\lambda} \lambda W &= G_{\lambda} (G_0^{-1} - G_{\lambda}^{-1}) \\ &= (G_{\lambda} - G_0) G_0^{-1} . \end{aligned}$$

This can be averaged directly because only G_{λ} depends upon the arrangement of the ions. Equation (3.12) now follows immediately upon taking the diagonal matrix element in momentum representation.

Writing

$$M(\lambda, E) = -\frac{1}{\pi} \left\langle \text{Im Tr} \left\{ \lambda \frac{d}{d\lambda} \ln(1 - G_0 \lambda W) \right\} \right\rangle_{\text{ave}} , \quad (3.13)$$

we have, from (3.12),

$$\begin{aligned} M(\lambda, E) &= \frac{1}{\pi} \frac{L^3}{(2\pi)^3} \int \text{Im} \left\{ \frac{\Sigma_{\lambda}(k, E)}{E - k^2 - \Sigma_{\lambda}(k, E)} \right\} d^3k \\ &= \frac{L^3}{2\pi^3} \int_0^{\infty} \text{Im} \left\{ \frac{\Sigma_{\lambda}(k, E)}{E - k^2 - \Sigma_{\lambda}(k, E)} \right\} k^2 dk , \quad (3.14) \end{aligned}$$

where L^3 is the normalization volume. In terms of $M(\lambda, E)$ equation (3.8) becomes

$$N(E) = N_0(E) + \int_0^1 \frac{M(\lambda, E)}{\lambda} d\lambda . \quad (3.15)$$

In (3.15) it is understood that $N(E)$ now represents the ensemble average number of states. It should be emphasized that, contrary to the effective mass approximation in Chapter 2, the present method of handling the energy dependence of the model potential is exact.

To gain some insight into our new formalism consider the simple case of a uniform potential $W = W_0(E)$, which is independent of position \underline{x} but depends on the parameter E . Then

$$\sum_{\lambda} (\underline{k}, E) = \lambda W_0(E)$$

and, from (3.14),

$$\begin{aligned} M(\lambda, E) &= \frac{1}{\pi} \sum_{\underline{k}} \text{Im} \frac{\lambda W_0(E)}{E - \underline{k}^2 - \lambda W_0(E)} \\ &= -\lambda W_0(E) n_0(E - \lambda W_0(E)) , \end{aligned} \quad (3.16)$$

where

$$\begin{aligned} n_0(E) &= -\frac{1}{\pi} \sum_{\mathbf{k}} \text{Im} \frac{1}{E - k^2} \\ &= \frac{L^3}{4\pi^2} E^{1/2} \end{aligned}$$

is the free-electron density of states. Substituting (3.16) into (3.15) and performing the integral we have,

$$N(E) = N_0(E - W_0(E)) .$$

Thus the effect of a uniform, energy dependent potential is, as expected, to shift the free-electron energy spectrum by an amount $W_0(E)$ which depends on the energy. The corresponding density of states is

$$n(E) = n_0(E - W_0(E)) \left(1 - \frac{dW_0}{dE}\right) . \quad (3.17)$$

We may compare this result with standard band structure calculation. Since the potential does not depend on position we have a unique E-k dispersion relation,

$$E(k) = k^2 + W_0(E) ,$$

from which

$$n(E) = \frac{L^3}{2\pi^2} k^2 \left(\frac{dE}{dk}\right)^{-1}$$

$$\begin{aligned} &= \frac{L^3}{4\pi^2} k \left(1 - \frac{dW_0}{dE} \right) \\ &= n_0 (E - W_0(E)) \left(1 - \frac{dW_0}{dE} \right) , \end{aligned}$$

in agreement with (3.17).

Although we have overcome the problem of an energy dependent model potential in calculating the number of states $N(E)$, we are now unable to determine any spectral information about the states. Just as the diagonal matrix element of the Green operator (1.1) yields the spectral function $\rho(k, E)$, (1.3) whose trace is the density of states per unit energy (1.5), so the diagonal matrix element of $\ln(H-E)$ will yield the quantity

$$\int_{-\infty}^E \rho(k, E') dE' .$$

But it was necessary for us to replace $\ln(H-E)$ by another operator with the same trace (using (3.7)) in order to do perturbation theory. Thus we have given up the possibility of obtaining information about the spectral function.

§3.3 Application to Bismuth

To apply Eqs. (3.14) and (3.15) in a practical calculation we have to evaluate $\Sigma_\lambda(k, E)$ for different values of the parameter λ between 0 and 1. We evaluate $\Sigma_\lambda(k, E)$ by solving self-consistently, as in Chapter 2, the integral equation

$$\Sigma_\lambda(k, E) = \eta \lambda u(k, k, E) + \frac{\eta \lambda^2}{(2\pi)^3} \int \frac{|u(k, k', E)|^2 a(q)}{E - (k')^2 - \Sigma_\lambda(k', E)} d^3k', \quad (3.18)$$

where $u(k, k', E)$ is again given by (2.19), but with the argument E_F replaced by E , and the other symbols have the same meaning as in (2.18) and (1.17). Note that since a nonlocal, energy dependent model potential will be used, the first order term depends on k and E , and therefore cannot be set equal to zero by a shift of the origin. In terms of diagrams we are approximating the complete series of irreducible diagrams by the partial sum in Figure 26, which is the analog of the series represented by Figure 2 (b) and (d).

We have used the same model potential and structure factor for bismuth as in Section 2.3. The numerical solution of the integral equation for the self-energy function also proceeded in the same manner, but of course this time both $u(k, k', E)$ and the angular integral $f(k, k', E)$ (See Eqs. (2.19) to (2.21)) must be evaluated at the appropriate energy. We

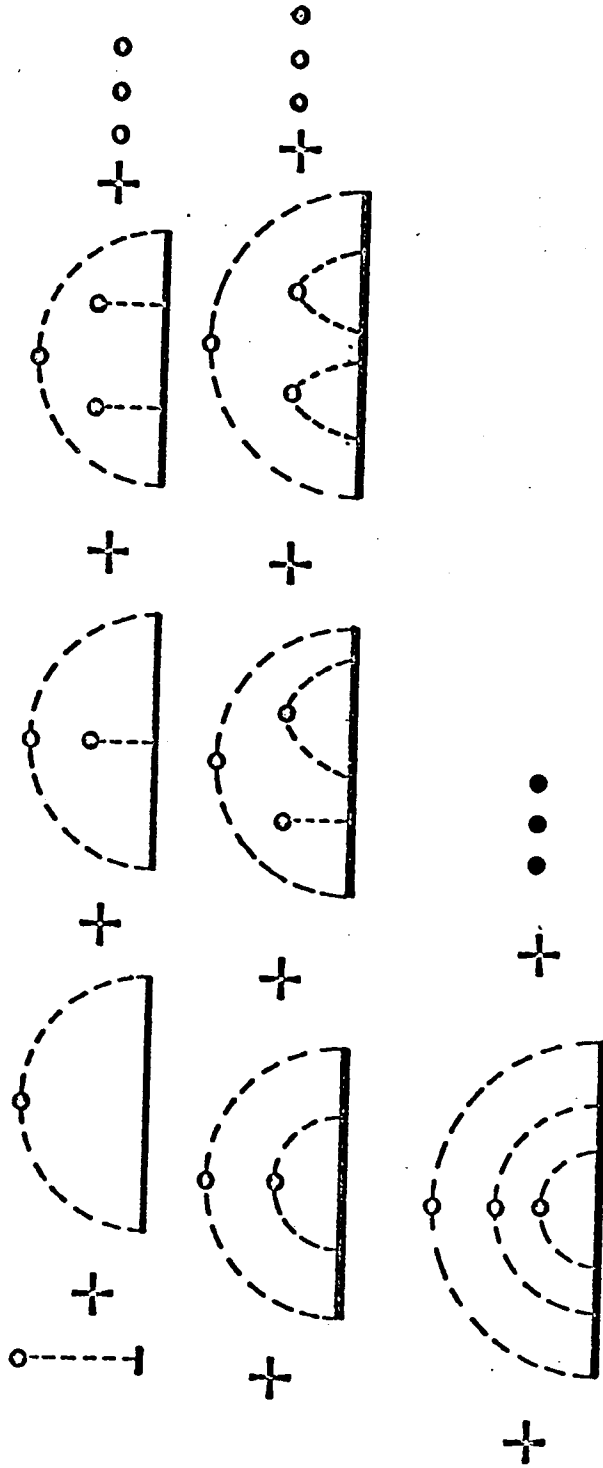


Figure 26 Diagrams summed by the integral Equation (3.18).

have made use of the assumed linear energy dependence of the model potential parameters $A_\ell(E)$, and hence of $u(E)$, to obtain the value of f at any energy E from its value at the Fermi energy. The results for $M(\lambda, E)/\lambda$ and $N(E)$ are shown in Figures 27 and 28. For convenience $N(E)$ has been expressed in number of electronic states per atom.

The numerical computation becomes inaccurate for very small values of λ . However, the limiting value of $M(\lambda, E)/\lambda$ as $\lambda \rightarrow 0$ can be easily obtained from (3.18) by treating λ as a perturbation parameter. The result for this limiting value is zero for negative E , and for positive E it is

$$-\frac{1}{4\pi^2} n u(\kappa, \kappa, E) \kappa, \quad \text{with } \kappa^2 = E.$$

Because the model potential parameters $A_\ell(E)$ are tabulated at the Fermi energy (Animalu, 1965), we must first estimate the position of E_F on our energy scale before we can begin the calculation. Using first order perturbation theory, we estimated it to be 0.246 on the scale of Figure 28. However, it turns out that $N(E)$ equals 5 electrons per atom at $E = 0.146$. In principle, one could correct this inaccuracy of the first order initial approximation by readjusting E_F , the energy for which we use the tabulated parameters $A_\ell(E_F)$, until it became self-consistent with the energy value for which $N(E)$ equals 5

Figure 27 $M(\lambda, E)/\lambda$ (per unit volume) versus λ for several values of E . See Eqs.(3.13) and (3.14) for the definition of this function.

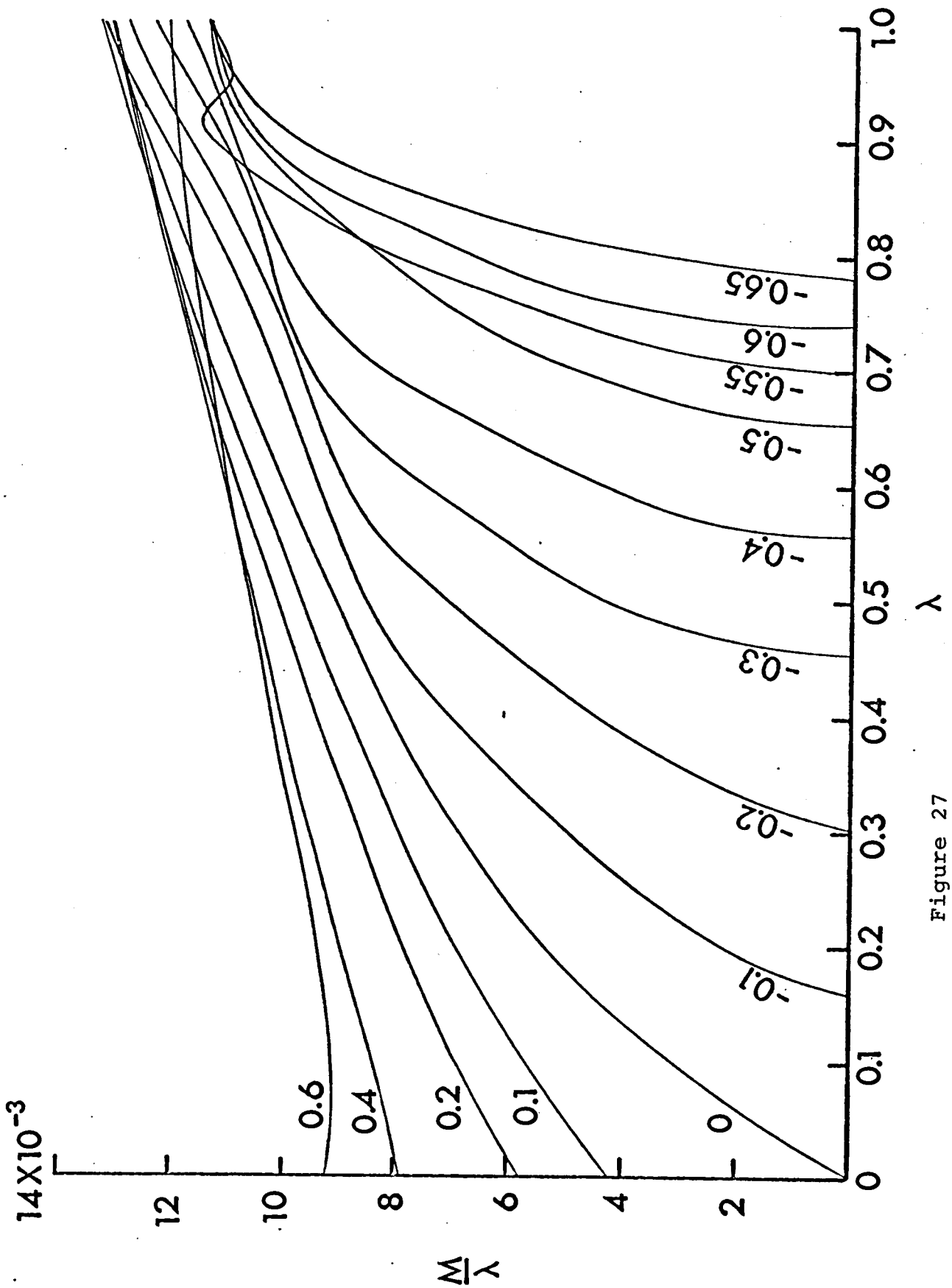


Figure 27

Figure 28 Number $N(E)$ of electronic states per atom below energy E , calculated for liquid bismuth at 300°C . Solid curve: calculated result. Dashed curve: best fitting free-electron curve, corresponding to $m^*/m = 0.63$. Dotted curve: obtained by integrating $n(E)$ curve (case 4) in Figure 9. Last two curves shifted so that all three curves coincide at $E = E_F$.

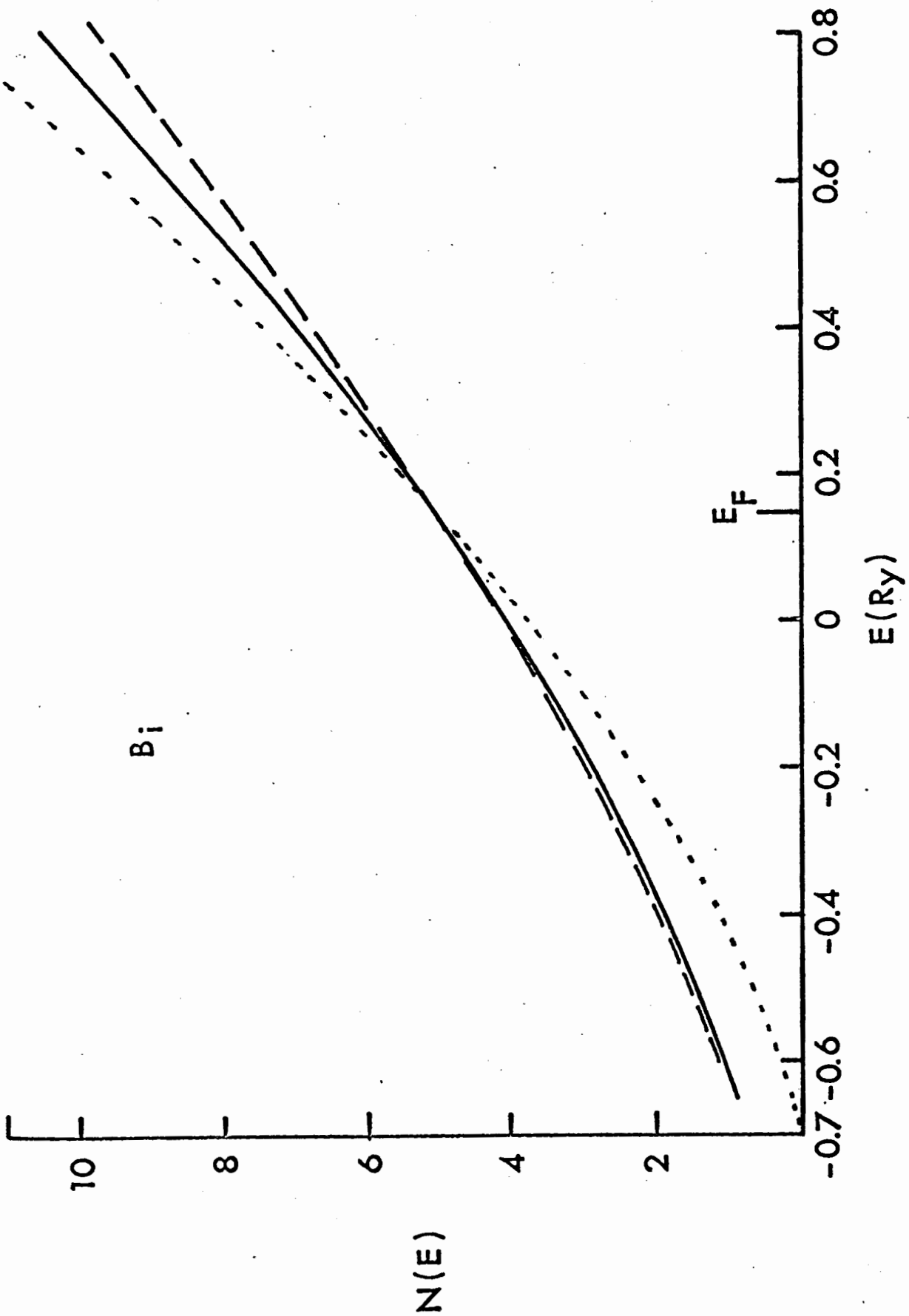


Figure 28

Figure 29 Similar to Figure 28 but $N^{2/3}$ plotted.
The free-electron (dashed) curve is now
a straight line.

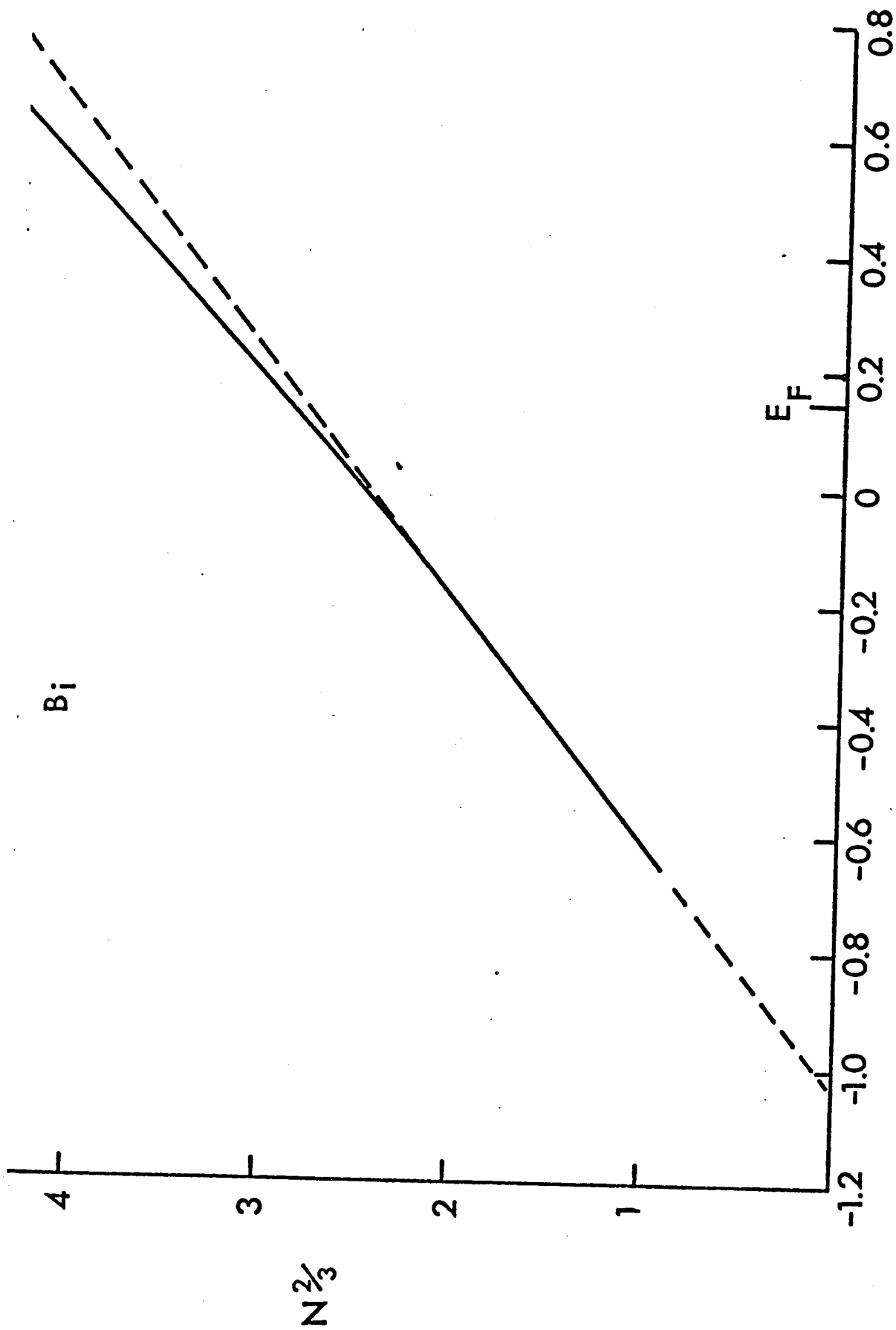


Figure 29

electrons per atom. Because of the very large amount of computer time needed for this calculation, we have not carried out this iteration to obtain a self-consistent Fermi energy. This means that the model potential form factor which was actually used in the calculation at the point marked E_F in Figure 28 was not the Fermi energy shell form factor shown in Figure 5, but instead it was the form factor corresponding to an energy shell 0.1 Ry lower. The difference between these two form factors is very small (~ 0.005 Ry), and it is not likely to have a significant effect on the final results.

§3.4 Discussion

The distribution of electron states (Figure 28) calculated for bismuth has very little structure, and does not differ greatly from a $E^{3/2}$ free-electron curve modified by an effective mass. (The zero of the energy scale has no absolute significance.) This can be seen more clearly in Figure 29, where we have plotted $N^{2/3}$ versus E . The lower portion of the curve is well fitted by a straight line, which we have extrapolated from our lowest computed point ($E = -0.65$) to the bottom of the band. We obtain a bandwidth of 1.18 Ry, compared with the free-electron bandwidth of 0.74 Ry and the bandwidth 0.861 Ry of Chapter 2. The corresponding bandwidth effective mass here is $\mu = m^*/m = 0.63$, compared with the first order estimate of 0.87 of Chapter 2.

The smaller value of the bandwidth effective mass may be attributed to higher order contributions, and in particular

to the energy dependence of the off-diagonal matrix elements of the model potential. The fact that $E(k)$ does not really exist for a disordered system may also be relevant.

Except for the difference in the effective masses obtained the results of this chapter are quite similar to those in Section 2.3 as far as the qualitative nature of structure is concerned. This is clear from a comparison of the curve (dotted line in Figure 28) obtained by integrating the previous $n(E)$ (case 4 of Figure 9) to the present $N(E)$ curve (solid line in Figure 28). There is no sharp structure in either case.

The curves of $M(\lambda, E)/\lambda$ suggest some structure near $E = -0.55$, but it does not show up on the curve of $N(E)$.

The model potential which we have used was considered to be the best available at the time when the calculation was begun. Since then it has been demonstrated (Evans et al. 1969, Evans 1970) that the linear extrapolation of the model potential parameters $A_\lambda(E)$ from the energies of excited ionic states to the energies of the conduction band in a metal (as was done by Animalu and Heine (1965)) may be inaccurate if the highest core level is a d-state. More reliable values of $A_\lambda(E)$ and dA_λ/dE at conduction band energies can be obtained by a nonlinear extrapolation using the quantum defect method (Ham 1955). The work of Evans (1970) and our calculations in Section 2.5 showed that this nonlinear extrapolation has important consequences for mercury, in which the highest core levels are very

close to the conduction band, but it is not known how important these effects would be for bismuth.

PART II

FREQUENCY-DEPENDENT CONDUCTIVITY

CHAPTER 4

FORMAL THEORY

§4.1 Introduction

The experimental results on the optical conductivity $\sigma(\omega)$ of most liquid metals can be fitted adequately to the Drude formula (see Faber 1966 for a review):

$$\sigma(\omega) = \sigma(0) / (1 + \omega^2 \tau^2), \quad (4.1)$$

where ω is the angular frequency and τ is the relaxation time. The case of mercury is an exception. There are two apparently contradictory sets of data. Ellipsometric measurements by Hodgson (1959, 1960, 1961, 1962), Smith (1967a) and Faber and Smith (1968) have yielded values substantially higher than those predicted by Eq. (4.1). Taken together with the recent low frequency determination by Faber and Comins (private communication), these results indicate a peak in $\sigma(\omega)$ at $\hbar\omega \sim 0.6$ eV as illustrated schematically in Figure 30. On the other hand, the reflectivity data of Schulz (1957), Wilson and Rice (1966) and Bloch and Rice (1969) agree with the predictions of the Drude theory to within a remarkable precision.

Several explanations have been advanced for this unusual optical behaviour of liquid mercury. Smith (1968) suggested that it may be understood in terms of the predominance of back-scattering of the electrons in mercury whereas Bloch and Rice

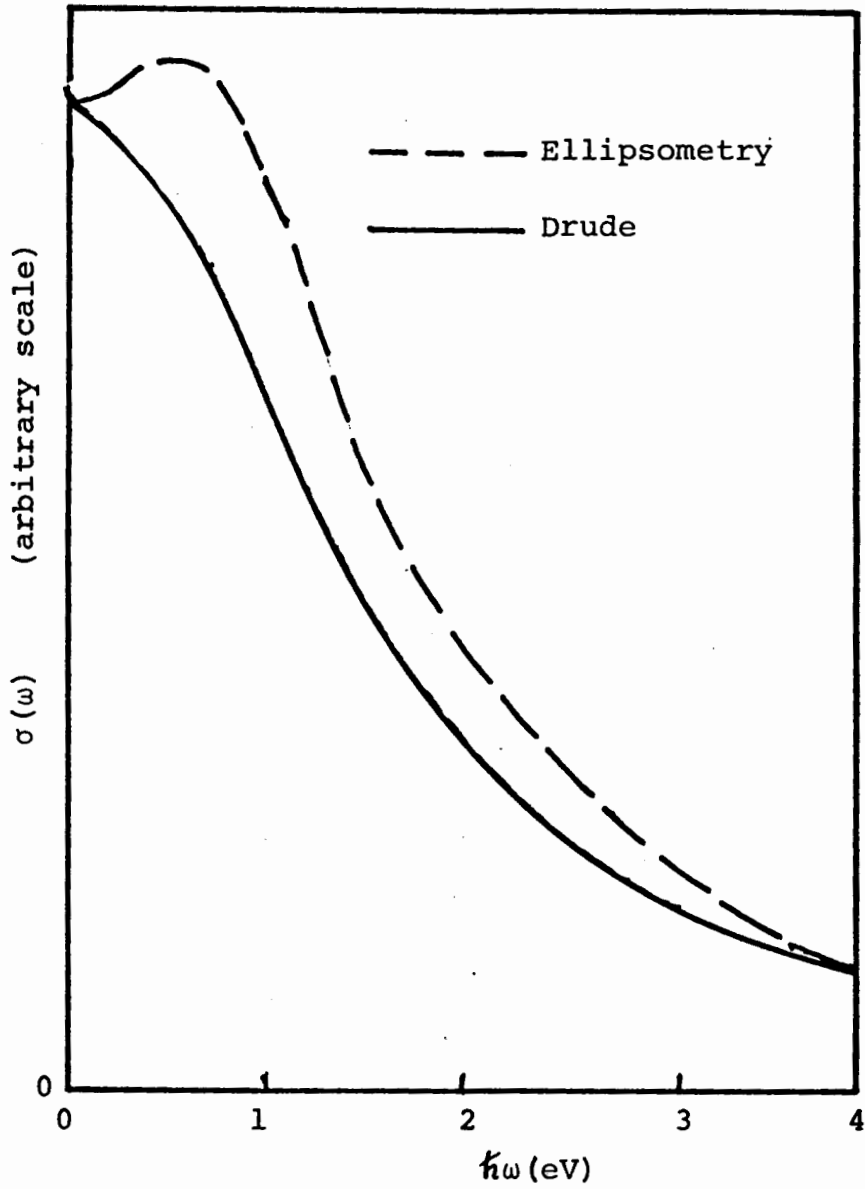


Figure 30. Schematic frequency variation of the optical conductivity of mercury as measured by ellipsometry.

(1969) surmised that the surface of mercury is not a geometric boundary, but a transition zone over which the properties of the system vary from those of the bulk metal to those of the contact medium and it is the sensitivity to such surface properties that give rise to the anomalous results obtained by ellipsometry. More pertinent to the present work is Mott's hypothesis (1966) that the abnormal optical properties of mercury, like its high d.c. resistivity, are due to the low density of states near the Fermi energy, a peak in $\sigma(\omega)$ occurring when the photon energy is sufficient to bridge the low-density region. In Section 2.5 we have found a dip in the density of electronic states $n(E)$ of mercury, although it is less severe than that suggested by Mott. It is therefore desirable to carry out an explicit calculation of the influence of $n(E)$ on the optical conductivity. In this chapter we shall reduce the Kubo-Greenwood formula (Kubo 1957, Greenwood 1958) to a form suitable for the present application. In order to make the calculations tractable certain approximations will be introduced. Various parametrized model Green functions corresponding to different densities of states will be used in Chapter 5 to evaluate $\sigma(\omega)$ numerically. The effect of $n(E)$ on the zero-frequency conductivity will also be studied.

§4.2 Reduction of the Kubo-Greenwood Formula

In the independent-electron model the Kubo-Greenwood formula for the frequency-dependent conductivity of a metal can be written (in units $\hbar = 1$) as

$$\sigma_{\mu\nu}(\omega) = \lim_{\eta \rightarrow 0^+} \frac{2i}{L^3} \sum_{\substack{\lambda, s \\ \lambda \neq s}} \frac{(j_\mu)_{\lambda s} (j_\nu)_{s\lambda}}{E_\lambda - E_s + \omega + i\eta} \frac{f(E_s) - f(E_\lambda)}{E_\lambda - E_s} \quad (4.2)$$

The notation is the conventional one: $f(E)$ is the Fermi-Dirac distribution function, j_μ stands for the μ th component of the one-electron current operator, and

$$(j_\mu)_{\lambda s} = \langle \psi_\lambda | j_\mu | \psi_s \rangle$$

where $|\psi_r\rangle$ denotes the eigenvector of the one-electron hamiltonian with the eigenvalue E_r . Only the absorptive part, which is equal to the real part in the absence of a magnetic field, needs to be considered, the imaginary part (corresponding to the dielectric constant) being related to it through the Kramers-Kronig relation. Thus

$$\text{Re } \sigma_{\mu\nu}(\omega) = \frac{2\pi}{L^3} \sum_{\substack{\lambda, s \\ \lambda \neq s}} (j_\mu)_{\lambda s} (j_\nu)_{s\lambda} \delta(E_\lambda - E_s + \omega) \frac{f(E_s) - f(E_\lambda)}{E_\lambda - E_s} \quad (4.3)$$

Now, if there is no magnetic field, the current operator is given by

$$\vec{j} = \frac{e}{m} \vec{p} \quad , \quad (4.4)$$

where \vec{p} is the canonical momentum. Expanding in terms of the

momentum eigenstates $|\underline{k}\rangle$ we have

$$(\dot{j}_\mu)_{rs} (\dot{j}_\nu)_{sr} = \frac{e^2}{m} \sum_{\underline{k}, \underline{k}'} k_\mu k'_\nu \langle \underline{k}' | \psi_r \rangle \langle \psi_r | \underline{k} \rangle \langle \underline{k} | \psi_s \rangle \langle \psi_s | \underline{k}' \rangle. \quad (4.5)$$

The result of inserting (4.5) into (4.3) and introducing the operator,

$$\rho(E) = \sum_\lambda |\psi_\lambda\rangle \langle \psi_\lambda| \delta(E - E_\lambda), \quad (4.6)$$

is

$$\begin{aligned} \text{Re } \sigma_{\mu\nu}(\omega) &= \frac{2\pi e^2}{m^2 L^3} \int dE \int dE' \sum_{\underline{k}, \underline{k}'} k_\mu k'_\nu \langle \underline{k}' | \rho(E) | \underline{k} \rangle \langle \underline{k} | \rho(E') | \underline{k}' \rangle \\ &\quad \times \delta(E - E' + \omega) \frac{f(E') - f(E)}{E - E'} \\ &= \frac{2\pi e^2}{m^2 L^3} \int dE \sum_{\underline{k}, \underline{k}'} k_\mu k'_\nu \langle \underline{k}' | \rho(E) | \underline{k} \rangle \langle \underline{k} | \rho(E - \omega) | \underline{k}' \rangle \\ &\quad \times \frac{f(E - \omega) - f(E)}{\omega}. \end{aligned} \quad (4.7)$$

It is convenient to introduce the Green operator

$$\begin{aligned} G(E) &= \frac{1}{E - H} \\ &= \sum_\lambda \frac{|\psi_\lambda\rangle \langle \psi_\lambda|}{E - E_\lambda}. \end{aligned} \quad (4.8)$$

The matrix elements of $\rho(E)$ can then be expressed as

$$\begin{aligned} \langle \underline{k} | \rho(E) | \underline{k}' \rangle &= -\frac{1}{\pi} \text{Im} \langle \underline{k} | G^+(E) | \underline{k}' \rangle \\ &= \frac{1}{\pi} \text{Im} \langle \underline{k} | G^-(E) | \underline{k}' \rangle, \end{aligned} \quad (4.9)$$

where

$$G^\pm(E) = \lim_{\eta \rightarrow 0^+} G(E \pm i\eta).$$

The formula for $\text{Re } \sigma_{\mu\nu}$ involves the operator product $\rho(E)\rho(E')$, which can be related to $G^\pm(E)$ by

$$\rho(E)\rho(E') = \frac{1}{2\pi^2} \text{Re} (G^+(E)G^-(E') - G^+(E)G^+(E')). \quad (4.10)$$

Generalizing the notation of Langer (1960) and Neal (1970) we introduce,

$$K_{\mu\nu}^{\pm\pm}(\underline{k}; E, E') \equiv \left\langle \sum_{\underline{k}'} k_\mu k'_\nu \langle \underline{k} | G^\pm(E) | \underline{k}' \rangle \langle \underline{k}' | G^\pm(E') | \underline{k} \rangle \right\rangle_{\text{ave}}. \quad (4.11)$$

In this notation (4.7) becomes, upon using (4.10),

$$\begin{aligned} \operatorname{Re} \sigma_{\mu\nu}(\omega) &= \frac{2\pi e^2}{m^2 L^3} \int dE \frac{f(E-\omega) - f(E)}{\omega} \\ &\times \sum_{\underline{k}} \frac{1}{2\pi^2} \operatorname{Re} \left\{ K_{\mu\nu}^{+-}(\underline{k}; E, E-\omega) - K_{\mu\nu}^{++}(\underline{k}; E, E-\omega) \right\}. \end{aligned} \quad (4.12)$$

For a liquid metal the ensemble averaging ensures isotropy, and so the conductivity tensor is diagonal,

$$\sigma = \frac{1}{3} \sum_{\mu} \sigma_{\mu\mu}.$$

If we define

$$K^{+-}(\underline{k}; E, E') = \sum_{\mu} K_{\mu\mu}^{+-}(\underline{k}; E, E'), \quad (4.13)$$

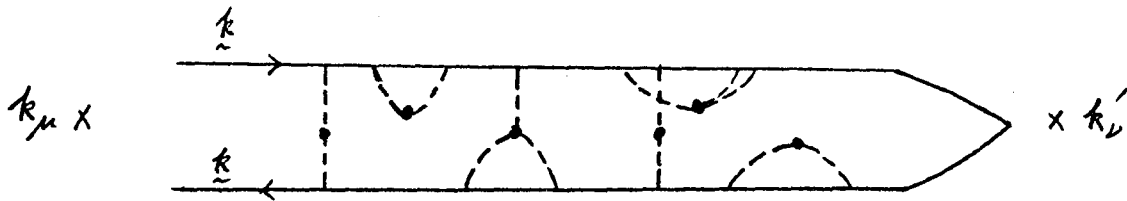
then (4.12) can be written as

$$\begin{aligned} \operatorname{Re} \sigma(\omega) &= \frac{1}{3\pi} \int dE \frac{f(E-\omega) - f(E)}{\omega} \\ &\times \left(\frac{e}{m}\right)^2 \frac{1}{(2\pi)^3} \int d^3k \operatorname{Re} \left\{ K^{+-}(\underline{k}; E, E-\omega) - K^{++}(\underline{k}; E, E-\omega) \right\}. \end{aligned} \quad (4.14)$$

Equation (4.14) is the frequency-dependent generalization of the expression for the d.c. conductivity given by Langer (1960) and Neal (1970). Our work is more closely related to that of Neal, who was also dealing with liquid metals whereas Langer was interested in the many-body effects on scattering by uncorrelated impurities.

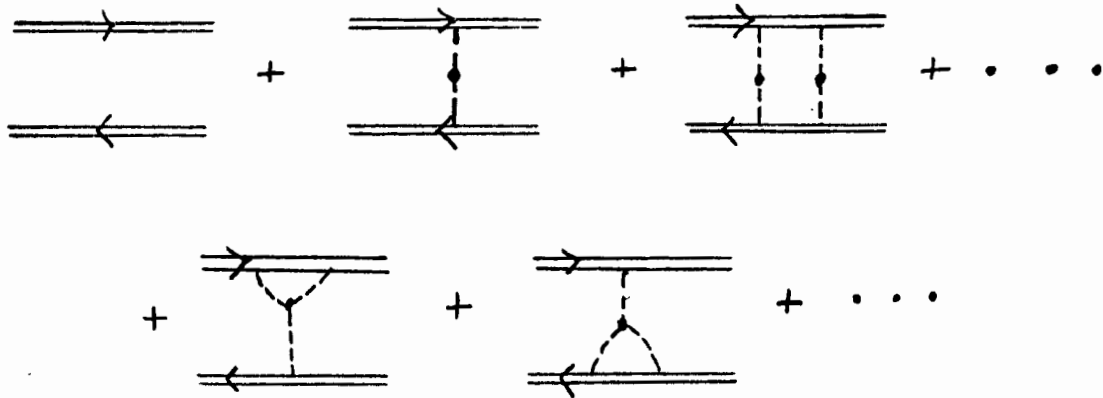
4.3 Diagrammatic Analysis

Using the expansion for $G = (E - H_0 - V)^{-1}$, where V is the total electron-ion scattering potential, we can provide a diagrammatic expansion for each of $K_{\mu\nu}^{++}$, $K_{\mu\nu}^{--}$, $K_{\mu\nu}^{+-}$, and $K_{\mu\nu}^{-+}$ defined by (4.11). For example, $K_{\mu\nu}^{+-}(k, E, E')$ is equal to the sum of all diagrams of the form



The notation here is similar to that in Section 1.4: an upper solid line $\frac{k}{\sim}$ represents a free propagator $G_0^+(k, E) = (E + i0^+ - k^2)^{-1}$, a lower solid line $\frac{k'}{\sim}$ represents $G_0^-(k', E) = (E + i0^- - (k')^2)^{-1}$, an intersection of two solid lines with a dashed line (or vertex) represents a matrix element $\langle k|v|k' \rangle$ of the scattering potential due to a single ion, and a node connecting n dashed lines represents a factor $N a_n(q_1, q_2, \dots, q_n)$,

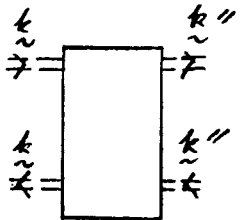
the continuous part of $C_n(q_1, \dots, q_n)$ defined by (1.16). All renormalization diagrams may be summed by replacing the free propagator line \overrightarrow{k} by $\overrightarrow{\underline{k}}$ which stands for the full propagator $G(k, E) = (E - k^2 - \Sigma(k, E))^{-1}$. The leading diagrams which remain are:



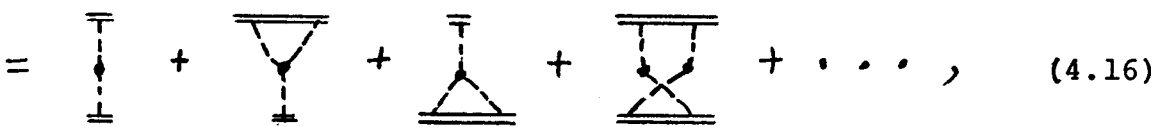
In analogy with the Dyson equation for the one-particle Green function we may write a Bethe-Salpeter type of equation (see e.g. Nozières 1964, section 6.1) for the ensemble average quantity,

$$\begin{aligned}
 & \langle \langle \overrightarrow{k} | G(\beta) | \overrightarrow{k}' \rangle \langle \overrightarrow{k}'' | G(\beta') | \overrightarrow{k} \rangle \rangle_{ave} \equiv \text{Diagram with shaded circle} \\
 & = \text{Diagram with two parallel lines} \times \delta_{\overrightarrow{k}, \overrightarrow{k}'} + \sum_{\overrightarrow{k}''} \text{Diagram with rectangle and shaded circle} \quad (4.15)
 \end{aligned}$$

where the upper (lower) horizontal line is associated with complex energy $z(z')$. Here we have introduced the irreducible interaction part,

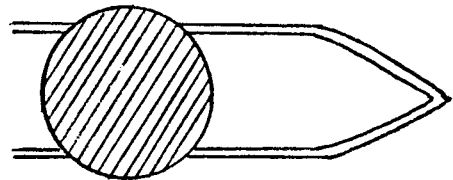
$$\frac{1}{L^3} W(\underline{k}, \underline{k}''; \bar{z}, \bar{z}') \equiv$$


(with external propagator lines removed)

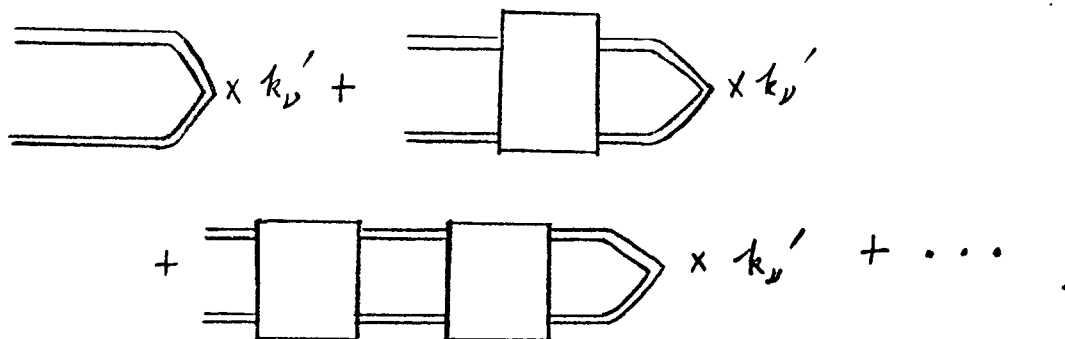
$$=$$


(4.16)

the sum of all irreducible interaction diagrams, which by definition cannot be divided into two by cutting both propagator lines but without cutting any interaction line. The quantity $K_{\mu\nu}$ is now represented by

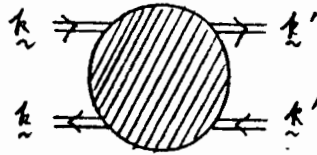
$$K_{\mu\nu}(\underline{k}; \bar{z}, \bar{z}') = k_\mu \sum_{\underline{k}'} \text{Diagram} \times k_\nu'$$


An iterative solution of the integral equation for $(\frac{1}{k_\mu})K_{\mu\nu}(k; z, z')$ would be expressed diagrammatically as:



(4.17)

An integral equation to determine $K(\underline{k}; z, z')$ of (4.13) can be obtained from (4.15). Defining a quantity $P(\underline{k}, \underline{k}'; z, z')$ by writing



$$\equiv \underline{G}(\underline{k}, z) \underline{G}(\underline{k}', z') P(\underline{k}, \underline{k}'; z, z'),$$

where $\underline{G}(\underline{k}, z)$ denotes the ensemble average of $G(\underline{k}, z)$, we have

$$P(\underline{k}, \underline{k}'; z, z') = \delta_{\underline{k}, \underline{k}'} + \frac{1}{(2\pi)^3} \int d^3 \underline{k}'' W(\underline{k}, \underline{k}''; z, z') \times \underline{G}(\underline{k}'', z) \underline{G}(\underline{k}'', z) P(\underline{k}'', \underline{k}'; z, z'). \quad (4.18)$$

By definition,

$$K(\underline{k}; z, z') = \sum_{\underline{k}'} \underline{k} \cdot \underline{k}' \underline{G}(\underline{k}, z) \underline{G}(\underline{k}', z') P(\underline{k}, \underline{k}'; z, z'). \quad (4.19)$$

Hence

$$K(\underline{k}; z, z') = \underline{k}^2 \underline{G}(\underline{k}, z) \underline{G}(\underline{k}, z') + \underline{G}(\underline{k}, z) \underline{G}(\underline{k}, z) \times \frac{1}{(2\pi)^3} \int d^3 \underline{k}'' W(\underline{k}, \underline{k}''; z, z') \underline{G}(\underline{k}'', z) \underline{G}(\underline{k}'', z') \times \sum_{\underline{k}'} \underline{k} \cdot \underline{k}' P(\underline{k}'', \underline{k}'; z, z'). \quad (4.20)$$

For an isotropic system $K(\underline{k}; z, z')$ will be independent of the direction of \underline{k} , $W(\underline{k}, \underline{k}''; z, z')$ will depend only on the relative angle of \underline{k} and \underline{k}'' , and $P(\underline{k}'', \underline{k}; z, z')$ will depend only on the relative angle of \underline{k}'' and \underline{k} . Choosing \underline{k}'' as a polar axis in doing the \underline{k}' sum, we have

$$\begin{aligned} \sum_{\underline{k}'} \underline{k} \cdot \underline{k}' P(\underline{k}'', \underline{k}'; z, z') &= \sum_{\underline{k}''} \frac{(\underline{k} \cdot \underline{k}'')(\underline{k}'' \cdot \underline{k}')}{(k'')^2} P(\underline{k}'', \underline{k}'; z, z') \\ &= \frac{\underline{k} \cdot \underline{k}''}{(k'')^2 g(k'', z) g(k'', z')} K(\underline{k}''; z, z'). \end{aligned} \quad (4.21)$$

Thus (4.20) reduces to

$$\begin{aligned} K(\underline{k}; z, z') &= g(k, z) g(k, z') \left\{ k^2 + \frac{1}{(2\pi)^3} \int d^3 k'' W(\underline{k}, \underline{k}''; z, z') \right. \\ &\quad \left. \times \frac{\underline{k} \cdot \underline{k}''}{(k'')^2} K(\underline{k}''; z, z') \right\}. \end{aligned}$$

Using isotropy again, this can be written as

$$\begin{aligned} K(\underline{k}; z, z') &= g(k, z) g(k, z') \left\{ k^2 + \int_0^\infty k k'' W_1(k, k''; z, z') \right. \\ &\quad \left. \times K(k''; z, z') dk'' \right\}, \end{aligned} \quad (4.22)$$

where

$$W_1(k, k''; z, z') = \frac{1}{(2\pi)^2} \int_0^\pi W(\underline{k}, \underline{k}''; z, z') \cos\theta \sin\theta d\theta, \quad (4.23)$$

with θ being the angle between \underline{k} and \underline{k}'' . Equations (4.22) and (4.23) are the same as (6.10) and (6.11) of Langer (1960).

§4.4 Approximations

In order to calculate the frequency-dependent conductivity we must sum all the irreducible diagrams in (4.16) to obtain $W(k, k''; z, z')$, perform the angular integration in (4.23) to get $W_1(k, k''; z, z')$ and then solve the integral equation (4.22) self-consistently for $K(k; z, z')$ which is to be substituted into (4.14) for $\text{Re } \sigma(\omega)$. Although we know how to enumerate the successive diagrams formally as in (4.16) and (4.17), a complete realistic calculation based on this scheme is obviously impossible at the present state of knowledge*. First, the evaluation of any diagram other than the simplest in (4.16) would require a knowledge of three-particle or higher correlation functions. Secondly, since the Kubo-Greenwood

* See, however, the recent contributions of Ashcroft and Schaich (1970), and Bringer and Wagner (1971). They studied only the d.c. conductivity, trying to sum a suitable set of irreducible interaction diagrams. In both cases a certain approximate relation expressing higher order ionic correlations in terms of the two-body correlation had to be made. The approximation (and hence the partial sum of diagrams) was different in the two cases.

formula (4.2) involves the matrix elements $\langle \psi_r | j_\mu | \psi_s \rangle$ of the current operator j_μ between true eigenstates $|\psi_r\rangle$, the one-electron Green function that enters (4.22) and other equations is the one corresponding to the true scattering potential, rather than the pseudopotential. Our attempt to find an explicit relation between the true and the pseudo Green functions has not been successful. To be able to carry on we have to do two things: (1) to introduce an approximation in the irreducible interaction, and (2) to work with fictitious liquid metals represented by parametrized Green functions.

If we assume that the scattering is isotropic in k-space, or equivalently, $W(k, k''; z, z')$ is orthogonal to the cosine term, then $W_1(k, k''; z, z')$ will vanish and (4.22) will reduce to

$$K(k; z, z') = \bar{G}(k, z) \bar{G}(k, z') k^2, \quad (4.23)$$

which merely states that the ensemble average of a product of two Green functions can be replaced by the product of their averages. This simplifies the calculation enormously but is not likely to be realized in practice. However, we may regard our assumption as defining a model for a liquid metal, the "isotropic scattering model", say. Calculations based on this model with parametrized Green functions may still indicate how much the structure of $n(E)$ will affect $\text{Re } \sigma(\omega)$.

The evaluation of (4.14) for $\text{Re } \sigma(\omega)$ can be simplified a little by taking the low temperature limit. This is legitimate since the typical temperature of a liquid metal is still very low compared with the Fermi temperature $T_F = E_F/k_B$, k_B being Boltzmann's constant. In this limit the Fermi-Dirac distribution function $f(E)$ is just a step function and (4.14) can be written, in the "isotropic scattering" approximation, as

$$\text{Re } \sigma(\omega) = \frac{1}{6\pi^3} \left(\frac{e}{m}\right)^2 \frac{1}{\omega} \int_{E_F}^{E_F+\omega} dE \int_0^\infty dk k^2 \text{Re} \{K^{+-}(k; E, E-\omega) - K^{++}(k; E, E-\omega)\}, \quad (4.24)$$

where E_{F_0} is the free-electron Fermi energy.

CHAPTER 5

NUMERICAL CALCULATION WITH MODELS

§5.1 The Lorentzian Model

Before introducing any model we note that, in the approximation of Section 4.4, (4.24) can be expressed in terms of the spectral function $\rho(k, E)$ (Eq. (1.3)) as

$$\text{Re } \sigma(\omega) = \frac{1}{3\pi} \left(\frac{e}{m}\right)^2 \frac{1}{\omega} \int_{E_F}^{E_F + \omega} dE \int_0^{\infty} k^4 \rho(k, E) \rho(k, E - \omega) dk, \quad (5.1)$$

which is equivalent to the formula that Faber (1966) obtained using Kramers-Heisenberg dispersion theory in the form quoted by Smith (1967b). Similarly, the zero-frequency limit obtained directly from (4.14) can be written as

$$\text{Re } \sigma(0) = \frac{1}{3\pi} \left(\frac{e}{m}\right)^2 \int_0^{\infty} k^4 \rho^2(k, E_F) dk, \quad (5.2)$$

which is equivalent to the formula given by Edwards (1958). Hence one only needs to model for the spectral function.

The simplest model to use is to choose a constant self-energy,

$$\Sigma = A + i\Gamma$$

In this case the real part A corresponds only to a constant energy shift and may be conveniently taken as zero. The Green function is then given by

$$G^{\pm}(k, E) = \frac{1}{E - k^2 \pm i\Gamma},$$

and the spectral function is a Lorentzian,

$$\rho(k, E) = \frac{1}{\pi} \frac{\Gamma}{(E - k^2)^2 + \Gamma^2}.$$

The calculation of the real part of the frequency conductivity (hereafter denoted simply by $\sigma(\omega)$) is now a matter of straightforward computation. We have cut off the k -integration in (5.1) at $10 k_F$ and evaluated $\sigma(\omega)$ from $\omega = 0$ to the free-electron Fermi energy E_{F_0} for the following values of Γ : 0.005, 0.01, 0.05, 0.1, 0.2, 0.4 (in units of E_{F_0}). The results have almost exactly the same frequency dependence as predicted by the Drude formula, and the product $\Gamma\sigma(0)$ remains constant for the various values of Γ . Defining a relaxation time τ such that $\sigma(\omega) = \frac{1}{2}\sigma(0)$ at $\omega = 1/\tau$ we find that τ is proportional to $1/\Gamma$. Thus all features of the free-electron theory are reproduced. It is suspected that it might be possible to prove analytically that evaluating the Kubo-Greenwood formula with the Lorentzian model would lead to the Drude formula, but we have not attempted to do this since complicated contour integrals are involved.

We cannot draw any definite conclusion regarding the effect of $n(E)$ on the frequency-dependent conductivity from our calculations with the Lorentzian model because the density of states corresponding to this model is not at all sensitive to the value of Γ . Simple integration gives

$$n(E) = \frac{\sqrt{2}}{4\pi^2} (E^2 + \Gamma^2)^{1/4} \left(1 + \frac{E}{E^2 + \Gamma^2}\right)^{1/2}. \quad (5.3)$$

For example, even when $\Gamma = 0.4 E_{F0}$, $n(E_{F0})$ from (5.3) differs from the free-electron value only by 2%.

§5.2 A Parametrized Model

The parametrized model introduced in Section 1.3 (Eqs. (1.9) and (1.10)) is suitable for studying the influence of the density of states $n(E)$ on the frequency-dependent conductivity because different $n(E)$ can be generated by varying the parameters a , b , c , and g . As is shown in Appendix I, this model automatically satisfies the sum rule for the spectral function. This is confirmed by numerical integration of $\rho(k, E)$ with respect to E , which yields 0.97 for an upper limit of $10 E_{F0}$ and 0.99 up to $40 E_{F0}$, for typical values of the parameters. We have calculated $\sigma(\omega)$ from this model for $a = 0.01$ to 0.1 , $b = 0.05$ to 0.5 , $c = -0.5$ and 0.1 to 0.5 , and $g = 0.6$ to 1.2 (in units for which $\hbar = 2m = k_F = 1$). Typical results are

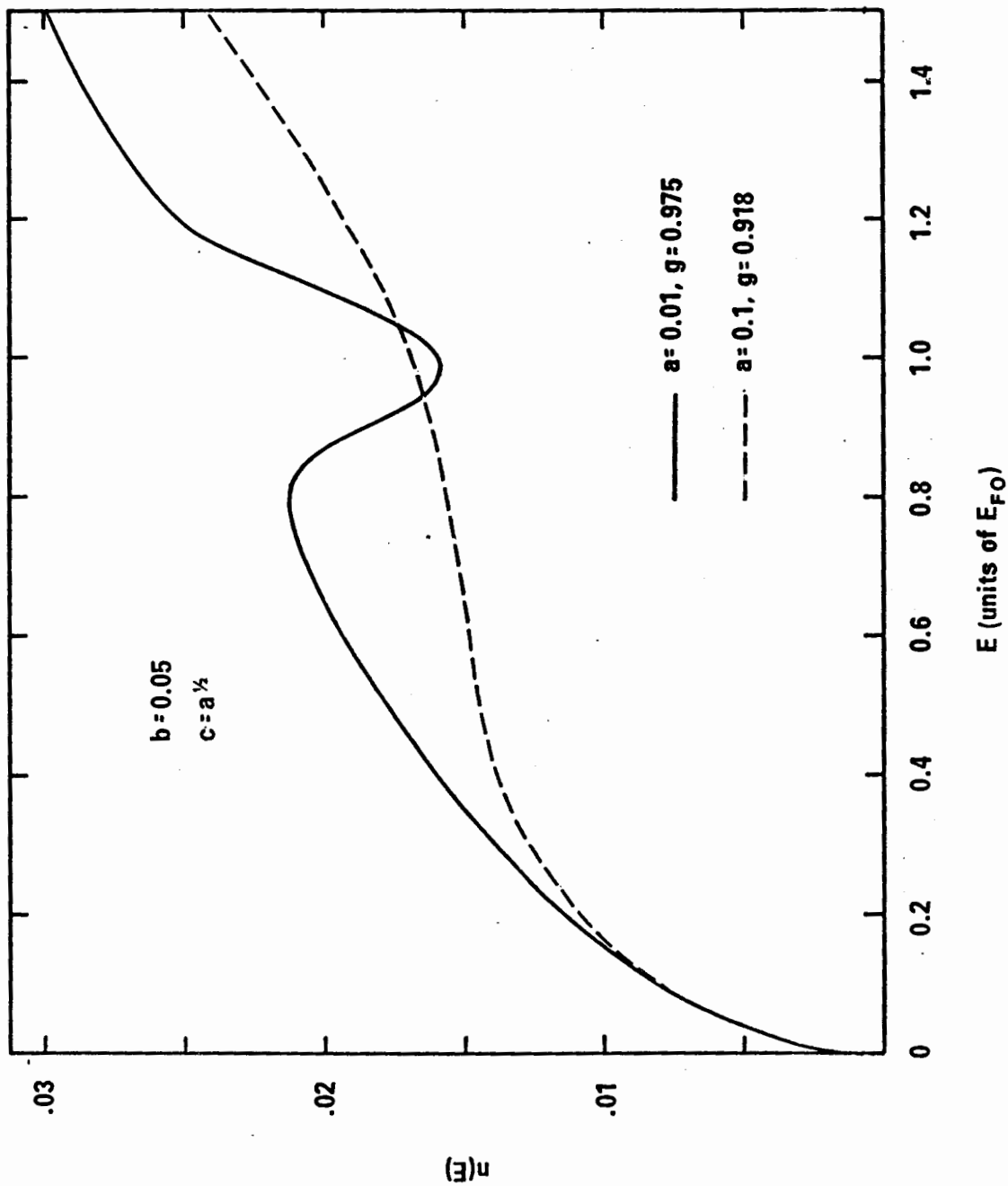


Figure 31 Density of states $n(E)$ using parametrized model Green function, a varied.

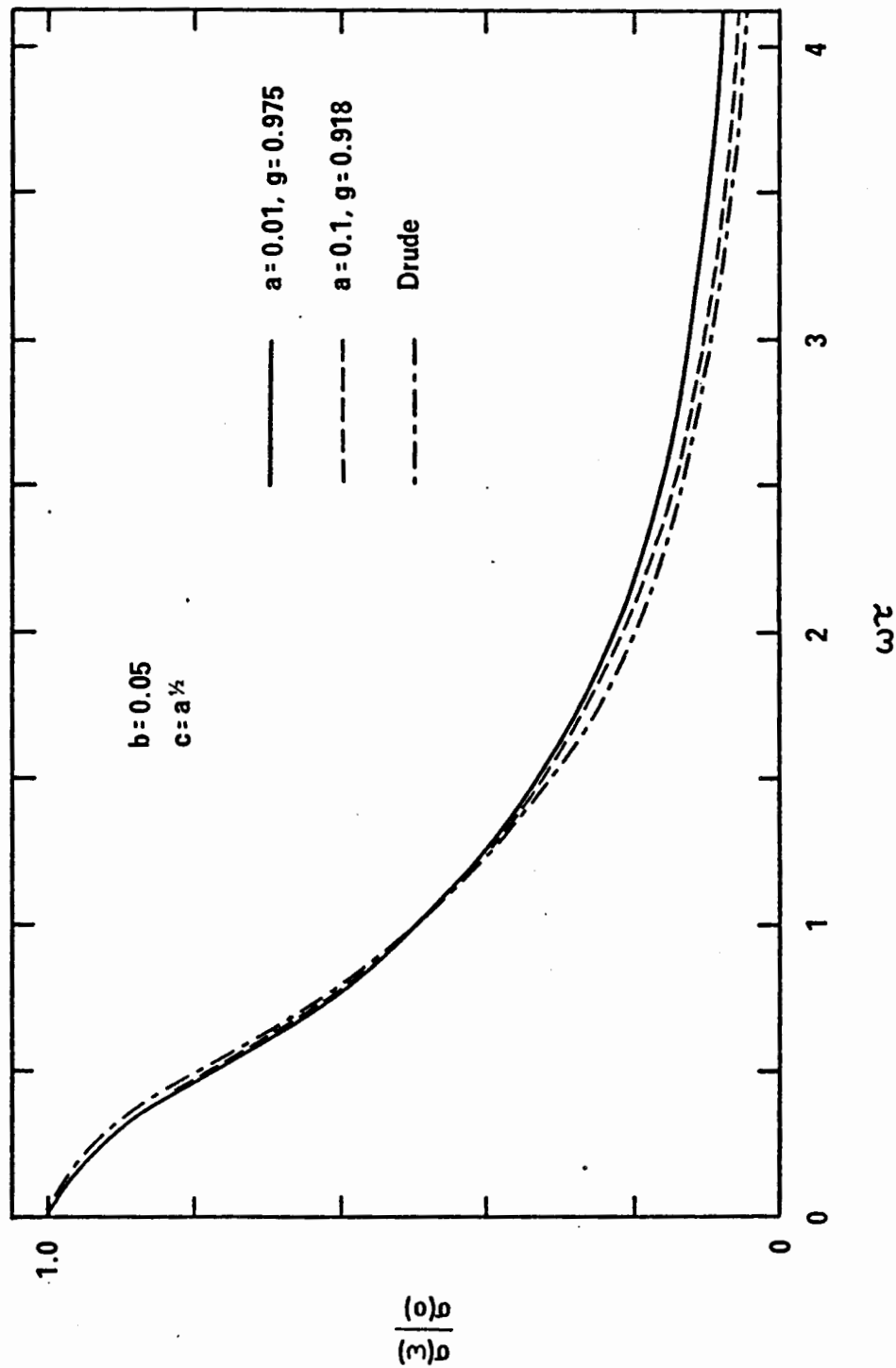


Figure 32 Frequency dependence of normalized optical conductivity corresponding to $n(E)$ of Figure 31; ω : frequency; τ : relaxation time.

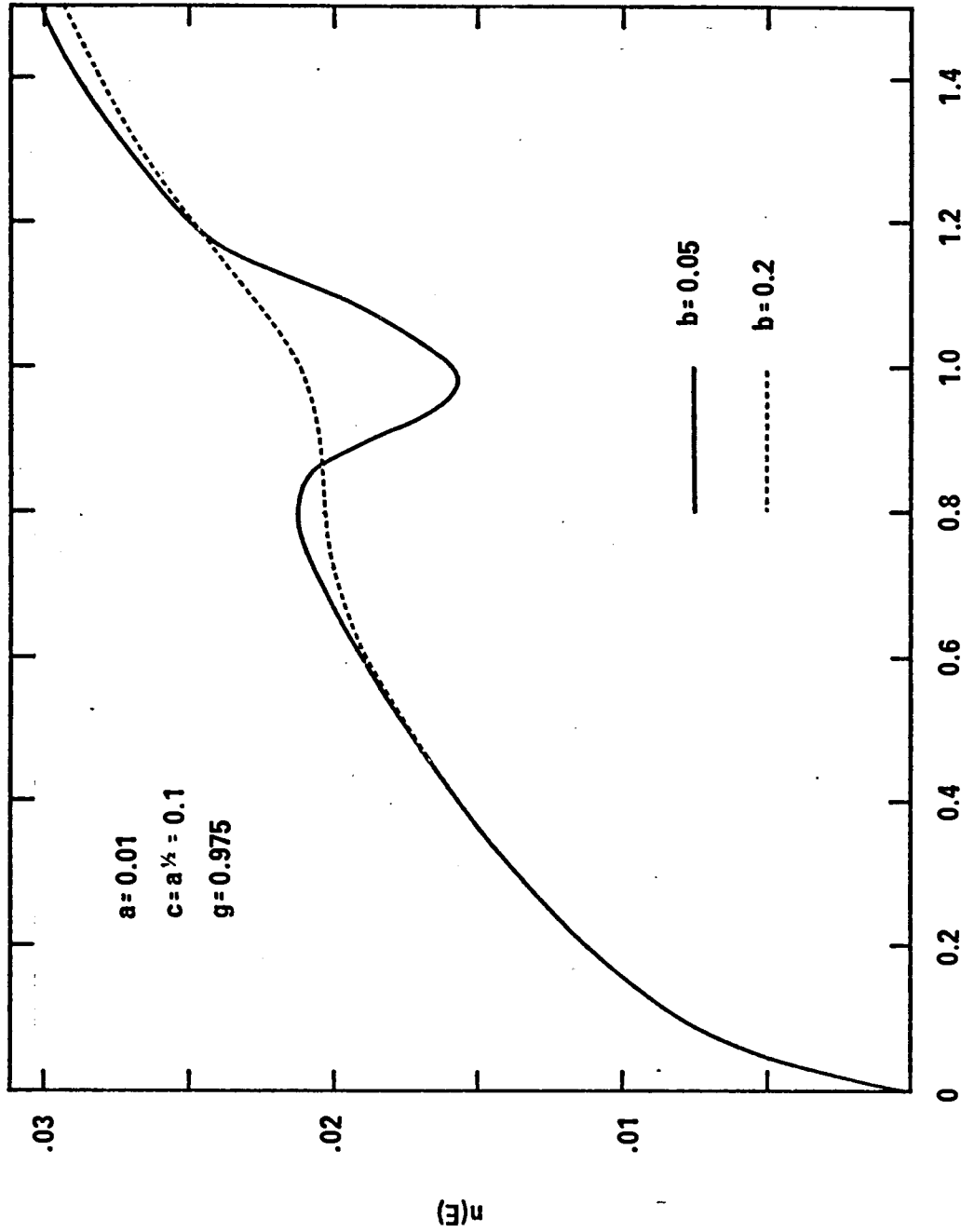


Figure 33 Density of states $n(E)$ using parametrized model Green functions, b varied.

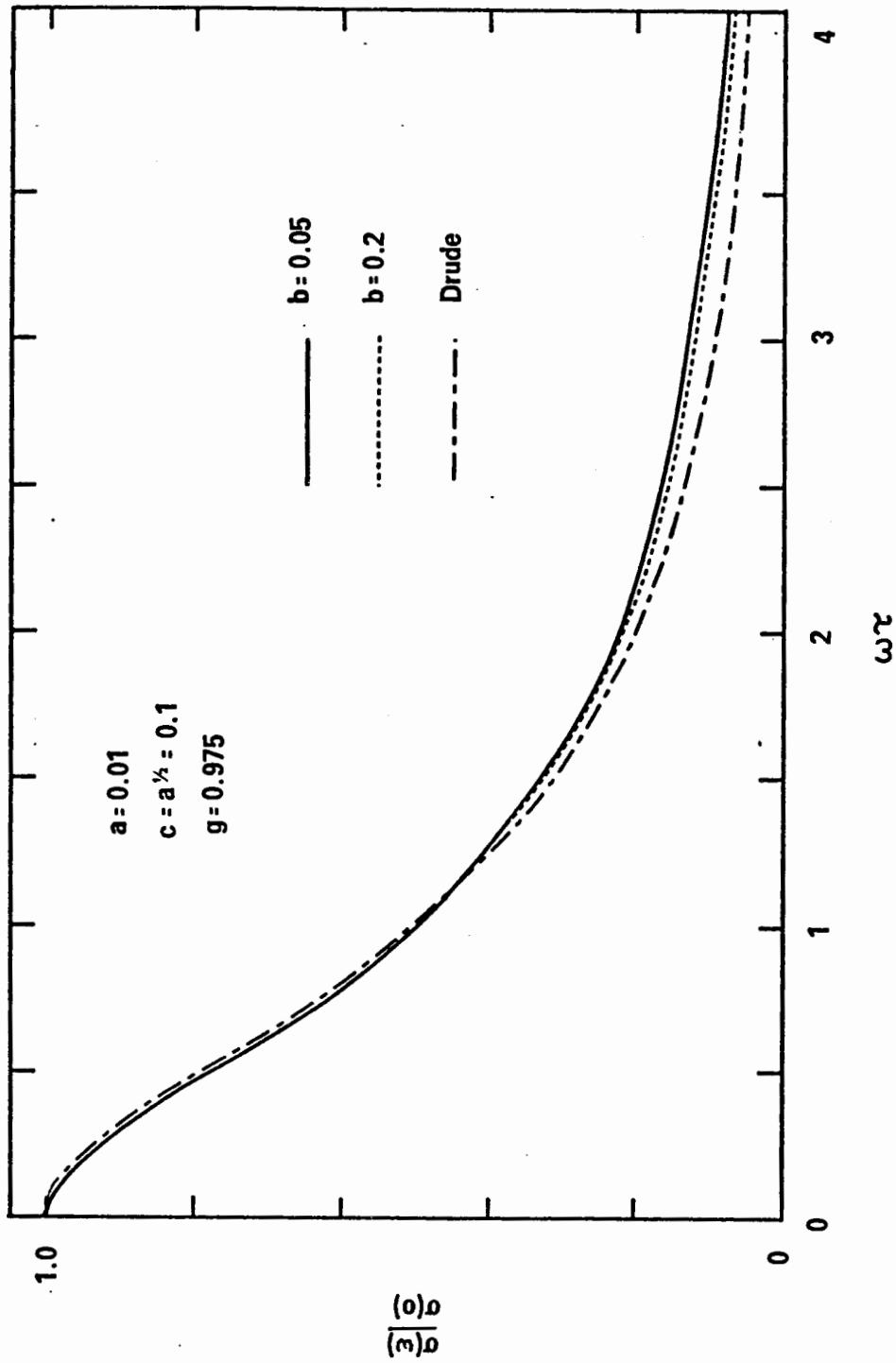


Figure 34 Frequency dependence of normalized optical conductivity corresponding to $n(E)$ of Figure 33; ω : frequency; τ : relaxation time.

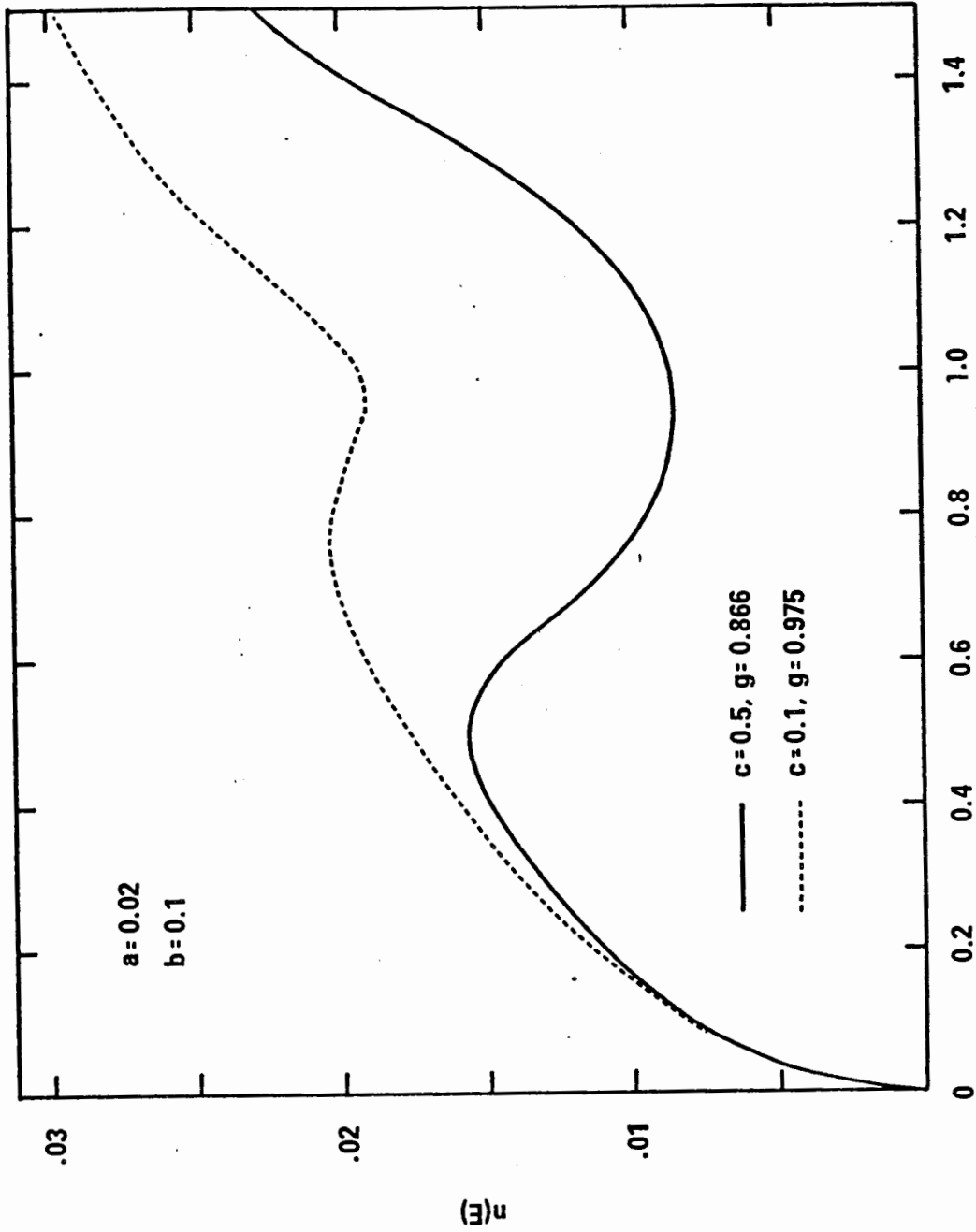


Figure 35 Density of states $n(E)$ using parametrized model
Green functions, c varied.

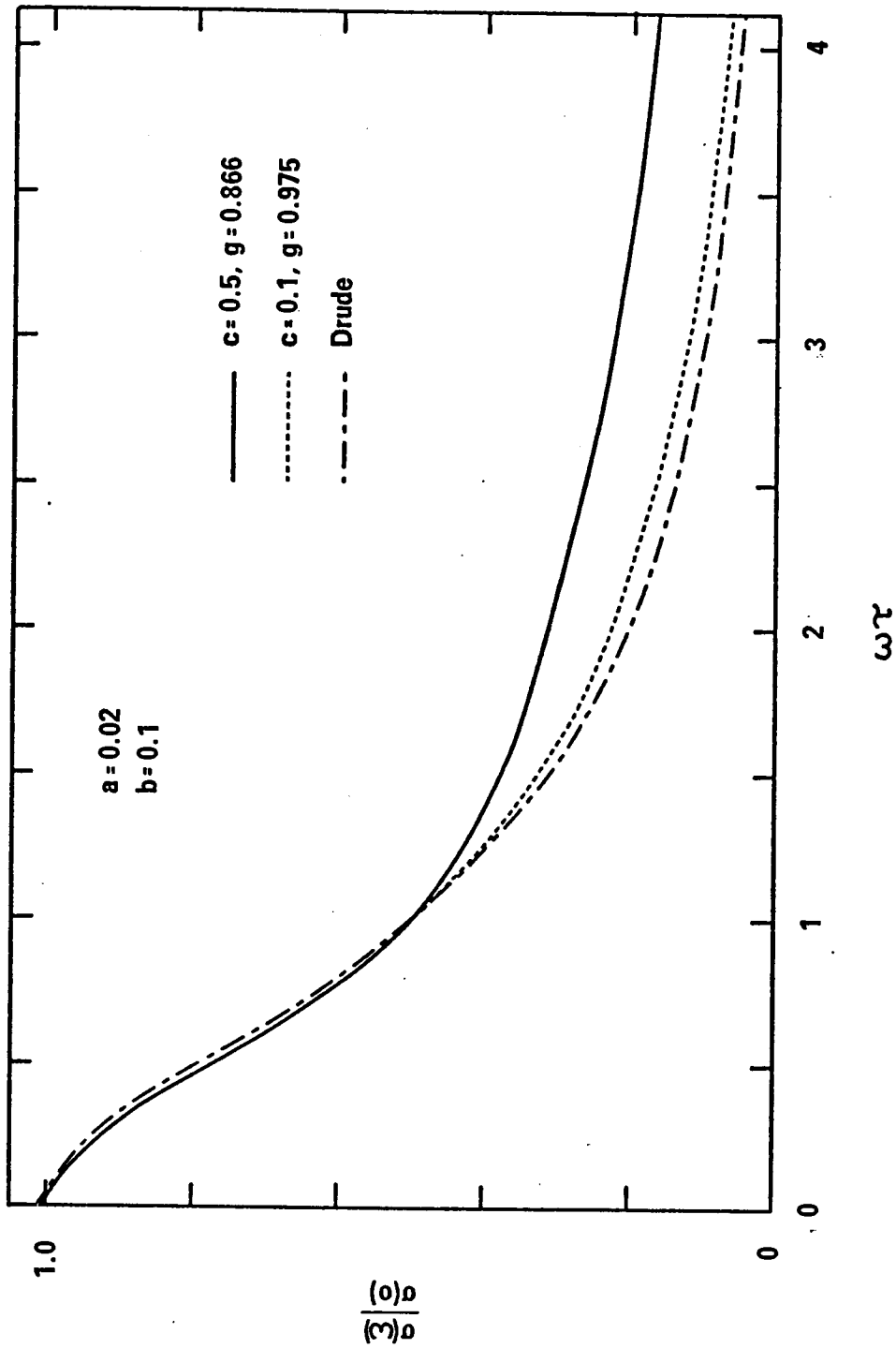


Figure 36 Frequency dependence of normalized optical conductivity corresponding to $n(E)$ of Figure 35; ω : frequency; τ : relaxation time.

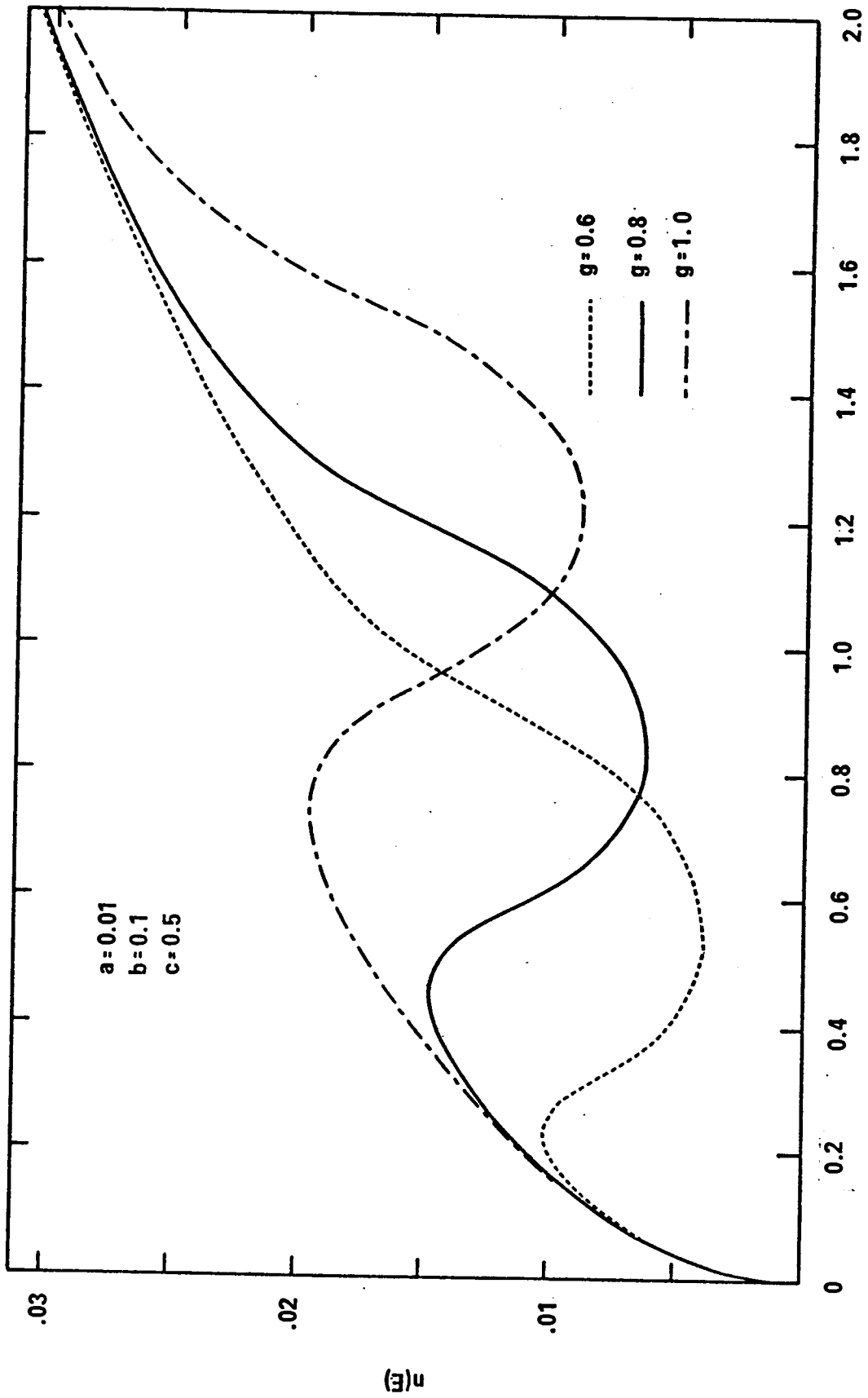


Figure 37 Density of states $n(E)$ using parametrized model
Green functions, g varied.

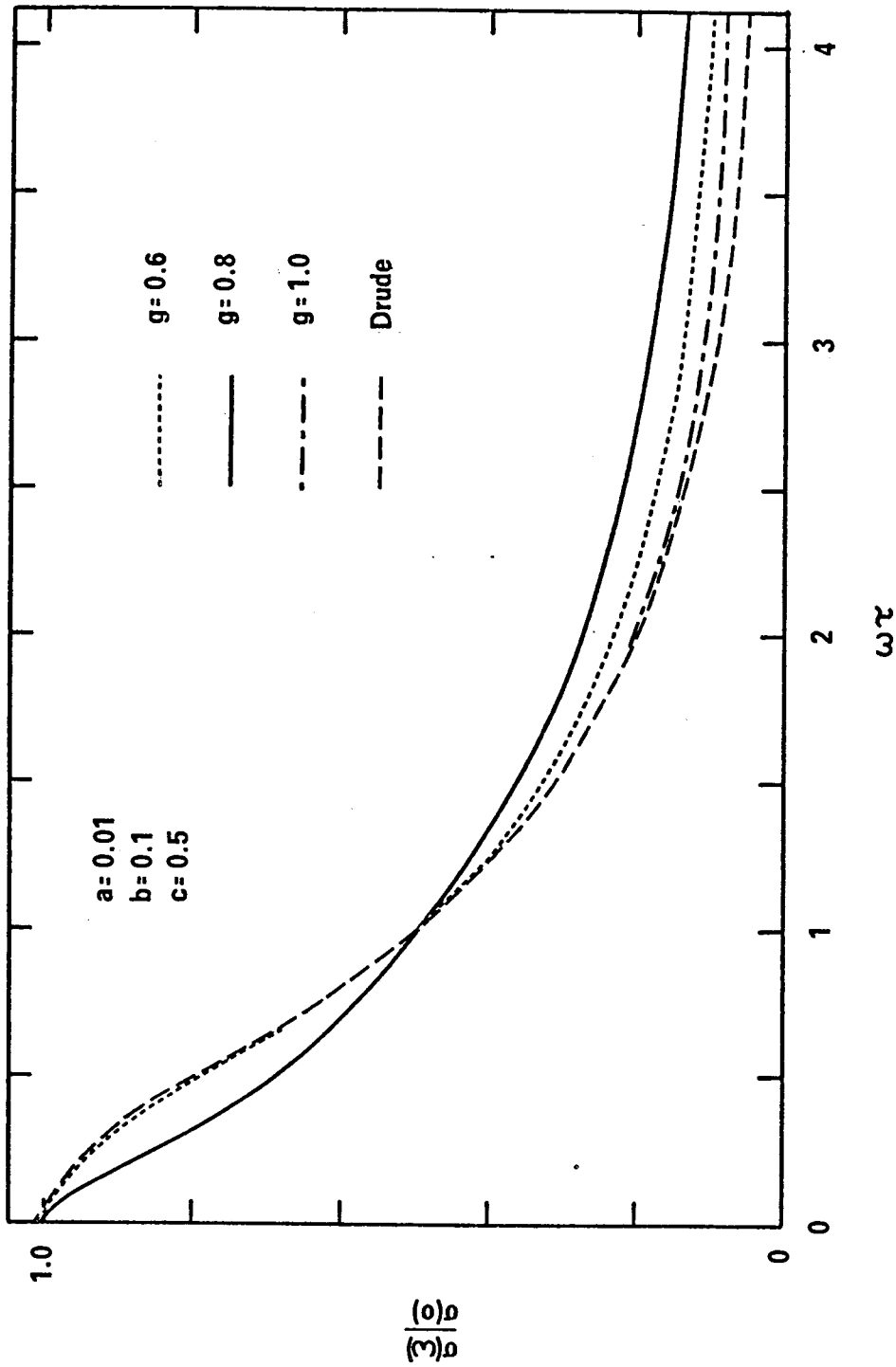


Figure 38 Frequency dependence of normalized optical conductivity corresponding to $n(E)$ of Figure 37; ω : frequency; τ : relaxation time.

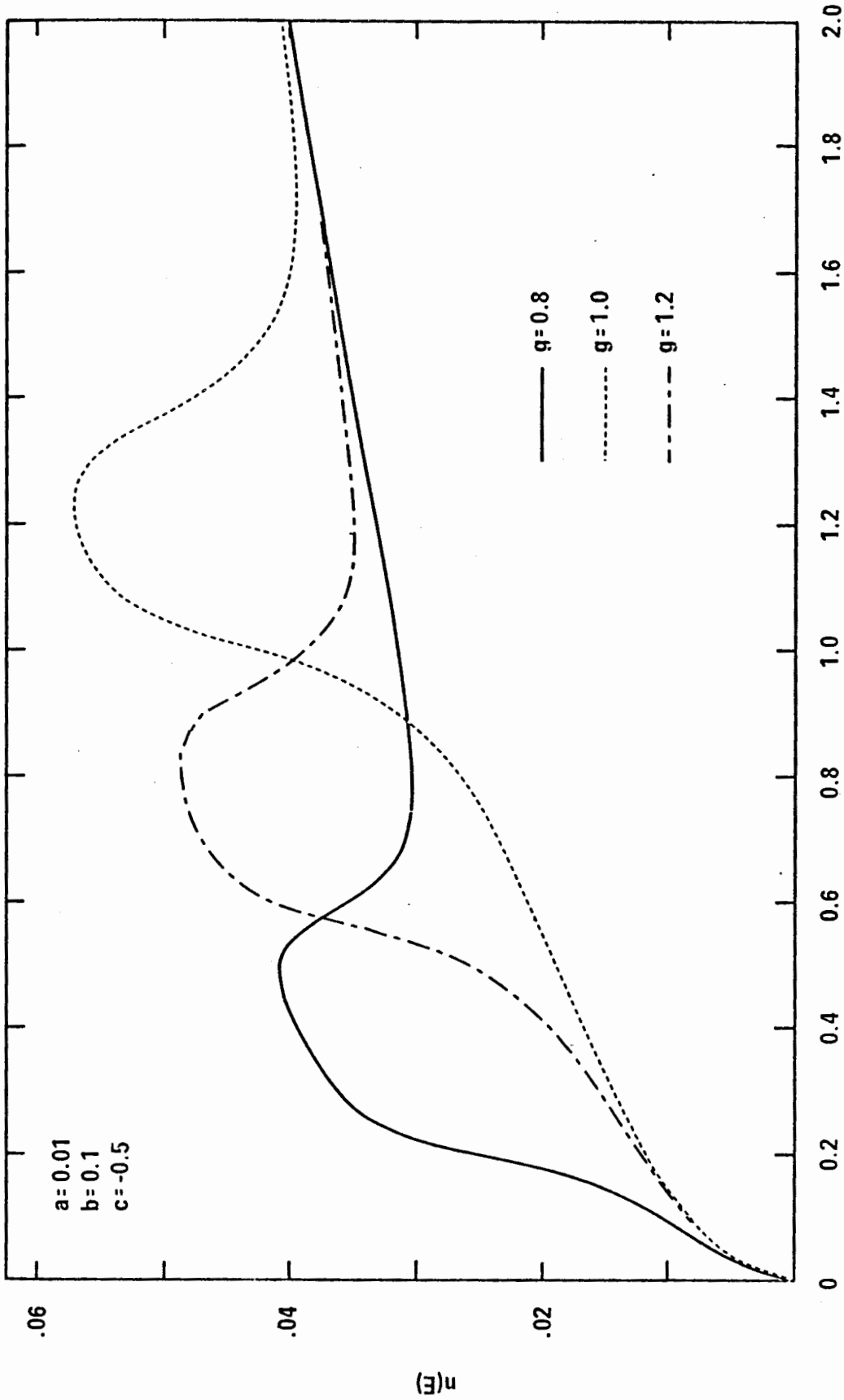


Figure 39 Density of states $n(E)$ using parametrized model Green Functions, g varied. Note that negative c gives enhanced $n(E)$.

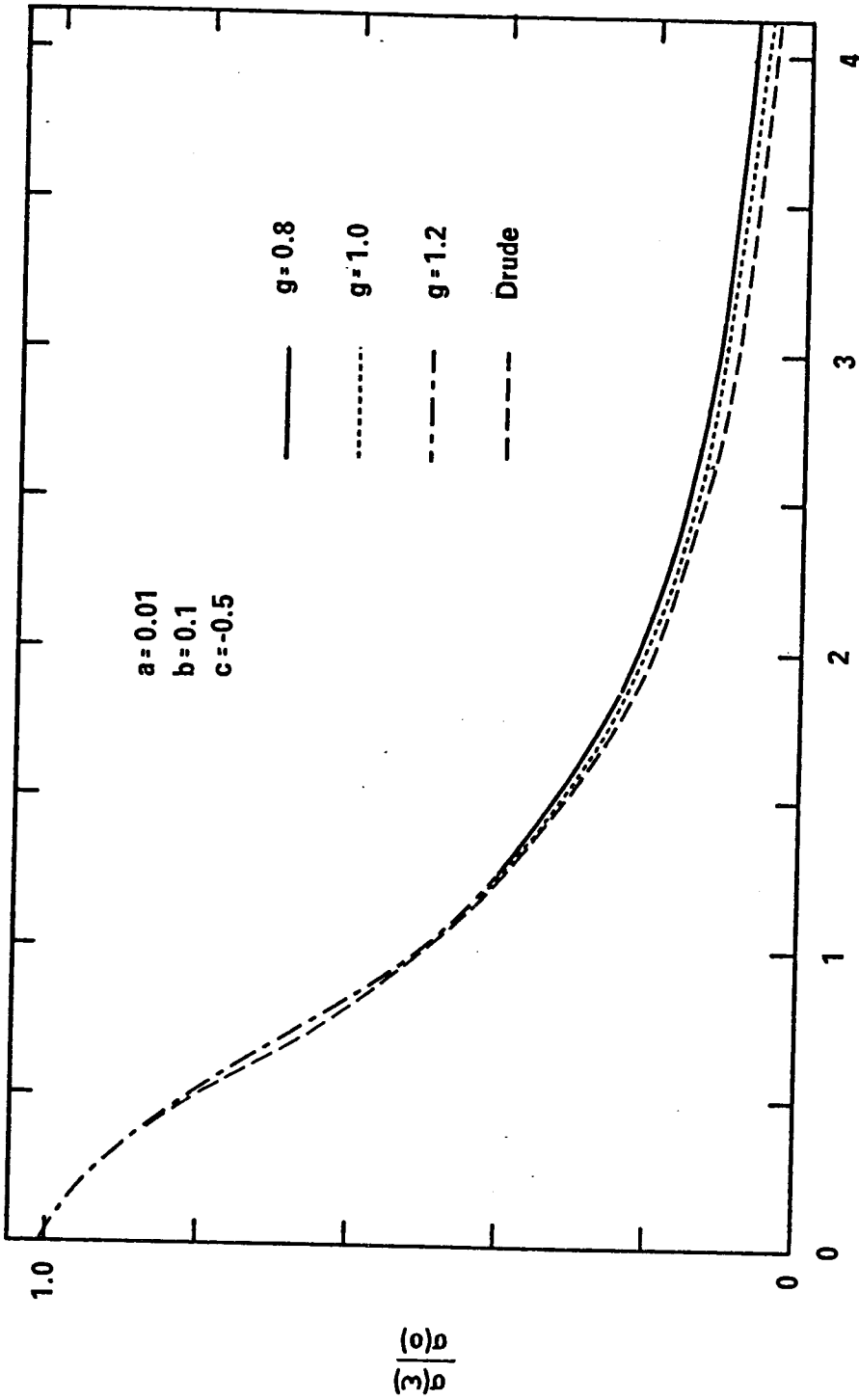


Figure 40 Frequency dependence of normalized optical conductivity corresponding to $n(E)$ of Figure 39; ω : frequency; τ : relaxation time.

shown in Figures 31-40. The corresponding $n(E)$ and $\sigma(\omega)$ curves are shown in consecutive figures. We have plotted the frequency dependence of the conductivity as normalized $\sigma(\omega)/\sigma(0)$ versus $\omega\tau$ curves in order that several curves can be displayed on the same scale. It may appear at first glance that the sum rule for $\sigma(\omega)$ due to n_t electrons per unit volume,

$$\frac{2m}{\pi e^2} \int_0^{\infty} \sigma(\omega) d\omega = n_t \quad , \quad (5.4)$$

has been violated in some cases. This is not so because the sum rule (5.4) applies only to the absolute values of $\sigma(\omega)$ and ω , and the values of $\sigma(0)$ and τ are different for the different curves. The particular parameter varied is a in Figures 31 and 32, b in Figures 33 and 34, c in Figures 35 and 36, and g in Figures 37-40. For the cases in Figures 31-36 the values of g were obtained by numerically solving the equation

$$\mathcal{E}(g) = g^2 + c \left\{ \frac{1}{2} - (1 + e^{g/a})^{-1} \right\} = 1 \quad , \quad (5.5)$$

so that the dip in $n(E)$ is located near E_{F0} .

In general, the structure in $n(E)$ is not very strongly reflected in the frequency dependence of $\sigma(\omega)$. For $\omega\tau < 1$ the values of $\sigma(\omega)/\sigma(0)$ are in close agreement with the Drude curve fitted at the two points $\omega = 0$ and $\omega = 1/\tau$; for $\omega\tau > 1$ the model

curves are slightly above the Drude curve, the discrepancy increasing with the depth of the depression in $n(E)$. The only cases that show substantial deviations from the Drude curve are those represented by the two solid lines in Figures 36 and 38, respectively. These correspond to very drastic structures, a wide region of severely reduced density of states at (solid line, Figure 35) or very close to (solid line, Figure 37) E_{F0} . From our experience in Part I of the thesis, the density of states in a simple liquid metal is not expected to exhibit a sharper structure than the solid curve in Figure 31, much less probable anything like the two extreme cases just mentioned. In fact, the calculated $n(E)$ for mercury can be fitted with the parameters $a = 0.04$, $b = 0.1$, $c = 0.2$, $g = 0.8$ which yield a $\sigma(\omega)$ in better agreement with the Drude formula than the dashed curve in Figure 34 because the dip in $n(E)$ for Hg does not occur exactly at E_F (nor E_{F0}). For all cases where there is a dip in $n(E)$, $\sigma(\omega)/\sigma(0)$ either falls slightly below or is practically identical with the Drude curve at frequencies $\omega < 1/\tau$. Even for the unrealistic cases in which there is a region of immensely enhanced density of states (Figure 39) $\sigma(\omega)/\sigma(0)$ rises only slightly above the Drude curve (Figure 40). In none of the cases considered did we find a frequency variation anywhere near the one illustrated in Figure 30. We conclude that within the framework of our model and approximations the optical conductivity of real liquid metals is quite insensitive to the structure of the electron density of states. It is not likely that $n(E)$ could affect $\sigma(\omega)$ in any

other way more important than directly through the product of the Green functions, which we have included in our calculations. An explanation for the anomalous optical properties of liquid mercury must be sought elsewhere.

E. D. Crozier (private communication) has measured the optical conductivity of Hg by ellipsometry using different interfaces and found the results to be almost independent of the interface material but results for the absolute reflectivity at oblique incidence depend on the nature of the interface and differ from both the ellipsometric and normal incidence reflectivity (Drude) results. These results are consistent with a surface transition region similar to the model of Bloch and Rice (1969). He proposes that the surface would produce an enhanced backscattering which would provide a mechanism for Smith's (1968) somewhat ad hoc hypothesis.

§5.3 Zero-Frequency Conductivity and Density of States

The dependence of the d.c. conductivity of a liquid metal on the density of states has been a subject of debate for some time. If one writes Ziman's (1961) nearly-free-electron formula in the form

$$\sigma_Z = \frac{1}{3} e^2 v_F^2 \tau_Z n(E_F) , \quad (5.6)$$

where v_F is the velocity of an electron on the Fermi surface, $n(E_F)$ is the density of states at that energy, and τ_Z is the

relaxation time calculated by lowest order perturbation theory, one expects that the conductivity σ_z should vary as $[n(E_F)]^{-2}$ because τ_z is proportional to $1/n(E_F)$ and v_F is given by $(\partial E(k)/\partial k)_F$ which is proportional to $1/n(E_F)$, if an E-k dispersion relation is assumed to exist. Edwards (1962) and later Ziman (1967) argued that the d.c. conductivity of a liquid metal should not depend on $n(E_F)$ because in a liquid the factor ev_F in (5.6) should be replaced by the 'Fermi current' j_F which they argued should be approximately equal to $e k_F/m$. (In a solid one can show by Bloch's theorem that the expectation value of the current is equal to e times the gradient of the energy (see e.g. Wilson 1953).) Faber (1966) agreed that the d.c. conductivity should not involve the density of states effective mass, defined as

$$\hat{\mu} = n(E_F)/n_0(E_{F_0}) \quad (5.7)$$

with $n_0(E_{F_0})$ being the free-electron value but he included some other correction factor. Mott (1966) expressed the opinion that there should be no dependence on $n(E_F)$ if it differs only slightly from $n_0(E_{F_0})$, but if $n(E_F) \ll n_0(E_{F_0})$ then the conductivity should be reduced, although he did not give an explicit functional dependence.

We have evaluated the expression (5.2) for the zero-frequency conductivity $\sigma(0)$ using the same parametrized model Green function as in Section 5.2. In Table III, the results

TABLE III
Dependence of Zero-Frequency Conductivity and
Relaxation Time on Density of States

a	b	c	g	Fig.	τ	$\hat{\mu}$	$\tau b \hat{\mu}$	$\hat{\sigma}$	$\hat{\sigma} / \hat{\mu}$	$\hat{\sigma} / \hat{\mu}^2$
0.02	0.50	0.141	0.964	0	0.770	0.902	0.347	1.072	1.188	1.318
0.04	0.50	0.200	0.949	0	0.766	0.866	0.331	0.981	1.133	1.309
0.06	0.50	0.245	0.937	0	0.755	0.844	0.319	0.939	1.112	1.318
0.10	0.50	0.316	0.918	0	0.765	0.818	0.313	0.871	1.065	1.302
0.01	0.20	0.100	0.975	33	2.020	0.834	0.337	0.849	1.018	1.221
0.02	0.20	0.141	0.964	0	2.000	0.790	0.316	0.780	0.988	1.251
0.04	0.20	0.200	0.949	0	2.128	0.754	0.321	0.692	0.918	1.218
0.08	0.20	0.283	0.927	0	2.299	0.733	0.337	0.622	0.848	1.157
0.04	0.10	0.200	0.949	0	4.651	0.683	0.318	0.580	0.849	1.242
0.08	0.10	0.283	0.927	0	4.926	0.687	0.339	0.556	0.810	1.178
0.01	0.05	0.100	0.975	31	8.333	0.626	0.261	0.552	0.881	1.407
0.02	0.05	0.141	0.964	0	9.804	0.626	0.307	0.498	0.796	1.271
0.04	0.05	0.200	0.949	0	10.000	0.634	0.317	0.522	0.823	1.297
0.06	0.05	0.245	0.937	0	10.000	0.649	0.325	0.536	0.826	1.273
0.10	0.05	0.316	0.918	31	10.000	0.667	0.333	0.542	0.813	1.219
0.02	0.05	0.100	0.975	0	9.434	0.703	0.331	0.624	0.888	1.263
0.02	0.10	0.100	0.975	35	4.405	0.770	0.339	0.719	0.934	1.214
0.02	0.10	0.500	0.866	35	4.255	0.340	0.144	0.182	0.536	1.578
0.01	0.10	0.500	0.600	37	5.181	0.632	0.327	0.330	0.523	0.828
0.01	0.10	0.500	0.800	37	2.062	0.304	0.063	0.226	0.745	2.450
0.01	0.10	0.500	1.000	37	4.525	0.490	0.222	0.401	0.820	1.675
0.01	0.10	-0.500	0.800	39	5.076	1.245	0.632	1.814	1.457	1.170
0.01	0.10	-0.500	1.000	39	4.673	1.518	0.709	2.184	1.439	0.948
0.01	0.10	-0.500	1.200	39	4.808	1.683	0.809	2.233	1.326	0.788

a, b, c, g are model parameters, the column Figure gives the serial number of the figure showing $n(E)$, 0 means not plotted, τ relaxation time, $\hat{\mu} = n(E_{F_0})/n_0$ (E_{F_0}), $\hat{\sigma} = \sigma(0)/\sigma_{FE}$

are compared with the density of states at E_F for different sets of parameters. The free-electron conductivity σ_{FE} was obtained from

$$\sigma_{FE} = \frac{n_e e^2 \tau}{m}, \quad (5.8)$$

where τ is the relaxation time deduced from the frequency-dependent conductivity curves, e , m the free-electron charge and mass, and n_e the number of valence electrons per unit volume, consistent with our choice of unit $k_F = 1$. For all cases that correspond to the kind of $n(E)$ that one can reasonably expect in simple liquid metals (all sets above the case $a = 0.02$, $b = 0.1$, $c = 0.1$, $g = 0.975$, inclusive) the ratio of the zero-frequency conductivity to the free-electron d.c. conductivity, $\hat{\sigma} \equiv \sigma(0)/\sigma_{FE}$, is approximately proportional to the square of the ratio of densities of states, $\hat{\mu} \equiv n(E_{F0})/n_0(E_{F0})$. Moreover, the relaxation time τ varies roughly as the reciprocal of $n(E_{F0})$, as expected from Ziman's theory and, of course, also as the reciprocal of the linewidth parameter b . The fact that the ratio $\hat{\sigma}/\hat{\mu}^2$ is not equal to 1 may indicate that a relaxation time slightly different from the optical τ or an effective number of valence electrons (see Faber 1966) should be used for the d.c. conductivity. The most serious discrepancy among this group occurs for the set $a = 0.01$, $b = 0.05$, $c = 0.1$, $g = 0.975$ which is associated with the sharpest structure in $n(E)$, with a dip more severe than the one we obtained for mercury. For those cases at the bottom quarter of the table,

which correspond to drastic structures, the dependence of τ and $\sigma(0)$ on $n(E)$ seems more complicated, but we can be quite sure that $\sigma(0)$ is not the same as σ_{FE} .

Let us compare our results with solid state theory and the arguments of the aforementioned authors. In a solid we have, from (5.6) and (5.8)

$$\hat{\sigma} \equiv \frac{\sigma(0)}{\sigma_{FE}} = \frac{1}{3} v_F^2 \frac{m}{n_e} n(E_F) . \quad (5.9)$$

As v_F is inversely proportional to $n(E_F)$, (5.9) predicts that $\hat{\sigma}$ is also inversely proportional to $n(E_F)$, which is obviously not what we found (c.f. the columns $\hat{\mu}$ and $\hat{\sigma}$ in Table III). Next consider Ziman's (1967) idea of replacing ev_F by $\frac{ek_F}{m}$ in (5.9), then $\hat{\sigma}$ would be proportional to $n(E_F)$. The values of $\hat{\sigma}/\hat{\mu}$ we obtained are not as constant as those of $\hat{\sigma}/\hat{\mu}^2$. This means that our findings are at variance with solid state theory and the opinions of various previous workers. Recalling that the density of states $n(E_F)$ is given by the integral of $k^2 \rho(k, E_F)$ (Eq. (1.5)) and the zero-frequency conductivity $\sigma(0)$ is given by the integral of $k^4 \rho(k, E_F)$ (Eq. (5.2)), our results sound quite plausible. In fact, if the spectral function $\rho(k, E)$ were a rectangular pulse, then $\sigma(0)$ would be exactly proportional to $[n(E_F)]^2$. Of course $\rho(k, E)$ is not a rectangular pulse in the actual case, only an approximate proportionality is to be expected.

There is one unnecessary approximation in our calculations. We have evaluated $\sigma(0)$, $n(E)$ and τ by using the free-electron Fermi energy E_{F_0} instead of the true Fermi energy E_F , to be determined by integrating the density of states up to the energy which will accommodate the n_e valence electrons. For the work in the preceding section this does not matter since we are only interested in the frequency dependence of the normalized optical conductivity--replacing E_F by E_{F_0} corresponds only to choosing a different energy scale. But when we want to compare the absolute value of $\sigma(0)$ with that of σ_{FE} , the results may be affected. It is hoped that in the near future some of the work in the present section can be repeated using the correct E_F .

CHAPTER 6

COMMENTS AND CONCLUSIONS

The calculations on liquid Bi, In, and Hg in this thesis, together with Ballentine's (1966) work on Zn and Al, suggest that the electronic structure of simple liquid metals (i.e. those other than transition or noble metals, which we have not treated) is nearly-free-electron-like (NFE). Nevertheless, solid state formulas should not be applied without caution. For instance, the density of states $n(E)$ calculated from $(\nabla_{\mathbf{k}} E(\mathbf{k}))^{-1}$ is not accurate, as we have illustrated by model calculations (Section 1.3). Another example is that $n(E)$ of liquid mercury is much more free-electron-like than Mott (1966) conjectured by analogy with the small band-overlapping in the solid (see Section 2.5).

We have made several different calculations for bismuth. Using the same local, energy independent model potential as Ballentine (1966), but without making his numerical approximations, we obtain a very similar electronic structure, except that the peak region which he found is slightly smoothed out. This structure is further reduced by an effective mass correction and by the use of a nonlocal model potential, the largest change occurring in the last step. The final $n(E)$ differs little from the free-electron parabola corresponding to the appropriate effective mass. This shows that the nonlocal and energy dependent nature of the model potential is of some significance. Calculation of the integrated density of states

(Chapter 3) by a method which remains exactly valid for energy dependent model potentials gives qualitatively similar structure, but a wider band indicating that the energy dependence of higher order terms may not be negligible.

Indium is found to be very free-electron-like (Section 2.4), but mercury has a substantial structure in $n(E)$ (Section 2.5). If one used the Heine-Abarenkov-Animalu (HAA) model potential for mercury, one would expect very little structure in $n(E)$ because the first zero of the form factor coincides with the main peak of the ionic structure factor resulting in very weak perturbation. However it has been shown (Evans 1970) that the linear extrapolation method used by HAA to obtain the model potential depth parameters is not valid for mercury because of the proximity of the d-states to the conduction band. Using the Evans model potential in which the depth parameters are calculated by the quantum defect method (Ham 1955) we are able to obtain some nontrivial structure for mercury.

It would be desirable to compare our results with experimental measurements. Unfortunately, no experiment to date determines the density of states directly. In soft X-ray emission from metals the intensity involves not only the density of states in the valence band but also the transition probabilities from the valence band to the vacant core levels. In fact, the analysis by Harrison (1968) suggested that the structure observed in the spectra reflects the variations in the transition probability (oscillator strength) more than in the

density of states. To make things worse the hole in the vacant core level interacts strongly with the electrons so that the measured intensity does not correspond to the unperturbed valence states. The situation is similar in the case of positron annihilation (Stewart and Roellig 1966), the electron momentum distribution being strongly perturbed by the positron. The major complication in the interpretation of photoemission data (see e.g. Berglund and Spicer 1964) is that one may need a detailed understanding of the possible energy losses of an electron leaving the metal. The Knight shift (Knight 1956) depends on two factors: the spin paramagnetic susceptibility of the conduction electrons, which is proportional to the density of states, $n(E_F)$ at the Fermi energy, and the penetration factor, $P_F = |\psi_F(0)|^2_{\text{ave}}$, the average probability density, at the nucleus, of electrons on the Fermi surface. The second factor P_F is more difficult to calculate than $n(E_F)$, so it is difficult to extract $n(E_F)$ from the Knight shift. One kind of experiment that appears promising is Compton scattering of X-rays (Eisenberger and Platzman 1970, also Platzman 1969, unpublished). Since the photon interacts only weakly with electrons, the experiment measures effectively the unperturbed momentum distribution. So far no such experiment has been done on a liquid metal.

Optical properties are even more difficult to interpret than the experiments mentioned above because, in addition to the problem of the transition probability, there are a large number of possible transitions for a given photon energy. Furthermore,

our model calculations in the "isotropic scattering" approximation (Section 5.2) suggest that the frequency dependence of the optical conductivity does not deviate significantly from the Drude formula even if $n(E)$ is quite different from the NFE form. This result is in agreement with most experimental observations, but it means that little information about $n(E)$ can be expected from optical spectra. On the basis of our model calculations the anomalous results for mercury obtained by ellipsometric methods do not seem to be caused by structure in $n(E)$. Perhaps they are due to surface effects.

We found the zero-frequency conductivity to be approximately proportional to the product of the free-electron conductivity and the square of the density of states at the Fermi energy (Section 5.3), in disagreement with semi-intuitive arguments based on the Boltzmann equation. This is another example showing that uncritical application of solid state theory to liquid metals may be misleading.

The current situation in liquid metals is not unlike solid state band-structure calculations in the "pre-Fermiology" era. Perhaps some experiments radically different from those discussed above need to be conceived before the electronic structure can be measured unambiguously.

APPENDIX I

THE ENERGY SUM RULE FOR THE GREEN FUNCTION

The Green function corresponding to a hamiltonian H that describes a physical system is defined as

$$\begin{aligned} G(\underline{k}, E) &= \langle \underline{k} | (E - H)^{-1} | \underline{k} \rangle \\ &= \sum_n \frac{|\langle \underline{k} | \psi_n \rangle|^2}{E - E_n} \end{aligned} \quad , \quad (I.1)$$

where $|\psi_n\rangle$ and E_n designate the eigenstates and eigenvalues of H .

The spectral function

$$\begin{aligned} \rho(\underline{k}, E) &= -\frac{1}{\pi} \text{Im} \{ \langle \underline{k} | G(E + i0^+) | \underline{k} \rangle \} \\ &= \sum_n |\langle \underline{k} | \psi_n \rangle|^2 \delta(E - E_n) \end{aligned} \quad , \quad (I.2)$$

must satisfy the sum rule,

$$\int_{-\infty}^{\infty} \rho(\underline{k}, E) dE = 1 \quad . \quad (I.3)$$

This is a consequence of the completeness of the set of states $\{|\psi_n\rangle\}$. Thus from (I.2) we have

$$\int_{-\infty}^{\infty} \rho(\underline{k}, E) \kappa E = \sum_n |\langle \underline{k} | \psi_n \rangle|^2 = 1$$

The sum rule is also a physical condition since it says that the total probability for a momentum eigenstate $|\underline{k}\rangle$ to have any energy is equal to unity.

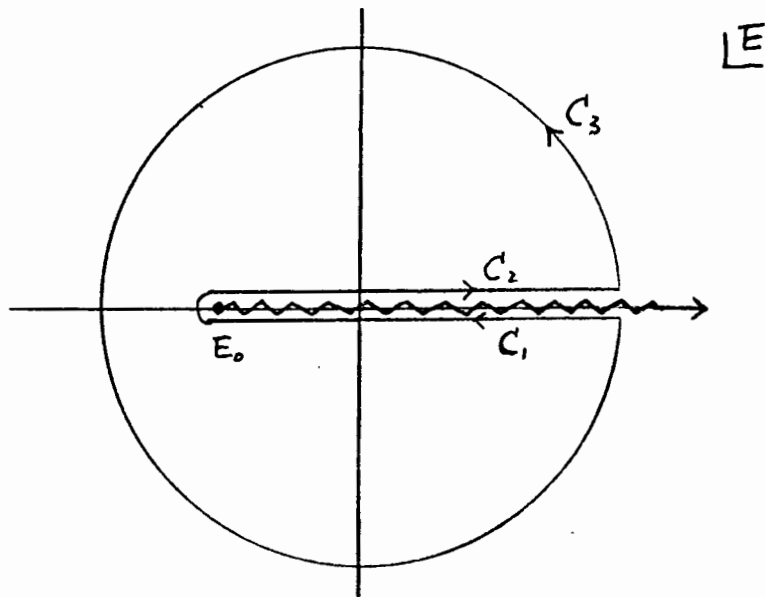
In a practical calculation the ensemble average Green function is usually expressed in the form,

$$G(\underline{k}, E) = \frac{1}{E - \kappa^2 - \Sigma(\underline{k}, E)} \quad , \quad (\text{I.4})$$

where the self-energy $\Sigma(\underline{k}, E)$ may be obtained either by perturbation theory as we did in Chapter 2 or from a parametrized model as in Chapter 5. We shall prove that the sufficient conditions for the Green function (I.4) to satisfy the sum rule (I.3) are:

- (1) It is analytic in the complex E-plane except for a number of poles on the real axis (for an infinite system these poles may coalesce to form a cut);
- (2) $G(\underline{k}, z^*) = G^*(\underline{k}, z)$ where z denotes a complex energy and the asterisk denotes complex conjugation; and
- (3) $\Sigma(\underline{k}, E)$ is an analytic function of E and tends to infinity more slowly than E .

Consider the integral of $G(\underline{k}, E)$ in the complex E-plane around the contour shown.



Here we have assumed that there exists a finite lower bound E_0 to the energy eigenvalue spectrum of H . Since $G(k, E)$ is analytic within the whole region enclosed by the contour $C = C_1 + C_2 + C_3$, we have

$$I \equiv \oint_C G(k, E) dE = 0 \quad . \quad (I.5)$$

From condition (3),

$$\begin{aligned} I_1 &\equiv \int_{C_3} G(k, E) dE \\ &= \int_{C_3} \frac{1}{E} dE \\ &= 2\pi i \quad . \end{aligned} \quad (I.6)$$

From condition (2),

$$\begin{aligned} I_2 &\equiv \int_{C_1} G(k, E) dE + \int_{C_2} G(k, E) dE \\ &= \int_{\infty}^{E_0} G(k, E + i0^-) dE + \int_{E_0}^{\infty} G(k, E + i0^+) dE \\ &= 2i \int_{E_0}^{\infty} \text{Im } G(k, E + i0^+) dE \\ &= -2\pi i \int_{E_0}^{\infty} \rho(k, E) dE \end{aligned} \tag{I.7}$$

But

$$I_1 + I_2 = I = 0 \quad ,$$

therefore

$$\int_{E_0}^{\infty} \rho(k, E) dE = 1 \quad ,$$

which is the required sum rule.

Note that the parametrized model,

$$G(k, E) = \frac{1}{E - \varepsilon(k) + i b E^{1/2}},$$

where

$$\varepsilon(k) = k^2 + c \left\{ [1 + e^{(g-k)/a}]^{-1} - [1 + e^{g/k}]^{-1} \right\}$$

satisfies all the conditions (1) to (3) and hence the sum rule.

On the other hand, the Lorentzian model,

$$G(k, E) = \frac{1}{E - k^2 + i\Gamma},$$

with Γ independent of E , does not satisfy condition (2), therefore the above proof for the sum rule does not apply. However, in this case it can easily be proved by direct integration that (I.3) is still satisfied.

APPENDIX II

TABLE IV MODEL POTENTIAL PARAMETERS ^(a)

		Bi	In	Hg
A_0	(a.u.)	2.38	1.32	1.05
A_1	(a.u.)	2.58	1.46	1.27
A_2	(a.u.)	0.25	1.10	0.98
$R_M^{(b)}$	(a.u.)	2.0	2.4	3.4
Ω	(a.u.)	234.2	183.6	166.1
Z		5	3	2
R_C	(a.u.)	1.4	1.74	2.12
α	(a.u.)	0	0	0.0781
E_{ic}	(Ry)	0.597	-0.45	0
$\frac{dA_0}{dE}$	(a.u.)	-0.57	-0.45	-0.42
$\frac{dA_1}{dE}$	(a.u.)	-0.62	-0.21	-0.40
$\frac{dA_2}{dE}$	(a.u.)	1.12	0	-0.30

(a) These quantities are defined in Section 2.3 or Section 2.5 and are evaluated at the Fermi energy E_F .

(b) R_2 in the case of Hg.

APPENDIX III

DIFFERENTIATION OF A FUNCTION OF AN OPERATOR WITH RESPECT TO A PARAMETER

Let $F(A)$ be a function of an operator A , which in turn is a differentiable function of a continuous parameter ξ . We wish to derive an expression for the derivative of $F(A)$ with respect to ξ . For simplicity we assume that $F(A)$ can be expanded in a power series,

$$F(A) = \sum_{n=0}^{\infty} C_n A^n . \quad (\text{III.1})$$

Since the operator A does not in general commute with its derivative, it is important to keep track of the order during differentiation. For instance, in the notation

$$\begin{aligned} A' &\equiv \frac{dA}{d\xi} , \\ \frac{d}{d\xi} A^2 &= A'A + AA' \\ &= 2A'A + [A, A'] , \end{aligned} \quad (\text{III.2})$$

where we have introduced the commutator,

$$[A, B] \equiv AB - BA . \quad (\text{III.3})$$

Continuing to derivatives of higher powers of A in this way one readily arrives at the general formula for any integral power,

$$\begin{aligned} \frac{d}{d\lambda} A^n &= n A' A^{n-1} + [A, A'] A^{n-2} + [A^2, A'] A^{n-3} + \dots \\ &\quad + [A^{n-2}, A'] A + [A^{n-1}, A'] \end{aligned}$$

(III.4)

$$= n A' A^{n-1} + \sum_{s=0}^{n-2} [A^{n-s-1}, A'] A^s.$$

Hence

$$\frac{d}{d\lambda} F(A) = A' \sum_{n=0}^{\infty} n c_n A^{n-1} + \sum_{n=0}^{\infty} c_n \sum_{s=0}^{n-2} [A^{n-s-1}, A'] A^s$$

(III.5)

$$= A' \frac{dF(A)}{dA} + S,$$

where, for convenience, the notation

$$S \equiv \sum_{n=0}^{\infty} c_n \sum_{s=0}^{n-2} [A^{n-s-1}, A'] A^s$$

(III.6)

has been introduced.

Now, by repeated application of the commutation rule,

$$[AB, C] = A[B, C] + [A, C]B, \quad (\text{III.7})$$

for any three operators A, B, and C, one can show

$$[A^m, B] = \sum_{p=0}^{m-1} A^{m-p-1} [A, B] A^p, \quad (\text{III.8})$$

Inserting this into (III.6) we have

$$\begin{aligned} S &= \sum_{n=0}^{\infty} c_n \sum_{s=0}^{n-2} \sum_{p=0}^{n-s-2} A^{n-s-p-2} [A, A'] A^{p+s} \\ &= \sum_{n=0}^{\infty} c_n \sum_{s=0}^{n-2} \sum_{r=s}^{n-2} A^{n-r-2} [A, A'] A^r \\ &= \frac{1}{2} \sum_{n=0}^{\infty} n c_n \sum_{r=0}^{n-2} A^{n-r-2} [A, A'] A^r. \end{aligned} \quad (\text{III.9})$$

In order to simplify (III.9) we again use (III.3) to shift all powers of A from the left to the right of the commutator, thus

$$A[A, A'] = [A, A']A + [A, [A, A']],$$

$$A^2[A, A'] = [A, A']A^2 + 2[A, [A, A']]A + [A, [A, [A, A']]],$$

.....

Let us adopt the following notation:

$$A^{(0)}\{B\} \equiv B,$$

$$A^{(1)}\{B\} \equiv [A, B],$$

$$A^{(2)}\{B\} \equiv [A, [A, B]],$$

.

.

.

$$A^{(t)}\{B\} \equiv [A, A^{(t-1)}\{B\}].$$

Then we can write

$$A[A, A'] = A^{(1)}\{A'\}A + A^{(2)}\{A'\}$$

$$A^2[A, A'] = A^{(1)}\{A'\}A^2 + 2A^{(2)}\{A'\}A + A^{(3)}\{A'\},$$

.....

In general, as can be shown by mathematical induction,

$$A^k[A, A'] = \sum_{h=0}^k \binom{k}{h} A^{(h+1)}\{A'\} A^{k-h}, \tag{III.10}$$

where $\binom{k}{h}$ is just the binomial coefficient,

$$\binom{k}{h} = \frac{k(k-1)(k-2) \dots (k-h+1)}{h!}$$

Equation (III.9) now becomes

$$S' = \frac{1}{2} \sum_{h=0}^{\infty} n C_n^h \sum_{\lambda=0}^{h-2} \sum_{k=0}^{h-\lambda-2} \binom{h-\lambda-2}{k} A^{(k+1)} \{A'\} A^{h-2-k} \quad (III.11)$$

With the aid of the combinatorial relation,

$$\sum_{s=m}^n \binom{s}{m} = \binom{h+1}{m+1} ,$$

Equation (III.11) simplifies, after some algebra, to

$$S' = \frac{1}{2} \sum_{h=0}^{\infty} n C_n^h \sum_{k=0}^{h-2} A^{(k+1)} \{A'\} \binom{h-1}{k+1} A^{h-k-2} \quad (III.12)$$

But

$$\begin{aligned} & \sum_{h=0}^{\infty} n C_n^h \binom{h-1}{k+1} A^{h-k-2} \\ &= \sum_{h=0}^{\infty} C_n^h n(n-1)(n-2) \dots (n-k-1) A^{n-k-2} \\ &= \frac{d^{k+2}}{dA^{k+2}} F(A) , \end{aligned} \quad (III.13)$$

therefore we finally have

$$S = \sum_{h=1}^{\infty} \frac{A^{(h)}\{A'\}}{2(h!)} \frac{d^{h+1}}{dA^{h+1}} F(A). \quad (\text{III.14})$$

Putting (III.14) back into (III.5),

$$\frac{d}{d\xi} F(A) = A' \frac{dF(A)}{dA} + \sum_{h=1}^{\infty} \frac{A^{(h)}\{A'\}}{2(h!)} \frac{d^{h+1}}{dA^{h+1}} F(A), \quad (\text{III.15})$$

which is the general formula we set out to derive.

If $A^{(t)}\{B\} = 0$ for $t = \ell$, then it is also equal to zero for all $t > \ell$. For example, if $[A, A'] = 0$, then

$$\frac{d}{d\xi} F(A) = A' \frac{dF(A)}{dA} ; \quad (\text{III.16})$$

if $[A, [A, A']] = 0$, then

$$\frac{d}{d\xi} F(A) = A' \frac{dF(A)}{dA} + \frac{1}{2} [A, A'] \frac{d^2 F(A)}{dA^2} \quad (\text{III.17})$$

and if $[A, [A, [A, A']]] = 0$, then

$$\frac{d}{d\xi} F(A) = A' \frac{dF(A)}{dA} + \frac{1}{2} [A, A'] \frac{d^2 F(A)}{dA^2} + \frac{1}{4} [A, [A, A']] \frac{d^3 F(A)}{dA^3} . \quad (\text{III.18})$$

REFERENCES

- Abarenkov, I.V. and Heine, V. 1965. *Phil. Mag.* 12, 529.
- Adams, P.D., Davies, H.A., and Epstein, S.G. (editors), 1966. "The Properties of Liquid Metals," Proc. Brookhaven Conference (Taylor and Francis: London).
- Adams, P.D. 1968. *Phys. Rev. Lett.* 21, 1324.
- Animalu, A.O.E. 1965. Technical Report No. 4, Solid State Theory Group, Cavendish Laboratory, Cambridge, England.
- Animalu, A.O.E. and Heine, V. 1965. *Phil. Mag.* 12, 1249.
- Ashcroft, N.W. and Schaich, W. 1970. *Phys. Rev.* B1, 1370.
- Austin, B.J., Heine, V., and Sham, L.J. 1962. *Phys. Rev.* 127, 276.
- Ballentine, L. E., 1965, Ph.D Thesis, Cambridge University.
- Ballentine, L.E. 1966. *Can. J. Phys.* 44, 2533.
- Ballentine, L.E. and Gupta, O.P. 1971. *Can. J. Phys.* 49, 1549.
- Berglund, C.N. and Spicer, W.E. 1964. *Phys. Rev.* 136, A1030.
- Bloch, A.N. and Rice, S.A. 1969. *Phys. Rev.* 185, 933.
- Borsa, F. and Barnes, R.G. 1966. *J. Phys. Chem. Solids* 27, 567.
- Bradley, C.C., Faber, T.E., Wilson, E.G., and Ziman, J.M. 1962. *Phil. Mag.* 7, 865.
- Bringer, A. and Wagner, D. 1971. *Z. Physik* 241, 295.
- Chan, T. and Ballentine, L.E. 1971a, *Phys. Lett.* 35A, 385.
- Chan, T. and Ballentine, L.E. 1971b . *Physics and Chemistry of Liquids* 2, 165.
- Cohen, M.L. and Heine, V. 1970. *Solid State Physics* 24, 37.
- Conte, S.D. 1965. "Elementary Numerical Analysis" (McGraw-Hill: New York).
- Cusack, N.E. 1963. *Reports on Prog. Phys.* 26, 361.
- Cusack, N.E. 1967. *Contemp. Phys.* 8, 583.
- Cyrot-Lackmann, F. 1966. *J. de Physique* 27, 627.

- Dy, K.S. and Wu, Shi-Yu 1971. Phys. Rev. B3, 1173.
- Edwards, S.F. 1958. Phil. Mag. 3, 1020.
- Edwards, S.F. 1962. Proc. Roy. Soc. A267, 518.
- Edwards, S.F. 1965. Proc. Phys. Soc. 85, 1.
- Eisenberger, P. and Platzman, P.M. 1970. Phys. Rev. A2, 415.
- Evans, R. 1970. J. Phys. C: Metal Phys. Suppl. No. 2, S 137.
- Evans, R., Greenwood, D.A., Lloyd, P., and Ziman, J.M. 1969. Phys. Lett. 30A, 313.
- Faber, T.E. 1966. Adv. Phys. 15, 547.
- Faber, T.E. and Ziman, J.M. 1965. Phil. Mag. 11, 153.
- Faber, T.E. and Smith, N.V. 1968. J. Opt. Soc. Am. 58, 102.
- Freed, K.F. and Cohen, M.H. 1971. Phys. Rev. B3, 3400.
- Greenwood, D.A. 1958. Proc. Phys. Soc. (London) 71, 585.
- Halperin, B.I. 1968. Adv. Chem. Phys. 13, 123.
- Ham, F.S. 1955. Solid State Physics 1, 127.
- Harrison, W.A. 1966. "Pseudopotentials in the Theory of Metals" (Benjamin: New York).
- Harrison, W.A. 1968. in "Soft X-Ray Band Spectra and the Electronic Structure of Metals and Materials", ed. D.J. Fabian (Academic Press: New York) p. 227.
- Heine, V. and Abarenkov, I.V. 1964. Phil. Mag. 9, 451.
- Hodgson, J.N. 1959. Phil. Mag. 4, 183.
- Hodgson, J.N. 1960. Phil. Mag. 5, 272.
- Hodgson, J.N. 1961. Phil. Mag. 6, 509.
- Hodgson, J.N. 1962. Phil. Mag. 7, 229.
- Hohenberg, P. and Kohn, W. 1964. Phys. Rev. 136, B 864.
- Jena, P. and Halder, N.C. 1971. Phys. Rev. Lett. 26, 1024.
- Jones, J.C. 1970. Ph.D. Thesis, McMaster University.
- Kaplow, R., Strong, S.L., and Averbach, B.L. 1965. Phys. Rev. 138, A 1336.

- Knight, W.D. 1956. Solid State Physics 2, 93.
- Kohn, W. and Sham, L.J. 1965. Phys. Rev. 140, A 1133.
- Koyama, R., Spicer, W.E., Ashcroft, N.W., and Lawrence, W.E.
1967. Phys. Rev. Lett. 19, 1284.
- Kubo, R. 1957. J. Phys. Soc. Japan 12, 570.
- Langer, J.S. 1960. Phys. Rev. 120, 714.
- Langer, J.S. 1961. Phys. Rev. 124, 1003.
- Lloyd, P. 1967. Proc. Phys. Soc. 90, 207; 217.
- Lloyd, P. 1968. in "Theory of Condensed Matter" (International Atomic Energy Agency: Vienna), p. 639.
- March, N.H. 1968. "Liquid Metals" (Pergamon: Oxford).
- Mott, N.F. 1966. Phil. Mag. 13, 989.
- Mott, N.F. 1967. Adv. Phys. 16, 49.
- Neal, T. 1970. Phys. Fluids 13, 249.
- North, D.M. Enderby, J.E., and Egelstaff, P.A. 1968.
J. Phys. C (Proc. Phys. Soc.) [2], 1, 1075.
- Nozières, P. 1964. "Theory of Interacting Fermi Systems"
(Benjamin: New York).
- Ocken, H. and Wagner, C.N.J. 1966. Phys. Rev. 149, 122.
- Phillips, J.C. and Kleinman, L. 1959. Phys. Rev. 116, 287;880.
- Platzman, P.M. 1969. Lecture Notes, C.A.P. Summer School,
Banff 1969 (unpublished).
- Rousseau, J., Stoddard, J.C., and March, N.H. 1970. Proc.
Roy. Soc., London, A 317, 211.
- Schneider, T. and Stoll, E. 1967. in "The Properties of Liquid Metals", ed. P.D. Adams et al. (Taylor and Francis: London), p. 731.
- Schulz, L.G. 1957. J. Opt. Soc. Am. 47, 64.
- Seymour, E.F.W. and Styles, G.A. 1964. Phys. Lett. 10, 269.
- Sharma, S.N. and Williams, D.L. 1967. Phys. Lett. 25A, 738.

- Shaw, R.W., Jr. 1968. Phys. Rev. 174, 769.
- Shaw, R.W., Jr. and Harrison, W.A. 1967. Phys. Rev. 163, 604.
- Shaw, R.W., Jr. and Smith, N.V. 1969. Phys. Rev. 178, 985.
- Smith, N.V. 1967a. in "The Properties of Liquid Metals",
ed. P.D. Adams et al. (Taylor and Francis: London), p. 629.
- Smith, N.V. 1967b. Phys. Rev. 163, 552.
- Smith, N.V. 1968. Phys. Lett. 26A, 126.
- Srivastava, S.K. and Sharma, P.K. 1969. Ind. J. Pure and
Appl. Phys. 7, 644.
- Stewart, A.T. and Roellig, L.O. (editors) 1966. "Positron
Annihilation" (Academic Press: New York).
- Sunström, Lorna, J. 1965. Phil. Mag. 11, 657.
- Taylor, A.W.B. 1966. Physica 32, 2030.
- Watabe, M. and Tanaka, M. 1964. Prog. Theor. Phys. 31, 525.
- Weaire, D. 1967. Proc. Phys. Soc. 92, 956.
- Weaire, D. 1968. J. Phys. C (Proc. Phys. Soc.) [2], 1, 210.
- Wilson, A.H. 1953. "The Theory of Metals", 2nd ed. (Cambridge
University Press: London).
- Wilson, J.R. 1965. Metallurgical Rev. 10, 381.
- Wilson, E.G. and Rice, S.A. 1966. Phys. Rev. 145, 55.
- Ziman, J.M. 1961. Phil. Mag. 6, 1013.
- Ziman, J.M. 1964. Adv. Phys. 13, 89.
- Ziman, J.M. 1965. "Principles of the Theory of Solids"
(Cambridge University Press: London).
- Ziman, J.M. 1967. in "The Properties of Liquid Metals", ed.
P.D. Adams et al. (Taylor and Francis: London), p. 551.
- Ziman, J.M. 1968. J. Phys. C (Proc. Phys. Soc.) [2], 1, 1532.
- Ziman, J.M. 1969a. J. Phys. C (Solid State Phys.) [2], 2, 1230.

Ziman, J.M. 1969b. "Elements of Advanced Quantum Theory"
(Cambridge University Press: London).

Ziman, J.M. 1969c. J. Phys. C (Solid State Phys.) [2], 2, 1704.